Massive Stars and High-Energy Emission in OB Associations

Proceedings of JENAM 2005 *Distant Worlds*,
July 4-7, 2005, Liège (Belgium)

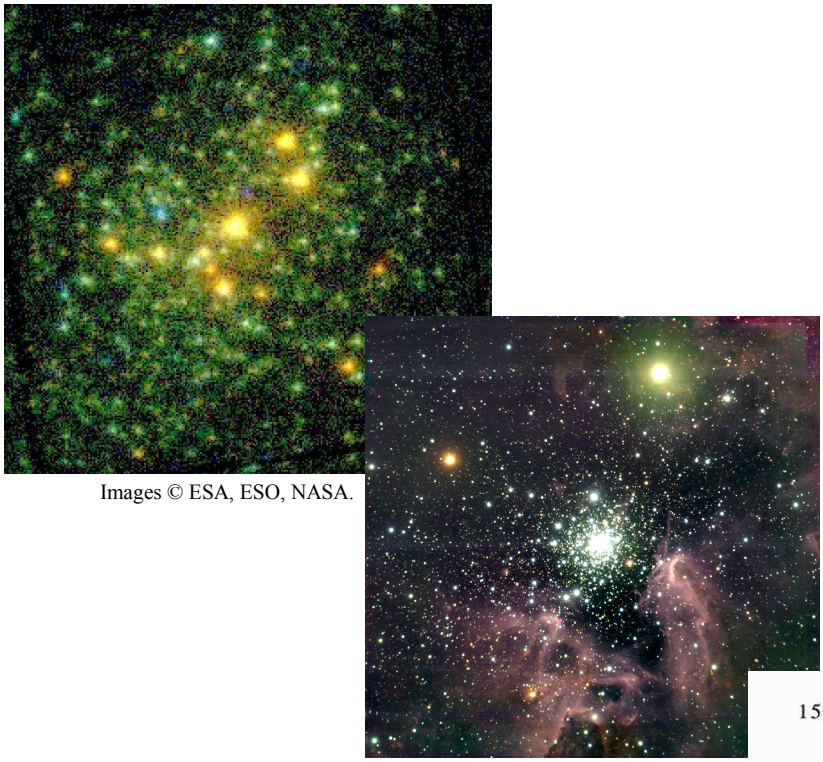

Images © ESA, ESO, NASA.

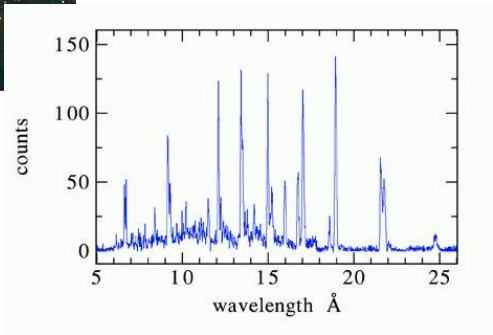

Institut d'Astrophysique et de Géophysique
Université de Liège
Allée du 6 Août 17, Bat. B5C
B4000-Liège (Belgium)

Edited by:
G. Rauw, Y. Nazé,
R. Blomme & E. Gosset

Dépôt légal : D/2005/0480/95

Foreword

About 35 astronomers including many experts in the field of massive stars attended the afternoon sessions of the JENAM 2005 workshop "Massive Stars and High-Energy Emission in OB Associations". In addition to the two plenary talks by Dr Ian Stevens and Prof Thierry Montmerle, two invited reviews by Prof Artemio Herrero and Dr Martin Guerrero as well as 12 contributed talks and nine posters were presented during the workshop. A good number of new exciting results obtained with modern high-resolution optical spectrographs and/or high-energy instruments onboard *XMM-Newton*, *Chandra* and *INTEGRAL* were presented and new questions were raised.

Several contributions were devoted to *non-thermal phenomena* associated with a subset of the massive stars. Many results presented at the workshop seem to demonstrate that non-thermal radio emission of early-type stars is a signature of *colliding winds* in binary systems. While this was already established for Wolf-Rayet stars, it becomes now more and more obvious for O stars as well. In this context, the participants emphasized the interest to search for non-thermal X-ray and γ-ray emissions from massive binaries. Such a hard X-ray – soft γ-ray emission could also arise from the collision of a supernova remnant with a stellar wind.

The topic of non-thermal emission is related to one of the most controversial issues of massive star research; their *magnetic fields*. Magnetic fields certainly play a major role in the generation of the non-thermal radio emission and they might lead to magnetically confined stellar winds (such as observed in θ Ori C). However, there are many questions that remain open as to the origin of these fields, their strengths as well as their origin (fossil vs. dynamo…). These properties are essential ingredients of any theoretical attempt to model the non-thermal processes. The participants expressed their hope that upcoming observational facilities as well as new developments in theoretical models will allow to better constrain the properties of magnetic fields in early-type stars.

New questions were also raised concerning the *origin of X-ray emission from massive stars*. Some observational as well as theoretical results cast doubt on the "standard model" (the shock – X-ray emission paradigm) for the production of X-rays from massive stars. Again, magnetic fields might play a key role here.

Another major question concerns the *duplicity* of massive stars and the *colliding wind phenomenon*. As a result of detailed analyses and high-quality data, we now have better statistics of the multiplicity of massive stars as well as a better knowledge of the observed properties of colliding wind systems over a broad range of stellar parameters. Some features were unexpected, others agree quite well with theoretical expectations. A question that was actively debated is whether or not all Wolf-Rayet stars that emit X-rays or that produce dust are binaries. Finally, wind-wind collisions or magnetic fields might also play a role in the enigmatic variability of some peculiar objects like the Of?p stars.

Some topics related to *star formation* were also discussed. Recent X-ray observations of massive star clusters reveal a wealth of secondary sources associated with pre-main sequence stars. A new temperature calibration of O-type stars further suggests that massive stars are significantly cooler than previously thought and may actually not appear on the zero age main sequence. These results are crucial for a better understanding of massive star formation and of many interaction processes between massive stars and their surroundings.

The participants of the workshop emphasized the need for more observations of massive stars in the high-energy domain (using *XMM-Newton*, *INTEGRAL* and *Chandra*) as well as in the radio domain and they decided to coordinate their efforts towards this endeavor.

It is our pleasure to thank Jean-Pierre Swings and Jean-Marie Vreux for their participation in the local organizing committee of this workshop, as well Denise Caro, Alain Detal and Sandrine Sohy who contributed significantly to the practical organization of the workshop.

The organization of the JENAM 2005 event was made possible through various grants received from the "Province de Liège", OPTICON, the European Astronomical Society (EAS), the European Space Agency (ESA), AMOS, the "Fonds National de la Recherche Scientifique" (FNRS), the Belgian Science Policy (Belspo), the "Université de Liège" and the "Communauté Française de Belgique". We are grateful to all these organizations for their financial support.

An electronic version of these proceedings is available at the link

http://www.astro.ulg.ac.be/RPub/Colloques/JENAM/proceedings/proceedings.html

Liège, November 2005

Gregor Rauw, Yaël Nazé, Ronny Blomme, Eric Gosset

Table of Contents

Sect. 3: High-energy emission from young open clusters

Contributed Talks

Posters

Section 1

Massive stars: general properties,

X-ray emission and peculiar objects

X-ray and gamma-ray emission from single and binary early-type stars

I.R. Stevens

School of Physics and Astronomy, University of Birmingham, Birmingham B15 2TT, UK

Abstract: Since their launch, both the *Chandra* and *XMM-Newton* satellites have provided us with a new and more detailed view of the high energy processes in massive stars. This paper reviews recent X-ray observations of a range of massive stars, both O-stars and Wolf-Rayet (W-R) stars, as well as both single early-type stars and binary systems, where colliding winds may well play a role. Results from high spectral resolution X-ray data will be reviewed, where the velocity structure of the individual line profiles can be resolved. Recent *INTEGRAL* gamma-ray observations of massive stars will be covered, as well as discussing the expected gamma-ray properties of early-type stars.

1 Introduction: massive stars

Massive stars are clearly important objects within a galaxy, impacting their environments via their radiation fields and dense, supersonic winds, and then via subsequent supernova explosions. Within our own galaxy there are many examples of early type stars, both single objects, binary stars and within young star clusters, such as NGC 3603. In many starburst galaxies there are very large numbers of young stars, which via the mass and energy injection from their stellar winds, can power the starburst phenomenon and drive strong superwinds out of the galaxy.

In this paper, the focus is on the high energy view of massive stars, particularly X-ray and gamma-ray emission from single and binary early-type stars, including both OB-stars and W-R stars. A complimentary review on the high energy emission seen from young stars in clusters is given by Montmerle (this proceedings).

The most obvious characteristics of OB and W-R stars are that they are massive, very luminous and have strong radiatively driven winds. It is these winds that allow early-type stars to interact directly with their environments and the observed high energy emission is directly associated with these winds as well.

The typical values for early-type stars winds are as follows: the winds are highly supersonic, with $v_\infty \sim 1000 - 3000$ km s^{-1}, and have mass-loss rates ($\dot{M}$) in the range of $\dot{M} \sim 10^{-7} - 10^{-4}$ M$_\odot$ yr^{-1}, with the more luminous stars having more massive winds. If we convert these numbers into typical kinetic energies, we find that $L_{wind} = 0.5\dot{M}v_\infty^2 \sim 10^{35} - 10^{38}$ erg s^{-1}. This should be contrasted with the bolometric luminosities, $L_{bol} \sim 10^{37} - 10^{40}$ erg s^{-1}. This means that the kinetic energy in the stellar wind is only a relatively small fraction of the total energy output of the stars (typically only 1% or so), but it is nonetheless very important. The stellar winds

of the most massive stars can result in a very significant degree of mass-loss (the most massive stars lose most of their mass via their stellar winds during their lifetime), with a major impact on evolution. We also know that massive stars are very often in binary systems with other massive stars (and often in triple or quadruple systems). The periods of these binaries range from a couple of days up to many years (or hundreds or thousands of years). The presence of two massive stars leads directly to the phenomenon of colliding stellar winds. Colliding stellar winds in early type binary systems are now recognised as an integral part of our understanding of hot stars. Signatures of colliding winds have been found at virtually all wavelengths, and in a variety of guises, ranging from X-ray emission directly from the shocked region, to IR emission from dust formation inferred to be a consequence of wind collision.

There have been several important recent missions that are impacting on our understanding of high energy emission from massive stars. At X-ray energies, the *Chandra* and *XMM-Newton* X-ray satellites were both launched in 1999 and are both still operating. These two satellites both have high resolution grating instruments, which give unprecedented levels of spectral resolution at X-ray energies, allowing significant velocity resolution of the X-ray emitting material. The spectral resolution of these instruments is a few hundred km s^{-1}, which compares favourably with the terminal velocities of these objects. In this paper the focus is more on the high resolution observations of X-ray line emission, rather than the broad-band continuum properties of early-type stars, these observations yielding greater insight into the dynamics of the winds. At gamma-ray energies, the *INTEGRAL* satellite was launched in 2003, and is sensitive to the hard X-ray and low energy gamma-ray region.

This paper is organized as follows: Section 2 reviews the observed X-ray emission from single OB and W-R stars, and the various attempts to model the X-ray line emission. Section 3 reviews the situation for X-ray emission from binary early type stars, and colliding stellar winds. Section 4 covers results from gamma-ray observations from the *INTEGRAL* satellite, and Section 5 concludes.

2 X-ray emission from single OB and W-R stars

X-ray emission from early-type stars was first detected by the *EINSTEIN* satellite in the late 1970's. This discovery was rather unexpected and the details of what causes the emission remains a subject of debate. The two main proposals were that the X-ray emission was either caused by substantial "base corona" or that the X-ray emission was distributed throughout the wind (Cassinelli & Swank 1983). The lack of substantial low energy X-ray absorption was interpreted as being evidence against the base corona model, and the distributed emission model is preferred nowadays.

The basic observational facts for OB stars are as follows. The X-ray luminosities are typically in the range of $L_X \sim 10^{30} - 10^{34}$ erg s^{-1}. The X-ray luminosity of the early-type stars scales with bolometric luminosity, with a rough scaling of $L_X \sim 10^{-7} L_{bol}$. This scaling applies for O stars down into the early B-stars. For stars of later spectral types the scaling is rather flatter and for these stars the X-ray emission comes (at least in part) from unresolved companions (such as white dwarfs and low-mass stars that emit coronal X-rays). The general behaviour of the X-ray emission form early-type stars is illustrated in Fig. 1, which is taken from Berghöfer et al. (1997), using data from the *ROSAT* satellite.

The X-ray spectra of early-type stars are usually reasonably soft. Because they are not usually very strong X-ray emitters, the spectra are usually fitted with one or two temperature thermal models. In many cases, the softer component has a temperature of $kT \sim 0.5$ keV. In a number of cases, particularly with higher quality spectra there is also a harder emission

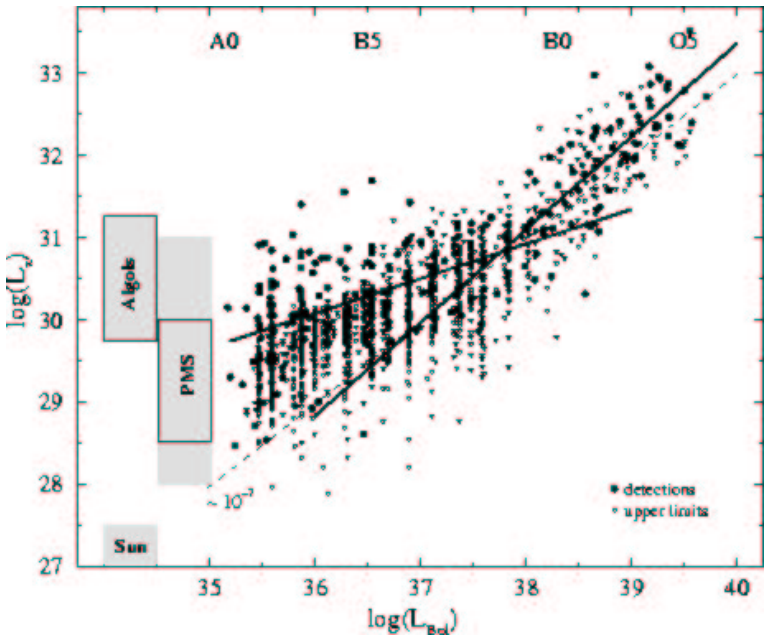

Figure 1: The X-ray luminosity (L_X) plotted against bolometric luminosity (L_{bol}), taken from Berghöfer et al. (1997). The solid lines represent regression lines for $L_{bol} \leq 10^{38}$ erg s^{-1} and $L_{bol} > 10^{38}$ erg s^{-1}. The dashed line shows $L_X = 10^{-7} L_{bol}$. The grey bars at the left side show typical ranges for the X-ray luminosity of Algol-type systems, pre-main sequence stars (PMS), as well as for the Sun.

component, with $kT \sim 2$ keV. There is some evidence for excess X-ray emission from (some) massive binary systems and this has been interpreted as being due to colliding stellar winds in such binary systems (see Section 4).

Radiatively driven winds are believed to be highly unstable, and the basic structure is expected to be punctuated by a whole host of shocks internal to the wind. These internal shocks will produce X-rays (Owocki, Castor & Rybicki 1988). Multiple shocks can also produce non-thermal particles and non-thermal radio and gamma-ray emission

In terms of the expected X-ray spectra from shocked heated gas, it will consist of continuum from thermal bremsstrahlung, but with strong contributions from line emission from the abundant atomic species, such as O, Ne, Mg, Si, S and Fe. The emission lines will come from predominantly hydrogen and helium-like ions of these elements. In contrast to this, non-thermal X-ray emission (from shock accelerated electrons for instance) will likely have a characteristic power-law shape. In reality, the emission from a given early-type star (single or binary) will have both thermal and non-thermal components (as we expect shocks to give rise to both forms of emission), and the thermal emission will certainly not be isothermal and will come from a range of different temperatures. Disentangling all these components from spectra with relatively few counts is rather challenging.

In addition to emission processes, absorption processes will also play a major role in the observed spectrum, as the abundant metals in the wind are very efficient at absorbing soft X-rays. For example, if we consider X-ray emitting material moving out in the wind of an O-star. From the point of view of the observer, material out in the wind on the far side of the star will be red-shifted and more heavily absorbed, and material on the near side will be blue-shifted and less heavily absorbed. This suggests that, for a spherical expanding wind, the resulting line profiles will be shifted towards the blue (with the red portions being more highly absorbed).

As mentioned earlier, one of the big advances in this field has been the launch of the *Chandra* and *XMM-Newton* satellites. The spectral resolution of the grating instruments on these satellites are around a few 100 km s^{-1}. With this resolution we are able to spectrally resolve the velocity structure of the emission lines in the X-ray spectra of early-type stars, and to gain new insights into the wind dynamics.

To return to the canonical result that $L_X \sim 10^{-7} L_{bol}$. We might expect the X-ray emission to scale as the wind density squared (the emission being due to free-free emission). This means that, as $\rho \propto \dot{M}/v_\infty$ for spherically symmetric winds, and as $\dot{M} \propto L_{bol}^{1.7}$ (Howarth & Prinja 1989), we might expect $L_X \propto L_{bol}^{3.4}$. This is obviously much steeper than observed, but we should also expect absorption to play a role, with an additional factor with $L_X \propto \exp(-c\tau)$ with c a constant and the optical depth $\tau \propto \dot{M}$. One explanation is that this absorption factor transforms the much steeper relationship for intrinsic X-ray emission into the observed linear relation. This seems rather contrived and is probably not the real explanation. Consequently, even this apparently very simple observed relationship for early-type stellar X-ray emission is not fully understood. What is clear is that the form of this relationship is a consequence of contributions from both emission and absorption (for soft X-rays, the $\tau \sim 1$ optical depth occurs at several stellar radii).

Interestingly, for OB stars in one young star cluster, namely NGC 6231 an even tighter relationship is seen. In this case all of the stars are at the same age and metallicity and this may be a clue as to what affects the relationship (Sana et al. 2005).

2.1 High resolution X-ray observations of single OB stars

Quite a number of single OB stars have now been observed with the *Chandra* and *XMM-Newton* grating instruments, and some examples and general results are discussed here. All the observed OB stars show Doppler broadened X-ray emission lines, from a range of highly ionized species. For example, Zeta Pup (an O4f star) shows strongly broadened and blue-shifted emission line profiles. The *Chandra* grating spectrum of Zeta Pup is shown in Fig. 2 (Cassinelli et al. 2001), with data from both the high energy (HEG) and medium energy (MEG) gratings. As can be seen, the spectrum is dominated by line emission from a range of (mostly) hydrogen- and helium-like ions. The line widths are typically around 850 km s^{-1} HWHM for Zeta Pup. In contrast to this, Delta Ori (O9.5 II) shows X-ray line profiles that are narrower, symmetric and largely unshifted (Miller et al. 2002), though the lines are still relatively broad (around 430 km s^{-1} HWHM, though this is much lower than the terminal wind velocity of 2000 km s^{-1}). As another example, moving to later type stars, Tau Sco (B0.2 V) has rather narrow lines (Cohen et al. 2003; Mewe et al. 2003). Tau Sco has a rather weak wind, certainly compared to Zeta Pup, which has a wind with a mass-loss rate around two orders of magnitude greater. This means that we can see deeper into the wind of Tau Sco.

As another example, multi-epoch X-ray observations of θ^1 Ori C (O5.5V) suggests that in this case we are seeing a magnetically confined wind. This star is both very young and shows evidence of being strongly magnetized (Gagné et al. 2005).

Typically, the observed X-ray lines are broader at shorter wavelengths, that is for lower ionization species and narrower for higher ionization species. This suggests that the X-ray emitting portions of the winds are cooler at greater distances from the star, where the wind is at higher velocities (and so the emission lines are broader). It is also clear from this that the observed X-ray emission comes from a range of radii (and densities). Interestingly, Tau Sco is an exception to this to this trend, with a rather weak trend in the opposite direction.

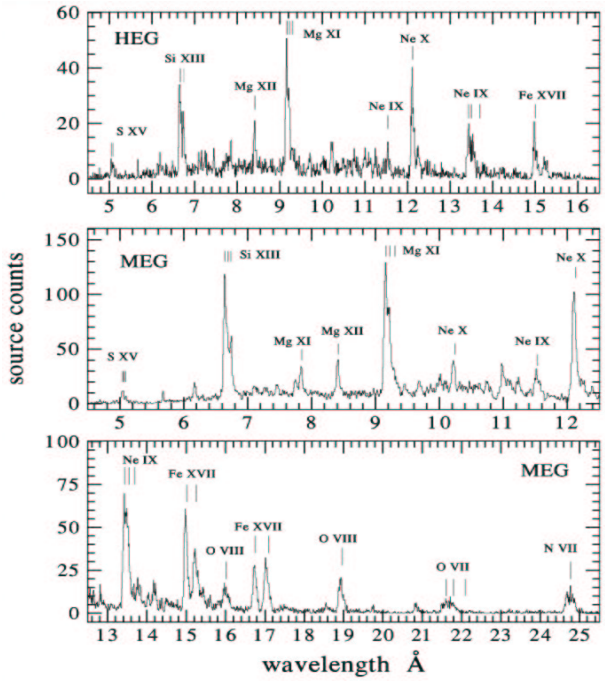

Figure 2: The *Chandra* spectrum of Zeta Pup, from Cassinelli et al. (2001), with data from HETGS HEG (top panel) and MEG (bottom panels). The ions responsible for the strongest emission lines are identified.

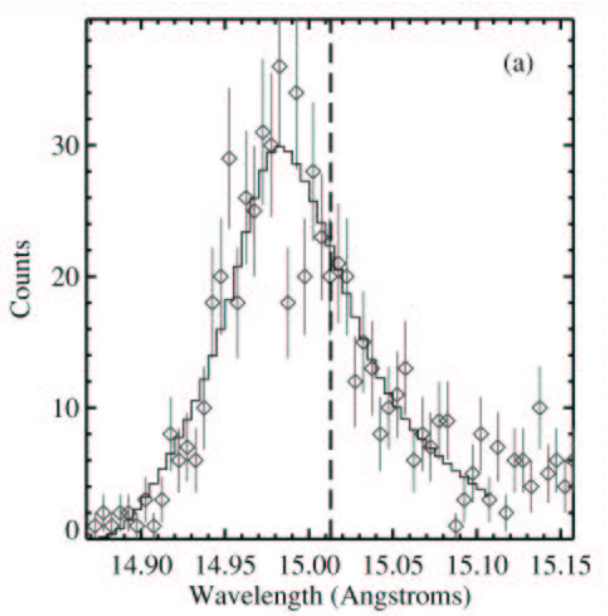

Figure 3: An example of the observed line profile and line fit, from the modelling work of Kramer et al. (2003). This is a fit to the Fe XVII line of Zeta Pup at 15.01Å, showing the broad blue-shifted profile.

2.2 X-ray line-profile modelling of single OB stars

Several different groups have attempted to model the observed line profiles from single OB stars. For example, one approach models the line emission using a highly structured wind model (Feldmeier et al. 2003; Oskinova et al. 2004), with many shocks. The X-rays come from the post-shock regions behind these shocks, and the X-rays suffer absorption by the underlying stellar wind and also from dense shells associated with the shocks (which can be rather opaque). Obviously in this model, red-shifted material, on the far side of the star, is more likely to be absorbed (having a longer path to traverse through the wind). This model is capable of reproducing the Zeta Oph emission lines.

Another approach have been adopted by Kramer et al. (2003). This is a simple phenomenological model, based on assumed distribution of X-ray material. The X-ray emitting material is assumed to be distributed throughout the wind, with the emissivity of the material given by a power-law distribution. The model also assumed an inner radius for the X-ray emission. Absorption by the stellar wind is also included, and this model is capable of reproducing the observed Zeta Pup emission lines, and implying that the X-ray emitting material extends well down into the inner regions of the wind. An example of the best fit to a Zeta Pup emission line from the modelling of Kramer et al. (2003) is shown in Fig. 3.

The message from this section is that there are several different approaches available to model the emission lines from OB stars. While these techniques are capable of well modelling the emission lines from some of the stars they are not capable of modelling all of the emission lines in a physically interesting way that yields new insight into the observed behaviour of these objects.

2.3 X-rays from single W-R stars

W-R stars, like OB stars, have radiatively driven winds, and given that W-R wind terminal velocities are comparable (or often greater) to those of O-stars we would expect single W-R stars also to be moderate X-ray emitters. One difference is that W-R stars tend to have substantially higher mass-loss rates than OB stars (implying higher levels of absorption).

While some W-R stars are strong X-ray emitters, those that are are usually binary systems, such as WR140 or Gamma Vel, it is true that some that are strong X-ray emitters are not always obviously binary systems. Here WR25 is an example (Raassen et al. 2003), and in this case it is strongly suspected that WR25 is a long-period binary system, possibly observed face-on.

In contrast to the binary W-R stars, there is less evidence of substantial X-ray emission from single W-R stars, particularly the WC subclass. For example, consider the WC W-R star WR114 (classified as a WC5). Oskinova et al. (2003) reported no detection of this star in a 16 ksec *XMM-Newton* observation, which implies $L_X < 4 \times 10^{-9} L_{bol}$. In contrast, Ignace et al. (2003) reported on *XMM-Newton* observations of WR1 (spectral type WN4) and did detect the system, with $L_X \sim 2 \times 10^{32}$ erg s^{-1}, slightly above the canonical L_X/L_{bol} value.

For the WN stars, the situation is rather unclear. For example, the WN8 star WR40 (HD 96548), which is considered a likely single star, has been observed with *XMM-Newton* by Gosset et al. (2004), and no detection was reported, conservatively implying $L_X < 2.6 \times 10^{-8} L_{bol}$. WR40 (and WN8 stars in general) has a relatively slow and dense wind, with $v_\infty < 1000$ km s^{-1}. Such a situation makes the absorbing column in the wind greater (as well as probably reducing the likely X-ray emission).

In summary, no single WC W-R star has been unambiguously detected in X-rays. The reason for this is unclear. It could be that the driving mechanism for W-R star winds is markedly different, and so the internal wind structure is different, lacking the shocks that are present in the winds of OB stars. Other possibilities include the lack of emission being due to the enhanced mass-loss rate of the winds (which means more of the X-ray emission is self-absorbed by the wind). Following from this, WC W-R wind material is much better at absorbing soft X-rays than solar abundance material, which may well help this effect.

3 X-ray emission from binary OB and W-R stars: colliding stellar winds

In a binary system consisting of a W-R and an OB star, the two stellar wind will collide at high velocities. This means that the observed X-ray emission may well have more than one component, the two individual winds, and the wind-wind collision region. In many systems it is likely that the wind-wind collision region dominates the X-ray emission. This also means that we would expect to see substantial X-ray orbital variability as the wind-wind collision region moves around the orbit (both due to varying absorption and changing separation for eccentric systems).

In addition to the X-ray emission, non-thermal radio emission is another important tracer of the wind-wind interaction. Shocks produce non-thermal electrons which in turn will produce synchrotron emission. To illustrate this, Dougherty & Williams (2000) studied 23 W-R stars at radio wavelengths. Of these 9 are clear non-thermal radio emitters. Of these 9 objects, 7 are definite binaries and the other 2 possible binaries. It seems to be the case that non-thermal radio emission implies binarity. However, the converse is not necessarily true. Some known binaries do not have any non-thermal emission, and have simple thermal radio spectra. These

tend to be the short period binary systems, and in these case the wind-wind collision region is buried deep within radio photosphere (and so any non-thermal emission is absorbed by the wind).

As an illustration, WR147 (spectral type WN8, with an OB companion) shows complex radio emission, with spatially separated thermal and non-thermal components. The radio components are separated by ~ 0.6 arcseconds. The thermal radio emission is associated with the wind of the W-R star, and the non-thermal radio emission is associated with the wind-wind collision (Williams et al. 1997).

We also expect X-ray emission from wind-wind collision and the two stars, and this system has been observed using the *Chandra* HRC instrument, which has a spatial resolution of 0.5 arcseconds. *Chandra* HRC observations show extended X-ray emission, centred on the wind-wind interaction zone, but also with emission from the W-R star (Pittard et al. 2002).

Returning to the grating instruments, the high spectral resolution means that we can, in principle, probe the dynamics of the wind-wind collision region. In addition we can do some more detailed physics from the line ratios of certain species. For example, helium-like lines have a triplet form, consisting of forbidden, intercombination and resonance ($f - i - r$) lines. The upper level of the f line is depopulated by electron collisions and/or UV photoexcitation, which means that the ratio $R = f/i$ is a diagnostic of wind density and UV field. Also, the mechanisms for populating the upper levels of the r, i and f lines have different temperature dependencies, which means that the ratio $G = (f + i)/r$ is a diagnostic of electron temperature.

3.1 Gamma Velorum: a colliding wind case study

As an illustration of high spectral resolution X-ray observations for colliding wind binary systems, here we look at results from a *Chandra* observation of the W-R binary Gamma Vel. Gamma Vel is the nearest W-R star (located at a distance of ~ 260 pc, although the distance is still the subject of some dispute and a higher value may also be possible), and consists of a W-R and an O-star of spectral types WC8+O7.5 (de Marco & Schmutz 1999). The system has an orbital period of $P_{orb} = 78.5$ days, with a moderate eccentricity of $e = 0.33$. The proximity of this system (and relative X-ray brightness) makes it a key object.

From a series of *ROSAT* observations, the system displays highly variable X-ray emission and is substantially brighter when the O-star is in front of the W-R star (Willis et al. 1995). This is broadly to be expected, as at this orientation, the emission from the wind-wind collision region will suffer much less absorption than at phases when the wind-wind collision region is behind the W-R star (the W-R star having the larger mass-loss rate).

The *Chandra* observation was taken during the X-ray "high state", with the O-star in front of the W-R star (see Fig. 4), and the results have been discussed in Henley et al. (2005) and Skinner et al. (2001). The main results are that the observed lines are generally unshifted, and have a mean FWHM of 1200 km s^{-1}. In addition, there is no correlation between measured line width and ionization potential or wavelength.

As has been discussed earlier, using high resolution line spectra, the $f - i - r$ triplets from He-like ions can be used to estimate the physical conditions. For example, the upper level of the forbidden line depopulated by electron collisions and/or UV photoexcitation and the ratio, $R = f/i$ is a diagnostic of n_e and UV field, which in turn can place constraints on location of the emitting plasma.

From the analysis of the $f - i - r$ line ratios for Gamma Vel, it seems likely that the Mg XI line originates closer to the O-star than the Si XIII. Given the respective excitation energies of these lines, we would expect this to be the other way round. We expect the hottest gas in

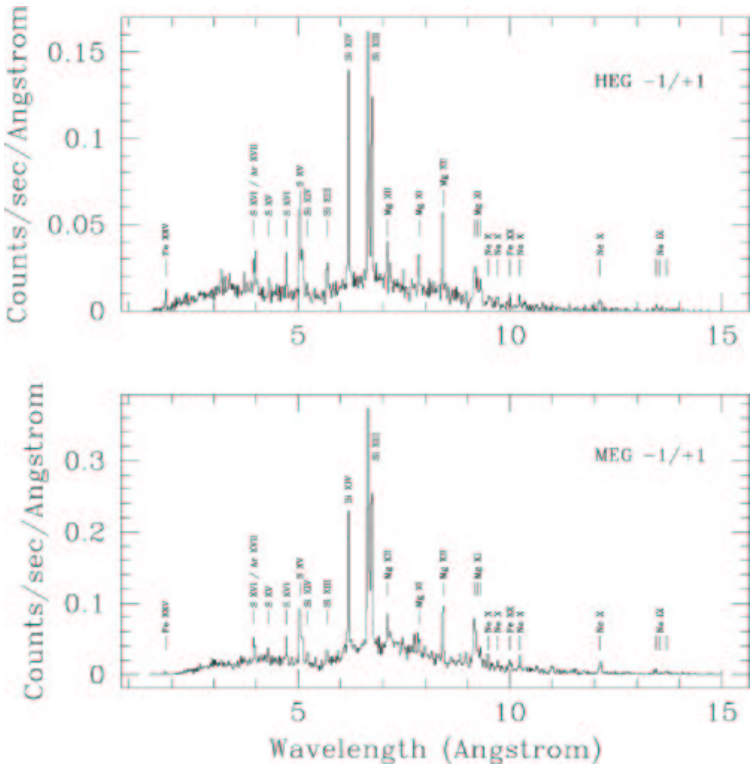

Figure 4: The *Chandra* Gamma Vel spectrum from Henley et al. (2005), showing data from both the high energy (HEG) and medium energy (MEG) gratings.

the system to be located near the line of centres of the system, with the temperature falling away from this point. The fact that we see things the other way round may be an indication of non-equilibrium ionization.

In addition, Schild et al. (2004) have reported on *XMM-Newton* observations of Gamma Vel, with one observation when the O-star is in front ("high state") and another when the O-star was behind ("low state"). Using spectral modelling of these two observations, to obtain the absorbing column, it is possible, along with estimates of the mass-loss rate, to place simple constraints on the 'clumping' factor of the wind. For Gamma Vel, Schild et al. (2004) derive a value of ~ 16, implying a rather highly clumped wind.

For the *Chandra* results, the emission lines were generally unshifted. This is rather unexpected, given the orientation of the system at the time of the observations, and the likely location of the shock surface (with unequal mass -loss rates). One possible explanation is that the shock cone in Gamma Vel is much wider than expected from basic wind parameters. A possible explanation for this wider shock is due to sudden radiative braking, as has been discussed by Gayley, Owocki & Cranmer (1997). In this scenario, the radiation field of the O-star can inhibit and decelerate the dominant wind of the W-R star. This in turn can quite substantially alter the location of the interface between the two winds, and results in a much wider shock angle. This is a result expected from theory, and these observations of Gamma Vel provide some evidence for the process at work.

Other colliding wind systems that have been well studied at X-ray energies with grating instruments include WR140 (Pollock et al. 2005) and Eta Car (Corcoran et al. in preparation). In these systems there are hints at some other physical effects at work - such as a substantial fraction of the wind kinetic energy going into proton acceleration rather than being thermalized in the shock (this is also seen in supernova remnants). This process can explain the narrower

than expected X-ray emission lines, and needs to be considered in more detail.

4 Gamma-ray emission from OB and W-R stars

Although X-ray emission from OB and W-R stars is now an established field, gamma-ray emission from early type stars is still in its infancy and awaiting the first unambiguous detection. There has been speculation about possible gamma-ray sources associated with massive stars, for example, possible correlations between unidentified high energy *CGRO* EGRET sources and early-type stars have been noted (Benaglia et al. 2001; Benaglia & Romero 2003), though these connections are certainly not unambiguous. The eventual detection of gamma-rays will provide some useful insights into the shock acceleration processes in these stars.

There are several different ways that early-type stars can generate gamma-ray emission, mostly related to shock accelerated particles (and often with binarity). Inverse Compton (IC) emission is the most likely to be the dominant emission mechanism. Shock accelerated electrons interact with the strong UV radiation fields of both stars to generate gamma-ray emission. This process is believed to generate a power-law spectrum and is likely to be the dominant emission mechanism at hard X-rays and gamma-rays from massive stars.

There are other gamma-ray emission mechanisms, such as pion decay, relativistic bremsstrahlung, and emission from the decay of radioactive ^{26}Al, which may be important in other contexts or in harder energy bands. For instance, the ^{26}Al emission is a result of stellar nucleosynthesis in W-R stars, followed by the subsequent distribution of the material via the strong stellar winds. This emission is diffuse in nature, but is concentrated on regions of recent star-formation (as the radioactive decay timescale for the ^{26}Al is comparable to the lifetimes of massive stars).

The recently launched *INTEGRAL* satellite has further opened up the possibility of detecting hot stars at softer gamma-ray energies. As part of a program to detect such emission we have used the *INTEGRAL* satellite to observe the Cygnus region, including three nearby W-R stars, namely WR140, WR146 and WR147. These three stars are expected to be some of the brightest gamma-ray emitters, amongst the early-type stars without compact companions.

Unfortunately, in spite of a long exposure time (and the detection of massive stars with a compact companion, such as Cyg X-1 and Cyg X-3), there has been no detection of these sources, and we still await a confirmed gamma-ray detection of a massive star. This is disappointing, but the upper limits will provide some useful constraints on the emission processes in these colliding wind systems.

5 Summary and conclusions

We have reviewed recent results on high energy emission from both single and binary massive stars. Although a convincing detection at gamma-ray energies is still lacking, some more constrained upper-limits are now being derived on the gamma-ray emission.

At X-ray energies, there has been substantial progress, with many new *Chandra* and *XMM-Newton* observations of single stars and binary stars. For the single stars, some patterns are beginning to emerge, but it is clear that there are differences in the X-ray line-profiles, with some stars having lines that are blue-shifted, other that are not, and some marked differences in line width. These may well be explained (in part) by differences in the mass-loss rates of the winds (and the resulting wind optical depths).

For the binary systems, we also now have some phase resolved observations of colliding stellar winds. For some systems, the simple colliding wind models work reasonably well, while for others there are some major discrepancies. These observations are pointing towards some clear deficiencies in the current state-of-the-art models, such as in the complex radiation hydrodynamics, non-thermal ionization effects and the possibility of a substantial amount of the wind energy going into non-thermal acceleration of particles and not into thermal emission.

It is clear that both more observations of a wider variety of systems and with better phase coverage and enhanced models are required to move the field forward.

References

Benaglia P., Romero G.E., 2003, A&A, 399, 1121
Benaglia P., Romero G.E., Stevens I.R., Torres D.F., 2001, A&A, 366, 605
Berghöfer T.W., Schmitt J.H.M.M., Danner R., Cassinelli J.P., 1997, A&A, 322, 167
Cassinelli J.P., Swank J.H., 1983, ApJ, 271, 681
Cassinelli J., Miller N., Waldron W., MacFarlane J., Cohen D., 2001, ApJ, 554, L55
Cohen D.H., de Messieres G.E., MacFarlane J.J., Miller N.A., Cassinelli J.P., Owocki S.P., Liedahl D.A., 2003, ApJ, 586, 495
de Marco O., Schmutz W., 1999, A&A, 345, 163
Dougherty S.M., Williams P.M., 2000, MNRAS, 319, 1005
Feldmeier A., Oskinova L., Hamann W.-R., 2003, A&A, 403, 217
Gagné M., et al. 2005, ApJ, 628, 986
Gayley K.G., Owocki S.P., Cranmer S.R., 1997, ApJ, 475, 786
Gosset E., Nazé Y., Claeskens J.-F., Rauw G., Vreux J.-M., Sana H., 2005, A&A, 429, 685
Henley D.B., Stevens I.R., Pittard J.M., 2005, MNRAS, 356, 1308
Howarth I.D., Prinja R.K., 1989, ApJS, 69, 527
Ignace R., Oskinova L.M., Brown J.C., 2003, A&A, 408, 353
Kramer R.H., Cohen D.H., Owocki S.P., 2003, ApJ, 592, 532
Mewe R., Raassen A.J.J., Cassinelli J.P., van der Hucht K.A., Miller N.A., Guedel M., 2003, A&A, 398, 203
Miller N., Cassinelli J., Waldron W., MacFarlane J., Cohen D., 2002, ApJ, 577, 951
Oskinova L., Feldmeier A., Hamann W.-R., 2004, A&A, 422, 675
Oskinova L., Ignace R., Hamann W.-R., Pollock A.M.T., Brown J., 2003, A&A, 402, 755
Owocki S.P., Castor J.I., Rybicki G.B., 1988, ApJ, 335, 914
Pittard J.M., Stevens I.R., Williams P.M., Pollock A.M.T., Skinner S.L., Corcoran M.F., Moffat A.F.J., 2002, A&A, 388, 335
Pollock A.M.T., Corcoran M.F., Stevens I.R., Williams P.M., 2005, ApJ, 629, 482
Raassen A.J.J., van der Hucht K.A., Mewe R., Antokhin I.I., Rauw G., Vreux J.-M., Schmutz W., Guedel M., 2003, A&A, 402, 653
Sana H., et al., 2005, MNRAS, (submitted)
Schild H., et al., 2004, A&A, 422, 177
Skinner S.L., Guedel M., Schmutz W., Stevens I.R., 2001, ApJ, 558, L113
Williams P.M., et al., 1997, MNRAS, 289, 10
Willis A.J., Schild H., Stevens I.R., 1995, A&A, 298, 549

X-ray survey of Wolf-Rayet stars in the Magellanic Clouds

M. A. Guerrero[1] and Y.-H. Chu[2]

[1]Instituto de Astrofísica de Andalucía,
Consejo Superior de Investigaciones Científicas (IAA-CSIC), Spain
[2]Department of Astronomy, University of Illinois at Urbana-Champaign, USA

Abstract: Systematic X-ray surveys of Wolf-Rayet (WR) stars in our Galaxy are hampered by the heavy obscuration in the Galactic plane, which prohibits the detections of WR stars, and by the uncertain distances to individual WR stars, which result in poorly determined luminosities. These problems are mitigated in the Large and Small Magellanic Clouds (MCs), because foreground and internal extinctions are small and distances are known. We have used archival *Chandra* ACIS and *ROSAT* PSPC and HRI observations of 128 WR stars in the MCs to search for X-ray emission from these stars. About 25% of the WR stars in this sample are detected with X-ray luminosities in the range 2×10^{32}–2×10^{35} ergs s^{-1}. The X-ray spectral analysis of the brightest WR stars reveals large absorption columns and high temperatures, similar to those seen in sources with colliding winds. The colliding-wind origin of the X-ray emission is further supported by the higher frequency of X-ray detections among WR stars in binary systems and by their higher X-ray luminosities compared to those of single WR stars. Among single WR stars, X-ray emission is mostly detected in WN6 stars, while single WC stars are not detected.

1 Introduction

A Wolf-Rayet (WR) star represents a late evolutionary stage of a massive star, when its H-rich envelope has been stripped off and CNO-Cylce H-burning (WN phase) or He-burning products (WC phase) are revealed at its surface. WR stars have the most powerful fast winds, with typical mass loss rates ($\dot{M}$) of a few $\times10^{-5}$ $M_\odot$ yr^{-1} (de Jager, Nieuwenhuijzen, & van der Hucht 1988) and terminal velocities (v_∞) of 1,000–3,000 km s^{-1} (Prinja, Barlow, & Howarth 1990), resulting in stellar wind mechanical luminosities ($L_{\rm w} \equiv \frac{1}{2}\dot{M}v_\infty^2$) of $10^{37} - 10^{38}$ ergs s^{-1}. The powerful stellar winds of WR stars are associated with three types of shocks that can produce X-ray emission:

- Shocks in the wind: Shocks in the wind itself are produced by stochastic or radiatively-induced instabilities and the post-shock gas reaches X-ray-emitting temperatures (Lucy & White 1980; Gayley & Owocki 1995). This is basically the same X-ray emission mechanism as for O and early B stars (Berghöfer et al. 1997), but WR winds are heavily enriched in metals (C, N, O) so that their X-ray emission is highly absorbed.

"Massive Stars and High Energy Emission in OB Associations"; Proc. JENAM 2005 *Distant Worlds*, Liège (Belgium), eds. Rauw et al., p. 13-20

- Colliding winds: In a WR+OB binary system, the WR wind collides with the companion's fast wind and generates shock-heated plasma at the interaction region, e.g., V444 Cygni (Corcoran et al. 1996). The physical conditions and X-ray luminosity of the hot gas at the collision zone vary along with the orbital phase of the binary system.

- Shocked wind in a circumstellar bubble: The fast wind of a WR star can blow a bubble in the ambient medium, and the bubble interior is filled with shocked stellar wind that emits X-rays (García-Segura, Mac Low, & Langer 1996). The X-ray emission is distributed and is expected to peak near the inner wall of the bubble shell.

Systematic X-ray surveys of WR stars using *Einstein* and *ROSAT* observations have been limited to our Galaxy (Pollock 1987; Pollock, Haberl, & Corcoran 1995; Wessolowski 1996). These studies suggest that (1) binary WR stars are brighter than single WR stars, (2) single WC stars are weaker X-ray sources than single WN stars, and (3) no simple $L_{\rm X}/L_{\rm bol}$ relationship appears to exist among single WN stars. These results did not take into account the unknown existence of binary companions, as Oskinova et al. (2003) and Oskinova (2005) have shown recently that *truly single* WC and late WN stars are not detectable in X-rays owing to the high opacity in their winds. It is difficult to extend X-ray observations to more WR stars in the Galaxy because the large absorption column densities in the Galactic plane prevent their detection. Furthermore, the uncertainties in the WR star distances directly affect the accuracy in their luminosity determination.

Chandra and *XMM-Newton* X-ray observatories, with their unprecedented angular resolution and sensitivity, make it possible to study the X-ray emission from WR stars in the nearby Large and Small Magellanic Clouds (LMC and SMC, or MCs), as illustrated recently by Portegies Zwart et al. (2002) and Nazé et al. (2002). The MCs have a foreground reddening $E_{B-V} \sim 0.04$–0.09 (Schwering & Israel 1991) and an internal reddening $E_{B-V} \sim 0.06$ (Bessell 1991), much smaller than the reddening in the Galactic plane, so the soft X-ray emission from single WR stars and WR bubbles can be more easily detected. Furthermore, WR stars in the MCs are at known distances, so their X-ray luminosities can be determined accurately. More importantly, there has been a systematic spectroscopic search for binarity for all WR stars in the MCs (Foellmi, Moffat, & Guerrero 2003a,b; Schnurr et al., in preparation), and this binary WR star database is invaluable in aiding the interpretation of their X-ray emission.

2 *Chandra* and *ROSAT* observations of WR stars in the Magellanic Clouds

The *Chandra* Archive[1] and *ROSAT* Archive[2] have been used to search for *Chandra* ACIS and *ROSAT* PSPC and HRI observations that include MC WR stars. Our search rendered 192 useful *Chandra* ACIS observations for 57 WR stars in the LMC and 9 WR stars in the SMC, *ROSAT* PSPC observations for 121 WR stars in the LMC and 11 WR stars in the SMC, and *ROSAT* HRI observations for 110 WR stars in the LMC and 11 WR stars in the SMC. This database includes X-ray observations of 128 WR stars, which correspond to ∼90% of the known WR stars in the MCs.

[1]The *Chandra* Archive is available using the *Chandra* Search and Retrieval Interface (*ChaSeR*) at the *Chandra* X-ray Observatory site (http://asc.harvard.edu).

[2]*ROSAT* archival data can be obtained from the anonymous ftp site legacy.gsfc.nasa.gov, or downloaded from the web site http://heasarc.gsfc.nasa.gov/W3Browse, maintained by the High Energy Astrophysics Science Archive Research Center (HEASARC) of Goddard Space Flight Center, NASA.

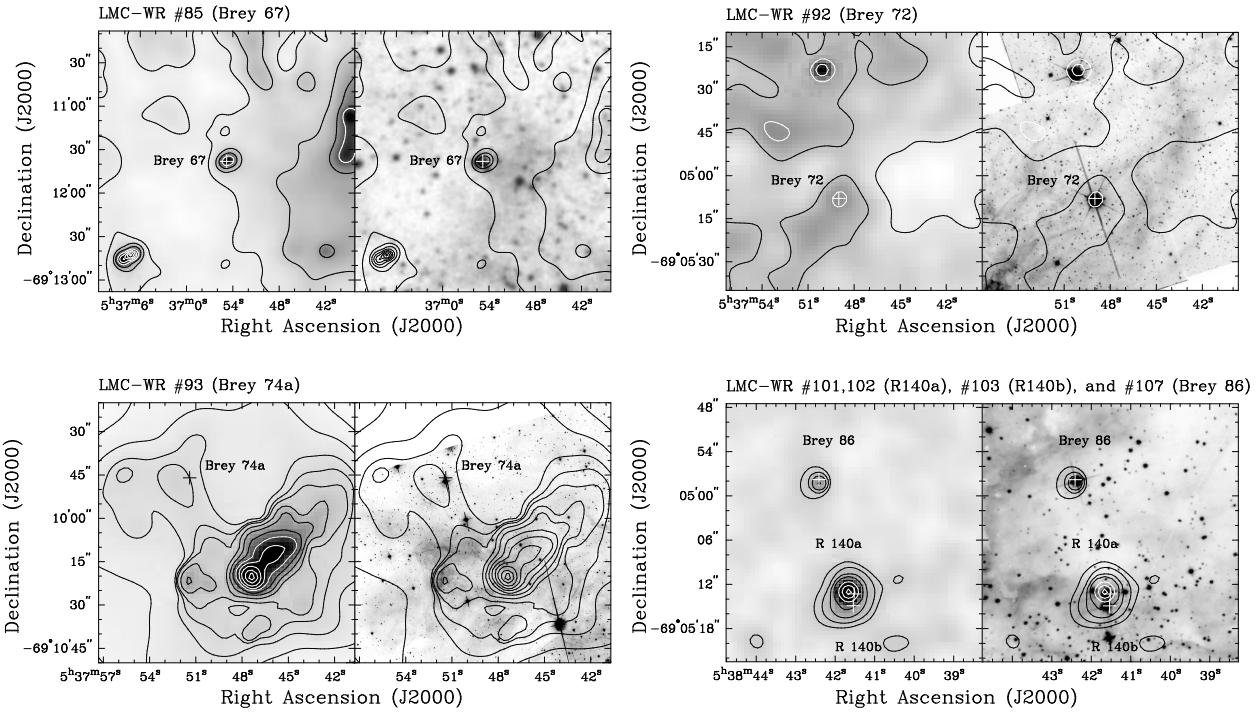

Figure 1: *Chandra* ACIS X-ray images in the 0.3–7.0 keV band and optical images of several WR stars in the LMC with detected X-ray emission. The position, number in the Breysacher et al. (1999) catalog, and names of the WR stars are marked. The contour levels have been chosen to highlight the X-ray emission and identification of WR stars.

To search for X-ray emission from WR stars in the MCs, we have extracted *Chandra* ACIS images in the 0.3–7.0 keV energy band, and *ROSAT* images in the 0.1–2.4 keV and 0.1–2.0 keV energy bands for the PSPC and HRI, respectively. We have used the positions of WR stars given by Breysacher, Azzopardi, & Testor (1999) in the LMC and by Massey, Olsen, & Parker (2003) in the SMC, and compared the X-ray images with optical images extracted from the Digitized Sky Survey[3] (DSS) or from the *Hubble Space Telescope* Archive when available. For each WR star, we have identified the star in the optical images and then searched for X-ray point source at the location of the star, and further searched for diffuse X-ray emission in its surroundings. Some examples of X-ray and optical images of WR stars with detected X-ray emission are shown in Figure 1.

X-ray emission is detected for the 34 WR stars listed in Table 1, which constitute ∼25% of all the MC WR stars surveyed. Table 1 also lists the spectral type, binarity or multiplicity status, and X-ray and bolometric luminosities of the WR stars. The bolometric luminosities have been compiled from the literature, or computed by applying a bolometric correction for WR stars as suggested by Schmutz, Hamann, & Wessolowski (1989) and Crowther & Smith (1997). For the latter case, we used v from Breysacher et al. (1999) and adopted a typical A_V

[3]The Digitized Sky Survey is based on photographic data obtained using the UK Schmidt Telescope and the Oschin Schmidt Telescope on Palomar Mountain. The UK Schmidt was operate by the Royal Observatory of Edinburgh, with funding from the UK Science and Engineering Research Council, until 1988 June, and thereafter by the Anglo-Australian Observatory. The Palomar Observatory Sky Survey was funded by the National Geographic Society. The Oschin Schmidt Telescope is operated by the California Institute of Technology and Palomar Observatory. The plates were processed into the present compressed digital form with the permission of these institutes. The Digitized Sky Survey was produced at the Space Telescope Science Institute under US government grant NAGW-2166.

Table 1: Spectral Type, Binarity, $L_{\rm X}$, and $L_{\rm bol}$ of WR Stars in the MCs with X-ray Emission

WR #	WR Name	Spec. Type	Binarity	$L_{\rm X}$ (ergs s^{-1})	$L_{\rm bol}$ (ergs s^{-1})
LMC-WR 10	Brey 9	WC5	M	$(6.7\pm1.1)\times10^{33}$	4.0×10^{38}
LMC-WR 19	Brey 16	WN4b+O5:	Y	$(3.2\pm0.4)\times10^{34}$	4.8×10^{39}
LMC-WR 20	Brey 16a	WC5+O	Y	$(8.4\pm1.3)\times10^{33}$	4.5×10^{38}
LMC-WR 38	Brey 31	WC4+O8I:	Y	$(5.4\pm1.4)\times10^{33}$	5.7×10^{39}
LMC-WR 39	Brey 32	WC4+O6V-III	Y	$(5.5\pm1.8)\times10^{33}$	2.2×10^{39}
LMC-WR 42	Brey 34	WN5b+(B3I)	Y	$(6.7\pm1.1)\times10^{33}$	2.5×10^{40}
LMC-WR 47	Brey 39	WN3	N	$(4.2\pm1.6)\times10^{33}$	6.8×10^{39}
LMC-WR 67	Brey 56	WN5ha	Y	$(1.2\pm0.2)\times10^{33}$	9.7×10^{38}
LMC-WR 77	Brey 65	WN7	Y	$(5\pm2)\times10^{32}$	1.0×10^{39}
LMC-WR 78	Brey 65b	WN6(+O8V)	Y	$(2.5\pm1.0)\times10^{32}$	1.3×10^{39}
LMC-WR 79	Brey 57	WN7h+OB	Y	$(5\pm2)\times10^{32}$	8.0×10^{38}
LMC-WR 80	Brey 65c	O4If/WN6	N	$(1.0\pm0.2)\times10^{33}$	1.2×10^{39}
LMC-WR 82	Brey 66	WN3b	N	$(5\pm2)\times10^{32}$	1.1×10^{39}
LMC-WR 85	Brey 67	WC4+OB	Y	$(8.6\pm0.9)\times10^{34}$	4.5×10^{39}
LMC-WR 92	Brey 72	WN6+B1Ia	Y	$(1.3\pm0.4)\times10^{33}$	5.9×10^{39}
LMC-WR 93	Brey 74a	O3If/WN6	N	$(8\pm3)\times10^{32}$	6.9×10^{38}
LMC-WR 99	Brey 78	O3If/WN6-A	N	$(1.3\pm0.2)\times10^{34}$	3.4×10^{39}
LMC-WR 100	Brey 75	WN6h	N	$(8\pm3)\times10^{32}$	2.8×10^{39}
LMC-WR 101,102	R140a	WN6	Y	$(1.5\pm0.1)\times10^{35}$	8.0×10^{39}
LMC-WR 103	R140b	WN6	Y	$(8\pm3)\times10^{32}$	1.5×10^{39}
LMC-WR 105	Brey 77	O3If/WN6-A	N	$(2.4\pm0.6)\times10^{33}$	8.8×10^{39}
LMC-WR 106,108,109,110	R136a	WN5h	Y	$(2.5\pm0.2)\times10^{34}$	1.9×10^{40}
LMC-WR 107	Brey 86	WNL/Of	Y	$(1.8\pm0.5)\times10^{33}$	1.0×10^{40}
LMC-WR 112	R136c	WN5h	M	$(6.1\pm0.4)\times10^{34}$	1.0×10^{40}
LMC-WR 114	Mk 35	O3If/WN6-A	N	$(1.0\pm0.3)\times10^{33}$	2.0×10^{39}
LMC-WR 116	Brey 84	WN5h	Y?	$(1.8\pm0.1)\times10^{35}$	1.2×10^{40}
LMC-WR 118	Brey 89	WN6h	N	$(1.5\pm0.5)\times10^{33}$	8.4×10^{39}
LMC-WR 119	Brey 90	WN6(h)	Y	$(1.2\pm0.4)\times10^{33}$	5.6×10^{39}
LMC-WR 125	Brey 94	WC5+O7	Y	$(1.6\pm0.3)\times10^{33}$	9.8×10^{38}
LMC-WR 126	Brey 95	WN4b+O8:	Y	$(1.6\pm0.4)\times10^{33}$	2.7×10^{39}
LMC-WR 127	Brey 95a	WC5+O6	Y	$(1.1\pm0.4)\times10^{33}$	1.1×10^{39}
SMC-WR 5	HD 5980	WN6h	Y	$(8.7\pm0.5)\times10^{33}$	1.2×10^{40}
SMC-WR 6	AV	WN4:+O6.5I:	Y	$(4.2\pm0.2)\times10^{34}$	7.1×10^{39}
SMC-WR 7	AV 336a	WN4+O6I(f)	Y	$(2.3\pm0.1)\times10^{33}$	4.0×10^{39}

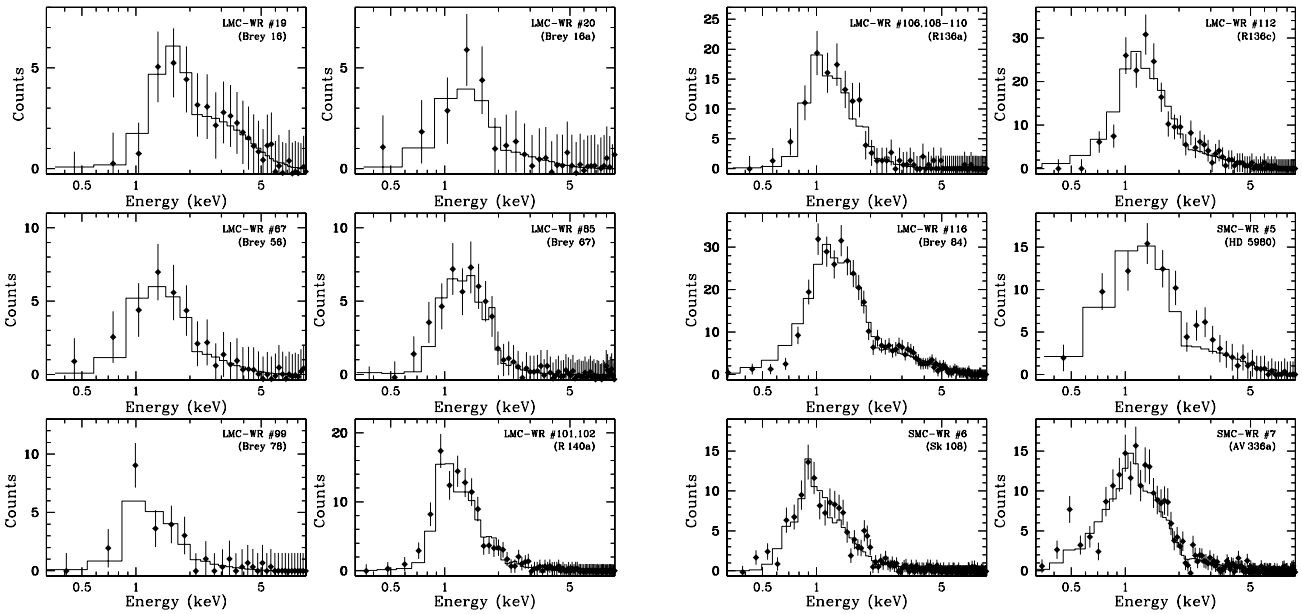

Figure 2: *Chandra* ACIS background-subtracted spectra of WR stars in the MCs with sufficient number of counts to allow a reliable spectral fit. The best-fit optically thin plasma emission models are overplotted on the X-ray spectra.

of 0.4 mag for the WR stars in the LMC, and used M_V from Massey et al. (2003) for the WR stars in the SMC. The X-ray luminosities of the WR stars in the MCs span a wide range, from a few $\times 10^{32}$ ergs s^{-1} to $\sim 10^{35}$ ergs s^{-1}.

3 X-ray spectral properties

The *Chandra* ACIS observations of WR stars with sufficient counts can be used to determine the physical properties of the X-ray-emitting gas and the amount of intervening absorbing material. The *Chandra* ACIS spectra of the 12 WR stars in the MCs with the largest number of counts are displayed in Figure 2. These spectra peak in the 0.7–2.0 keV band, with very few counts below 0.5 keV, and in some cases with high-energy tails extending above 5 keV. Interestingly, the integrated spectrum of all the X-ray-faint WR stars has a spectral shape similar to the spectra shown in Fig. 2. The X-ray spectral properties of the WR stars in the MCs are suggestive of high plasma temperatures and large amounts of absorption. This is confirmed by spectral fits to the observed background-subtracted spectra using an optically thin plasma emission model. The best-fits, overplotted on the spectra of Fig. 2, indicate plasma temperatures from $\sim$1 keV up to $\sim$7 keV, with absorption column densities much larger than the typical extinction for the MCs.

4 Frequency of X-ray detection

The frequency of X-ray detection among different subgroups of WR stars in the MCs is listed in Table 2. This table shows that detectable X-ray emission is more frequently associated with WR stars in known binary systems or WR stars with absorption lines that are commonly interpreted as evidence for binary companions. Indeed, all WC stars with detectable X-ray emission are in binary systems, and only 9 out of 80 putatively single WN stars show X-ray

Table 2: X-ray Detection Among Subgroups of WR Stars in the MCs

Sub-Group	Number of Detections	Number of WR Stars	Frequency
Single WR Stars	9	90	10±4%
Binary WR Stars	25	43	58±20%
WC Stars	7	21	33±20%
WN Stars	27	112	24±7%
Single WC Stars	0	9	0%
Single WN Stars	9	80	11±5%
Binary WC Stars	7	12	60±40%
Binary WN Stars	18	32	56±23%

emission. These results indicate that detectable X-ray emission from WR stars in the MCs is preferentially associated with binary systems, independent of whether they are of WN or WC types. It is understandable that if the X-ray emission from WR stars in binary systems arises from colliding stellar winds, the X-ray detection rate would not be strongly dependent on the spectral type of the WR stars. Indeed, Table 2 shows that binary WN stars and binary WC stars have similar X-ray detection rates.

The frequency of X-ray emission is subdivided by detailed spectral types and shown in Figure 3-*left*. X-ray emission from WR stars in the MCs is most frequently detected in WN6 stars, regardless of their binarity status. WC5 stars also have a high X-ray detection rate, but the sample has only four objects and all are in binary systems. WR stars with spectral type WN4, WN5, WN7, and WC4 are also detected frequently, but only in binary systems. It is noticeable that WN stars of spectral types WN2, WN3, and WN7–10 are rarely detected in X-rays: only 4 out of 36 are detected. WN4 is the most common spectral type, but WN4 stars have a similar low X-ray detection rate, $\sim$0.1.

The distributions of $L_{\rm X}$ and $L_{\rm X}/L_{\rm bol}$ for WR stars in the MCs are shown in Fig. 3-*right*. The sharp fall-off of the $L_{\rm X}$ distribution at luminosities below 10^{33} ergs s^{-1} reflects the survey limit. At the high luminosity end, there is a significant fraction of WR stars with $L_{\rm X} > 10^{34}$ ergs s^{-1}, well above the highest $L_{\rm X}$ observed for Galactic WR stars (Oskinova 2005). These X-ray-bright WR stars are all confirmed or likely members of binary systems or tight OB associations (Table 1). The distribution of $L_{\rm X}/L_{\rm bol}$ shows a marked peak at $\sim 5\times10^{-7}$ and a secondary peak at $\sim 10^{-5}$ (Fig. 3). It is tempting to interpret this double-peaked distribution as a result of two different populations: X-ray-faint single WR stars and X-ray-bright binary WR stars. However, the $L_{\rm X}/L_{\rm bol}$ distribution of WR stars in binary systems also shows a double-peaked shape, and the apparently single WR stars show only the $\sim 5\times10^{-7}$ peak. Therefore, we speculate that among WR stars in binary systems, the bright objects produce enhanced X-ray emission via colliding stellar winds, and the faint objects show X-ray emission from the WR stars themselves, similar to single WR stars.

5 Discussion

The X-ray survey of WR stars in the MCs has shown that WR stars in binary systems are much more frequently detected than single WR stars and that WR stars in binary systems have higher $L_{\rm X}/L_{\rm bol}$ than the apparently single WR stars. Similar trends have been reported

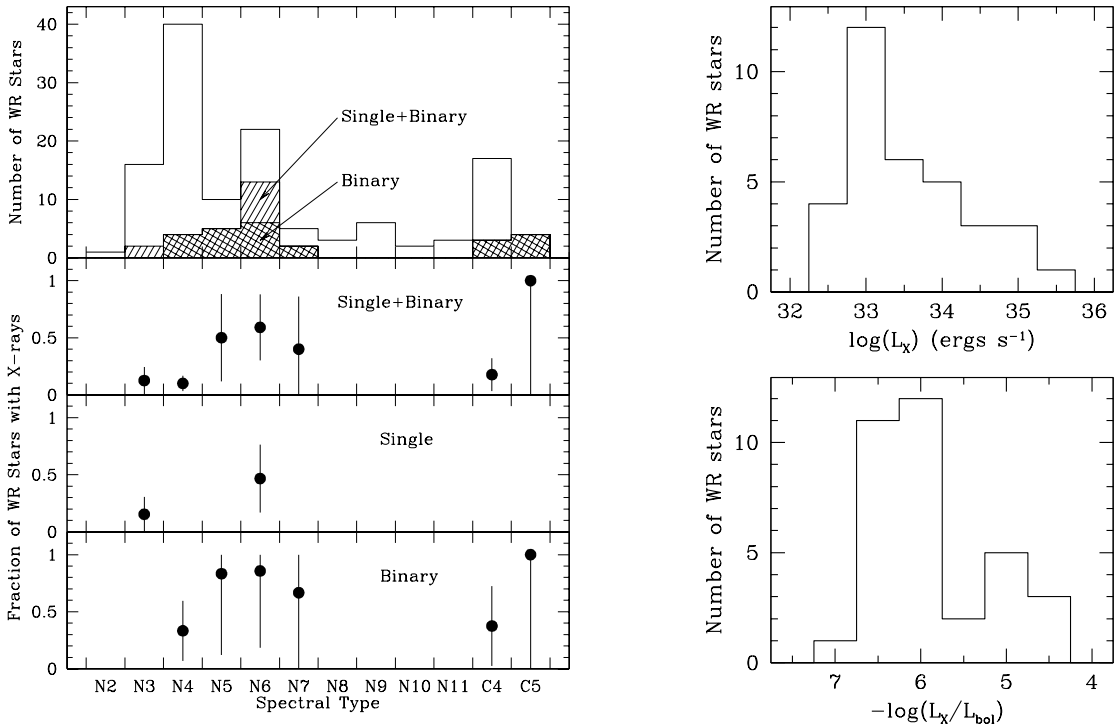

Figure 3: *(left)* Distribution and fraction of occurrence of X-ray emission from WR stars in the MCs by spectral sub-types *(top panels)*. The bottom panels separate the fraction of occurrence among single and binary WR stars. *(right)* $L_{\rm X}$ and $L_{\rm X}/L_{\rm bol}$ distributions of WR stars in the MCs with detected X-ray emission.

for Galactic WR stars (Pollock 1987), but it is possible to use the large number of WR stars in the MC sample to statistically examine their X-ray emission properties. In the MC sample, we find the X-ray-emitting WR stars in binary systems can be divided into two categories: (1) X-ray-faint binaries with $L_{\rm X}/L_{\rm bol}$ $\sim$5$\times$10^{-7}, and (2) X-ray-bright binaries with $L_{\rm X}/L_{\rm bol}$ $\sim$10^{-5}. The $L_{\rm X}/L_{\rm bol}$ relationship for X-ray-faint WR binaries is similar to this of apparently single WR stars in the MCs, but somewhat steeper than the $L_{\rm X}/L_{\rm bol}$ $\sim$1.2$\times$10^{-7} relationship found for Galactic O stars (Sana 2005, this proceeding). Therefore, the colliding winds do not contribute significant emission to the X-ray-faint WR binaries in the MCs. In contrast, the X-ray-bright WR binaries in the MCs are 30 times brighter than the single WR stars in the MCs, and at least 10 times brighter than their Galactic counterparts. The enhanced X-ray luminosities of these X-ray-bright WR binaries are most likely contributed by the colliding stellar winds. This conclusion is supported by the high plasma temperatures and large absorption column densities indicated by the best-fit models for their *Chandra* ACIS spectra.

As for single WR stars in the MCs, this survey shows that detectable X-ray emission is present only for a narrow range of spectral types: WN3 and WN6. Most notably, single WC, late WN, WN4, and WN5 stars are not detected in X-rays, in spite of their large number in our MC survey sample. The lack of detectable X-ray emission from single WR stars of these spectral types is firmly established by this survey for the MCs. Similar results have been reported for Galactic WR stars. Oskinova et al. (2003) have determined that single Galactic WC stars lack X-ray emission and, more recently, Oskinova (2005) has shown that single Galactic WN8 stars also do not show detectable X-ray emission. The lack of X-ray emission from WC and late WN stars is most likely caused by the high opacity in their stellar winds, but it is not clear why single WN4 and WN5 stars do not have detectable X-ray emission.

Acknowledgements

This research was partially supported by NASA/CXO grant GO 0-1004X and by grant PNAYA 2002-00376 of the Spanish MEC (cofunded by FEDER funds). MAG also acknowledges support from the Spanish program Ramón y Cajal.

References

Berghöfer T.W., Schmitt J.H.M.M., Danner R., Cassinelli J.P., 1997, A&A, 322, 167
Bessel M.S., 1991, A&A 242, 17
Breysacher J., Azzopardi M., Testor G., 1999, A&AS, 137, 117
Corcoran M.F., Stevens I.R., Pollock A.M.T., Swank J.H., Shore S.N., Rawley G.L., 1996, ApJ, 464, 434
Crowther P.A., Smith L.J., 1997, A&A, 320, 500
de Jager C., Nieuwenhuijzen H., van der Hucht K.A., 1988, A&AS, 72, 259
Foellmi C., Moffat A.F.J., Guerrero M.A., 2003a, MNRAS, 338, 360
Foellmi C., Moffat A.F.J., Guerrero M.A., 2003b, MNRAS, 338, 1025
García-Segura G., Mac Low M.-M., Langer N., 1996, A&A, 305, 229
Gayley K.G., Owocki S.P., 1995, ApJ, 446, 801
Lucy L.B., White R.L., 1980, ApJ, 241, 300
Massey P., Olsen K.A.G., Parker J.Wm., 2003, PASP, 115, 1265
Nazé Y., Antokhin I.I., Rauw G., Chu Y.-H., Gosset E., Vreux J.-M., 2004, A&A, 418, 841
Oskinova L.M. 2005, MNRAS, 361, 679
Oskinova L.M., Ignace R., Hamann W.-R., Pollock A.M.T., Brown J.C., 2003, A&A, 402, 755
Pollock A.M.T., 1987, ApJ, 320, 283
Pollock A.M.T., Haberl F., Corcoran M.F., 1995, IAU Symposium, 163, 512
Prinja R.K., Barlow M.J., Howarth I.D., 1990, ApJ, 361, 607
Portegies Zwart S.F., Pooley D., Lewin W.H.G., 2002, ApJ, 574, 762
Schmutz W., Hamann W.-R., Wessolowski U., 1989, A&A, 210, 236
Schwering P.B.W., Israel F.P., 1991, A&A 246, 231
Wessolowski U., 1996, in *Röntgenstrahlung from the Universe*, Würzburg meeting proceedings, 75

Parameters of massive stars in the Milky Way and nearby galaxies

A. Herrero[1,2] and F. Najarro[3]

[1]Instituto de Astrofisica de Canarias, C/ Vía Láctea s/n, E-38200 La Laguna, Spain
[2]Departamento de Astrofísica, Universidad de La Laguna, Avda. Astrofísico Francisco Sánchez, s/n, E-38204, Spain
[3]Instituto de Estructura de la Materia, CSIC, C/Serrano 121, E-28006 Madrid, Spain

Abstract: We present in this contribution a review of recent results of parameters of massive OB stars in the Milky Way, the Magellanic Clouds and nearby spirals. The review is timely because of the strong lowering of the temperature scale of Galactic OB stars produced by the new model atmospheres, including sphericity, blanketing and mass-loss, that are also discussed, and because of the boost suffered by extragalactic stellar physics in the last years. The effects on the determination of mass-loss and the Modified Wind Momentum-Luminosity Relationship are discussed, and a comparison with evolutionary models is provided. We finally present a comparison of abundances from OB stars and H II regions in Orion and M 33.

1 Introduction

Massive stars play a key role in many astrophysical fields, from the interaction with their sorrounding medium to the origin of GRBs and the possible reionization of the Universe. Therefore, the interpretation of a large number of data and observations relies on our knowledge of the stellar parameters and evolution of these stars. This, on the other hand, is very model dependent. A simple example may be given by the energy emitted by a starburst region. Assuming that this is the energy emitted by the recently formed stars, the derived IMF will depend on the prediction of the stellar emergent fluxes for stars of a given mass. This relation, on the other hand, will rely not only upon our calibration of effective temperature against spectral type, but also on the wind density of the star.

2 The new temperature scale for Galactic massive OB stars

Since NLTE models are available, the temperature scale of massive OB stars has been determined using model atmospheres to fit a given ionization equilibrium. Helium, being the atom used to spectroscopically classify the earliest stars, has become the traditional temperature indicator for these objects. Of course, the resulting temperature scale is model dependent.

Very recently a number of calculations from different authors have strongly changed the temperature scale of massive OB stars. These calculations have been based on new families of model

"Massive Stars and High Energy Emission in OB Associations"; Proc. JENAM 2005 *Distant Worlds*, Liège (Belgium), eds. Rauw et al., p. 21-29

atmospheres that include sphericity, mass-loss and line-blanketing, in addition to NLTE. The combination of all these factors results in temperatures that are much cooler than those hitherto assumed.

Vacca et al. (1996) presented a compilation of the spectroscopic determinations of effective temperatures of massive OB stars. They gave preference to the most recent calculations, that at that time were mostly based on plane parallel, hydrostatic, unblanketed model atmospheres. Their temperature scale for supergiants can be seen in Fig. 1-left.

The first calculations pointing to a cooler temperature scale were those from Martins et al. (2002), who used CMFGEN (Hillier & Miller 1998), a code with all the improvements indicated above. These authors limited their calculations to OB dwarfs, so that the influence of mass-loss effects were negligible. Therefore, the main differences with Vacca et al. were clearly due to line-blanketing. These differences could reach up to 4 000 K for early types, and decreased towards O9 and B0 types.

The work from Martins et al. was followed by a series of papers with similar results. Herrero et al. (2002) gave a temperature scale for supergiants in Cyg OB 2 using FASTWIND (Santolaya-Rey et al. 1997; Puls et al. 2005), another code with NLTE, sphericity, mass-loss and (in this case approximated) line-blanketing. They found differences up to 8 000 K. In this case both mass-loss and line-blanketing, played a role. These authors also showed that two stars with the same spectral type and luminosity class may have different effective temperatures if their wind densities are different. Repolust et al. (2004) presented an analysis of 24 stars, based on a slightly improved version of FASTWIND that confirmed these trends. These same trends have also been confirmed by Martins et al. (2005) who have calculated models with CMFGEN and have given a new temperature scale for massive OB stars of different luminosity classes. These temparature scales agree quite well with those from Repolust et al., and confirm that new models result in effective temperatures that are several thousands Kelvin cooler for early and intermediate spectral types, decreasing towards late spectral types. The different temperature scales can be seen in Fig. 1-left.

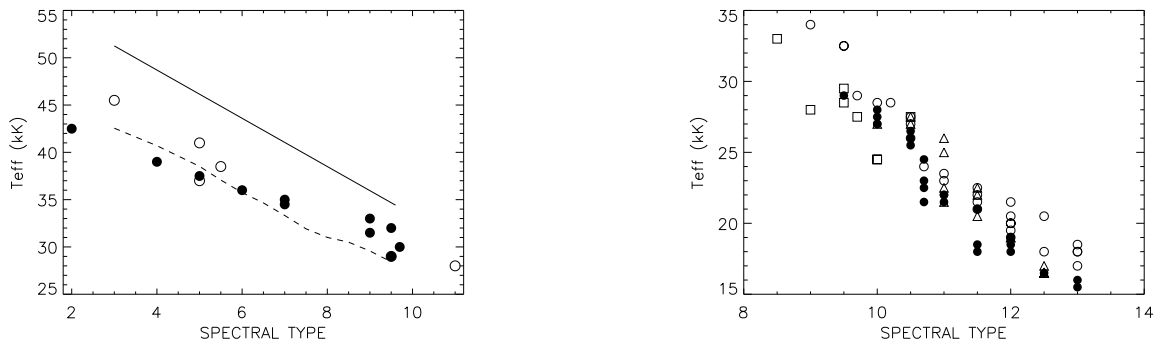

Figure 1: **(Left)** The temperature scale for Galactic O supergiants. The solid lines are for the Vacca et al. (1996) scale, the dashed line for the scale defined by Martins et al. (2005) (the one the authors define as the theoretical scale), filled symbols are data from Repolust et al. (2004) and open symbols are data from Herrero et al. (2002). **(Right)** Temperature scale for B supergiants in the Galaxy and the Magellanic Clouds. Circles are for the Galaxy: open, for McErlean et al. (1999) and solid for Crowther et al. (2005). Triangles are for the SMC (Trundle et al. 2004, 2005) and squares for the LMC (Evans et al. 2004)

OB stars in the Magellanic Clouds have been analysed by Massey et al. (2004, 2005) using FASTWIND. Their results confirm that supergiants are 3000–4000 K cooler than dwarfs of the same spectral type at any metallicity. However, a clear trend of temperature with metallicity at a given spectral type and luminosity class is not seen: authors obtain that SMC dwarfs and supergiants are hotter than Milky Way counterparts, but while LMC dwarfs seem to extend the SMC scale, LMC supergiants seem to extend the Milky Way scale.

For types O9–B0 there is no clear difference between temperature scales from different authors

or metallicities. It is then not strange that a comparison of temperatures scales for B supergiants results in no apparent difference between Galactic (from McErlean et al. 1999, Crowther et al. 2005), LMC (Evans et al. 2004) and SMC analyses (Trundle et al. 2004, 2005), although the new results for Galactic B supergiants by Crowther et al. (2005) indicate for them lower temperatures than the older (plane-parallel and hydrostatic) scale from McErlean et al. We can see all these scales in Fig. 1-right. The very large scatter at a given spectral type and the low number of data points, which can be attributed to the different wind densities, mask any effect due to metallicity.

The change in the temperature scale has been due to the spectacular progress on the development of the model atmospheres, which has been essentially driven by allowing the treatment of metal line blanketing. The effects of line blanketing were anticipated several decades ago (e.g., Mihalas, 1978) and have been incorporated in a number of modern codes. Results presented in this review are mainly based on FASTWIND (Puls et al. 2005) and CMFGEN (Hillier & Miller 1998). The reader is referred to Herrero & Najarro (2005) for more details about this ensemble of codes, and to Puls et al. (2005) for a thorough discussion concerning the description of the above codes and a detailed comparison of FASTWIND and WM-Basic (Pauldrach et al. 2001) and CMFGEN.

Figure 2 displays the effects of line blanketing on the He and H ionization structure of a O3If star. For the case presented in Fig. 2 we have selected three different models. The first one (solid) corresponds to a blanketed model with $T_{\rm eff}$=45.5kK, log g=3.7 and R=15.6$R_\odot$. The second model (dashed) has same parameters but no blanketing, while the third one (dash-dot) is hotter $T_{\rm eff}$=50kK, log g=3.8 and R=14.6$R_\odot$ and reproduces equally good the observed spectra of the O supergiant as well as the observed V magnitude. All models have the same wind-strength parameter $Q = \dot{M}/(R_* v_\infty)^{1.5}$.

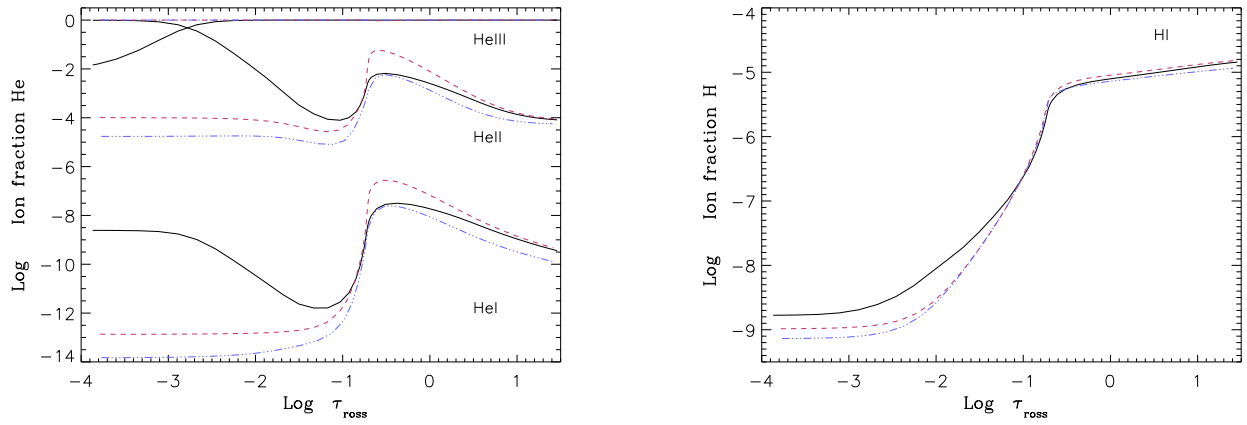

Figure 2: Effects of line blanketing on the helium **(left)** and hydrogen **(right)** ionization structure of a O3If supergiant.

From Fig. 2 we see that blanketing (solid) severely enhances the He ionization in the line formation region with respect to the cool unblanketed model (dash), so that a degree of He ionization similar to the hot unblanketed model (dash-dot) is obtained by decreasing $T_{\rm eff}$ by almost 5000 K. As the flux is blocked and a certain amount of photons are backscattered, flux (luminosity) conservation demands a more efficient diffusion in the inner photosphere. Since this effect is controlled by the temperature gradient (diffusion approximation) the temperature is increased in this region (back-warming). In other words, the basic diagnostic for temperature determinations in O stars, namely the He ionization balance reacts strongly to blanketing and causes the observed reduction on the effective temperature scale. Inspection of the impact of blanketing on the H ionization structure of O stars (Fig. 2-right) tells us that only minor changes are produced in the ionization degree of H and, therefore, only small variations should be expected in the inferred mass loss rates (assuming they are derived from Hα, as He II 4684Å would be severely altered). Finally, it should be noted that the relatively strong wind of the star blocks the He II ionizing radiation and forces recombination of He III to He II, with important implications on the number of He II ionizing photons.

Given the importance of blanketing and the strong revision to stellar parameters that the inclusion of this effect has lead to, it is crucial to compare thoroughfully different atmospheric codes and check for consistency among them. Important cross-tests have been carried out for each code (see Puls et al. 2005). Encouragingly, excellent agreement is found throughout most of the parameter domain among these codes.

3 Mass loss in massive stars

3.1 The Wind Momentum Luminosity Relation (WLR)

Since the winds of hot stars are driven by radiation, one should expect a tight relationship between the mechanical momentum of the stellar wind and the photon momentum. Actually, the theory of radiative driven winds (Castor et al. 1975; Abbott & Klein 1975; Pauldrach et al. 1986; Kudritzki et al. 1989) predicts that the "modified stellar wind momentum" depends directly on luminosity through the Wind Momentum Luminosity Relation (**WLR**)

$$logD_{mom} = logD_0 + xlog(L/L_{\odot}), \qquad D_{mom} = \dot{M}v_{\infty}(R_*/R_{\odot})^{0.5} \tag{1}$$

where the coefficients D_0 and x are a function of spectral type and luminosity class. Further, the coefficient controlling the dependence on luminosity, x, is determined by the statistics of the thousands of metal lines driving the wind, so a different WLR has to be established for each metallicity environment (see Kudritzki & Puls 2000, for a thorough discussion). During the last decade an enormous effort has been made to calibrate the WLR as function both of spectral type and metallicity and compare the results with the predictions by theory (Puls et al. 2000; Vink et al. 2000, 2001).

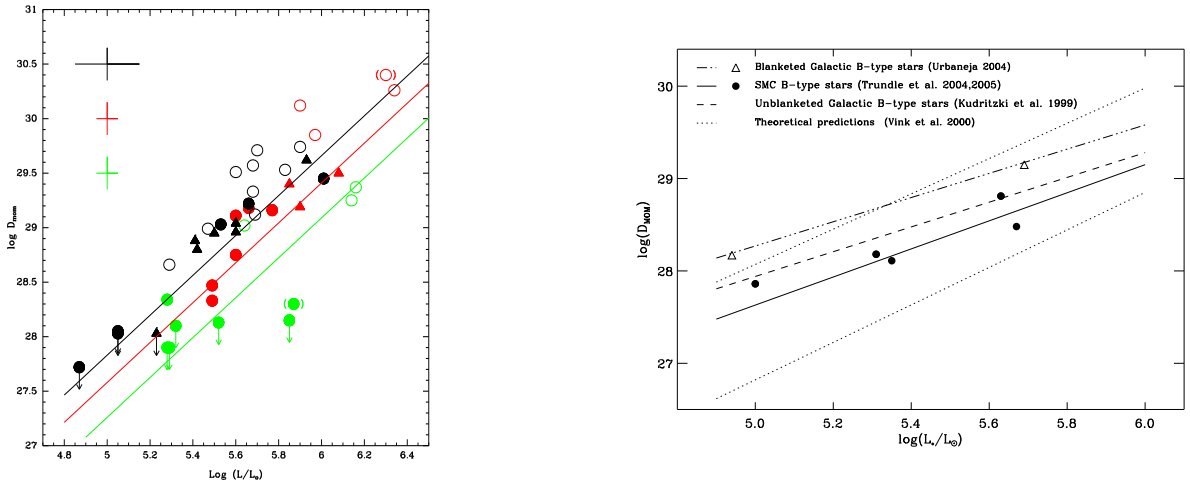

Figure 3: Metallicity scaling of the WLR for O and B supergiants. **(Left)** Z scaling for O supergiants (adapted from Massey et al. 2005). **(Right)** Z scaling for B supergiants (Kudritzki et al. 1999; Urbaneja 2004; Trundle et al. 2005). (dash-dot): linear regression to galactic stars with blanketed models (Urbaneja 2004); (dashed): unblanketed galactic (Kudritzki 1999); (solid): blanketed SMC (Trundle et al. 2005); (upper dotted) theoretical galactic predictions (Vink et al. 2000); (lower dotted) theoretical SMC predictions (Vink et al. 2001). Note the considerable correction to the modified wind momenta for B-supergiants due to line blanketing

Results on the metallicity dependence of the WLR for O stars and B supergiants and their comparison with theoretical predictions are displayed in Fig. 3. From Fig. 3-right we see how the modified momenta of galactic B-supergiants obtained with blanketed models (Urbaneja 2004) agree much better with theoretical predictions than those obtained with unblanketed models (Kudritzki et al. 1999),

although a significantly different slope is obtained. The whole worsens in the case of the SMC, where the WLR obtained from blanketed models (Trundle et al. 2005) differs severely from theoretical predictions (Vink et al. 2001). In the case of O stars, the situation is significantly improved. From Fig. 3-left (see Massey et al. 2005, and references therein) we see how the theoretically predicted WLRs for O stars in the Galaxy, LMC and SMC are reasonably well reproduced by spectroscopic studies.

3.2 Clumping

From Fig. 3-left, we also note, however, that some of the supergiants present "too large" modified momenta (higher mass loss rates). This effect was realized by Herrero et al. (2002). Repolust et al. (2004) confirmed this effect and suggested that clumping could account for excess of modified momenta on those supergiants showing Hα in emission (see Fig. 4). Hence the presence of clumping in the wind, i.e. the region where Hα emission was arising would lead to an overestimate of the true mass loss rate of the star. The existence of clumping was postulated on theoretical grounds by Owocki et al. (1988), who showed that radiation driven winds are inherently unstable and that would lead to the formation of a highly structured wind (clumping). Observationally, evidence of clumping in O stars has been found on the far ultraviolet P V line (Crowther et al. 2002; Hillier et al. 2003; Massa et al. 2003) and in the infrared continua (Blomme et al. 2002, 2003). Thus, assuming that wind inhomogeneities were responsible for the observed discrepancies in O supergiants, Repolust et al. (2004) estimated that a clumping factor of f=0.2 (leading to a correction of $-.36$ dex in the modified wind momenta of these stars) was enough to account for these "outliers". These results of these clumping corrected momenta are shown in Fig. 4 and provide much better agreement with the theoretical predictions.

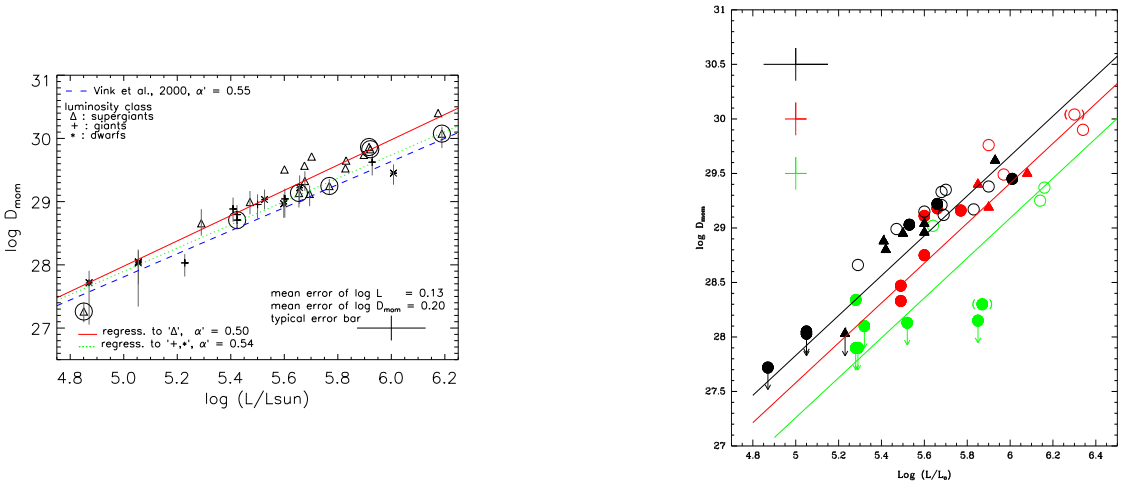

Figure 4: Hints of Clumping WLR. **(Left)** Galactic WLR for O stars (from Repolust et al. 2004). The enhanced modified momenta obtained for the supergiants showing emission in Hα suggest the presence of clumping in the winds of these stars. **(Right)** Z dependent clumping corrected WLR for the Galaxy, LMC and SMC (from Massey et al. 2005). The mass loss rates of the stars showing Hα in emission have been corrected assuming a clumping value of f=0.2

3.3 Thin winds

Puls et al. (1996) showed that the observed WLR for O-type dwarfs exhibited a severe curvature toward very low wind momenta for luminosities lower than $logL/L_{\odot} = 5.3$. Herrero et al. (2002) obtained a very low value for the mass-loss rate of the O9.5V star 10 Lac (more than one order of magnitude below the theoretically predicted), and recently Bouret et al. (2003) and Martins et al. (2004, 2005b) have obtained similar results on analysis of O dwarfs in the SMC and the Galaxy.

Therefore, there is a breakdown of the WLR for low luminosity O dwarfs. One important conclusion from the above studies is that the discrepancy in the mass loss rates obtained seems not to be related to metallicity, as it is present on both the Galactic and SMC stars.

However, present results based on UV studies may suffer from effects such as X-rays, advection or adiabatic cooling, whereas most mass-loss rates for dwarfs derived so far are only upper limits, due to the insensitivity of the usual mass-loss estimator Hα on low mass-loss rates. Consequently, a detailed investigation by means of *sensitive mass-loss diagnostics* in dwarfs over a larger sample is crucial to confirm their very weak-wind nature. Bα may well be this diagnostic, in view of its strong sensitivity to $\dot{M}$, particularly for very weak winds (see Najarro et al. 1998, Herrero & Najarro 2005).

4 Comparison with evolutionary models: the mass discrepancy

One of the best ways to advance in our knowledge is the comparison of results from different theories and models. The comparison of evolutionary and atmosphere models is a permament source of inspiration for new findings and improvements in these models.

Herrero et al. (1992) found in the first extensive NLTE analysis of massive O stars that the masses derived from the spectroscopic analysis were systematically lower than those derived from the evolutionary tracks after placing the stars on the Hertzsprung-Russell Diagram. The difference between the evolutionary and spectroscopic masses, that they called *mass discrepancy* was too large to be attributed to uncertanties in the determined parameters, and therefore a systematic effect due to some failure in the models, either atmospheric or evolutionary, was suspected.

The new model atmospheres have considerably improved the situation, as can be seen in Figs. 19 and 20 of Repolust et al. (2004) (see also the discussion in Repolust et al. 2004, or Herrero & Najarro 2005). Although the agreement is not perfect, the situation is much better than in the paper by Herrero et al. (1992), where most of the stars were far from the 1:1 relation, particularly the supergiants.

What's the situation in the Magellanic Clouds? One would expect that it should be better, because the major contribution to the error in the Galactic stellar masses (the distance uncertainty) is reduced. Further, the main reason for the failure of the model atmospheres (the presence of strong winds) should have a considerably lower impact in the low metallicity environment of the Magellanic Clouds. However, results from Massey et al. (2004, 2005) do not support this view. These authors find that a large number of stars both in the LMC and the SMC show the mass discrepancy. Even more, the mass discrepancy is found both for dwarfs and supergiants (this is however consistent with winds having a small effect in the discrepancy). This different behaviour of Galactic and Magellanic Clouds comparisons is a new challenge for our knowledge of the stellar structure at different metallicities.

5 Massive stars and H II regions

5.1 Trapezium stars

M42 in Orion is the reference H II region. Very recently, Esteban et al. (2004) have reanalysed the nebular abundances in Orion and found oxygen values only slightly higher than those of the Sun, the F-G dwarfs or the B dwarfs (see their Table 15). In fact the small difference they find is due to the assumption that a small fraction of oxygen is trapped into dust. Thus, Esteban et al. obtain an oxygen abundance in M42 of 8.65 dex for the gas phase, increasing to 8.73 dex when a correction for dust depletion is taken into account.

In view of their interest, Simon-Díaz et al. (2005) have recently newly analysed the Trapezium stars. These objects provide the most direct comparison to M42 abundances. Dwarfs with spectral types close to O9-B0 are ideal for the determination of the oxygen abundance, because they contain

a lot of O II lines. The dominant star in the Trapezium, $^1\theta$ Ori C, being an earlier type, has been excluded from this study.

To get an oxygen abundance as accurate as possible Simon-Díaz et al. (2005) set up a very detailed model atom and did a very careful study of the behaviour of each individual multiplet, by following the procedure described in Simon-Díaz et al. for each one of them. This procedure is designed such that it is easy to detect the anomalous behaviour of individual lines within multiplets, whatever the reason (uncertainties in the atomic parameters, unknown blends, etc.). These lines can then be removed from the analysis.

While this is a long way, it is rewarding. Simon-Díaz et al. (2005) have thus obtained the oxygen abundance of Trapezium stars. Their result - an average oxygen abundance of 8.63±0.06 dex - is much lower than other determinations (see Cunha & Lambert 1994) but compares very well with the abundance obtained by Esteban et al. (2004) for the gas phase of M42: 8.65±0.03 dex. This excellent agreement between the results from the spectroscopic analysis of stars and photoionized regions gives us confidence in both kinds of analyses.

5.2 Massive stars in M 33 and NGC 300

Now we can proceed to more difficult tasks, as for example the determination of the stellar radial oxygen gradient in M 33 to compare it with the one obtained from H II regions. The first steps in this direction were given by Monteverde et al. (1997, 2000). However, these authors only analysed four B-supergiants in M 33, while very recently, Urbaneja et al. (2005a) have presented an analysis with 12 M 33 stars. All these authors followed procedures similar to those of Simón-Díaz et al. (2005) (actually Simón-Díaz et al. followed and improved the procedures of these authors). The result, seen in Fig. 5, shows an excellent agreement between the radial oxygen gradient derived from stars and from H II regions (taken from Vilchez et al. 1988). Very recent results from Crockett et al. (2005) confirm these trends. Of course, error bars are now larger in both kind of objects than they were for Orion, and this is affecting the conclusion that we can derive from the data. For the stars this is not a matter of resolution, but more of SNR. An idea of the impressive state-of-the art of extragalactic stellar spectroscopy can be seen in Urbaneja et al. (2005a).

However, these results still have to be improved to place really serious constraints on the chemical evolutionary models of M 33. Firstly, the central steep rise of the oxygen abundance, although present in both sets of data (the recent data by Crockett et al. do not include this region), has to be confirmed, as it relies on only two objects; secondly, data still do not allow to distinguish between a linear gradient troughout M 33, and a different slope in the inner and outer regions (or some other possibility of this kind); and thirdly, actually a radial gradient is not what is needed, as two objects at the same radial distance from the center may actually be kiloparsecs away: a map of isoabundances on M 33 is really needed.

Urbaneja et al. (2005a) not only determined oxygen abundances for the B-supergiants, but also Si and Mg abundances. The abundances of these elements follow the trend displayed by the oxygen abundances, although with shallower gradients. This difference in the gradients cannot be explained at this point using the present theories of stellar and galactic structure and evolution.

The situation in M 31 is less clear. Results from Trundle et al. (2002) and Venn et al. (2000) do not show evidence of a radial O gradient (the former authors obtain a similar result for Si and Mg). This is in apparent contradiction to results from H II regions (see the above authors), but we have to take into account the much more limited range in galactocentric distance of these works and the much less favourable inclination of M 31 as compared to M 33.

M 33 and M 31 do not constitute the limit. The recent work by Urbaneja et al. (2005b) about B supergiants in NGC 300 (at 2.2 Mpc) shows how it is possible to extend this kind of work beyond the Local Group, still obtaining individual abundances of chemical elements in spite of a reduced resolution, although with larger error bars. These authors obtain stellar results that are consistent with H II regions. However, only for a particular calibration of the R_{23} index. In this way, stellar

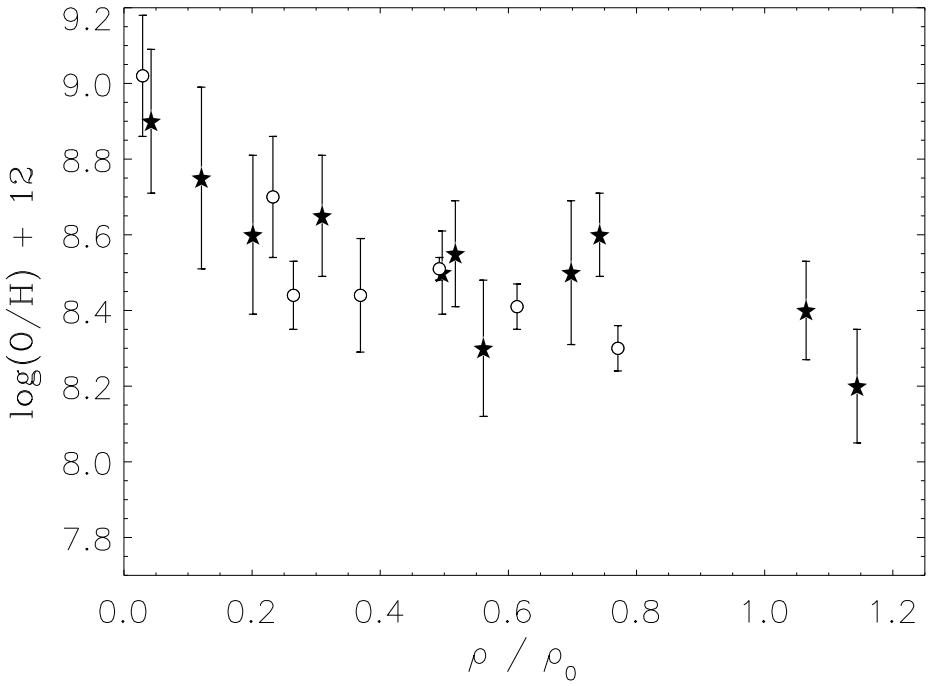

Figure 5: Comparison of the stellar and H II regions radial O gradient in M 33. The abcissa gives the deprojected distance to the center of M 33 in units of the Holmberg radius ρ_0 (28.77 arcmin). Stars are represented by asteriscs, while H II regions are represented by circles (from Urbaneja et al. 2005a)

results not only support the H II regions data (or they don't!), but may also help to distinguish between different calibrations in H II regions.

Acknowledgements

We would like to thank the organizers of the workshop for their kind invitation, and their patience with the manuscript, and C. Trundle, S. Simón-Díaz and M. Urbaneja for their help with some of the figures. They and other collaborators (they know who they are) are thanked for many very interesting discussions. F.N. acknowledges PNAYA2003-02785-E grant and the Ramon y Cajal program. This work has been supported by the spanish MEC through projects AYA2004-08271-C02-01 and 02.

References

Blomme R., Prinja R.K., Runacres M.C., Colley S., 2002, A&A, 382, 921
Blomme R., van de Steene G.C., Prinja R.K., Runacres M.C., Clark J.S., 2003, A&A, 408, 715
Bouret J.C., Lanz T., Hillier D.J., et al., 2003, ApJ, 595, 1182
Castor J.I., Abbott D.C., Klein R.I., 1975, ApJ, 195, 157
Crockett N.R., Garnett D.R., Massey P., Jacoby G., 2005, ApJ, submitted
Crowther P.A., Hillier D.J., Evans C.J., et al., 2002, ApJ, 579, 774
Cunha K., Lambert D.L., 1994, ApJ, 426, 170
Esteban C., Peimbert M., García-Rojas J., et al., 2004, MNRAS, 355, 229

Evans C.J., Crowther P.A., Fullerton A.W., Hillier D.J., 2004, ApJ, 610, 1021
Herrero A., Kudritzki R.P., Vílchez J.M., et al., 1992, A&A, 261, 209
Herrero A., Puls J., Najarro F., 2002, A&A, 396, 949
Herrero A., Najarro F., 2005, in Proc. of the workshop *Stellar Populations*, Cozumel, June 2005, ASP Conf. Ser., D. Valls-Gabaud & M. Chavez eds., in press
Hillier D.J., Miller D.L., 1998, ApJ, 496, 407
Hillier D.J., Lanz T., Heap S.R., 2003, ApJ, 588, 1039
Kudritzki R.P., Pauldrach A., Puls J., Abbott D.C., 1989, A&A, 219, 205
Kudritzki R.P., Puls J., 2000, ARA&A, 38, 613
Kudritzki R.P., Puls J., Lennon D.J., Venn K.A., Reetz J., Najarro F., McCarthy J.K., Herrero A., 1999, A&A, 350, 970
Martins F., Schaerer D., Hillier D.J., 2002, A&A, 382, 999
Martins F., Schaerer D., Hillier D.J., Heydari-Malayeri M., 2004, A&A, 420, 1087
Martins F., Schaerer D., Hillier D.J., 2005, A&A, 436, 1049
Martins F., Schaerer D., Hillier J., Meynadier F., Heydari-Malayeri M., Walborn N., 2005b, A&A, 441, 735
Massa D., Fullerton A.W., Sonneborn G., Hutchings J.B., 2003, ApJ, 586, 996
Massey P., Bresolin F., Kudritzki R.P., Puls J., Pauldrach A.W.A., 2004, ApJ, 608, 1001
Massey P., Puls J., Pauldrach A.W.A., et al., 2005, ApJ, 627, 477
McErlean N.D., Lennon D.J., Dufton P.L., 1999, A&A, 349, 553
Mihalas D., 1978, *Stellar Atmospheres*, 2nd Edition, Freeman, San Francisco
Monteverde M.I., Herrero A., Lennon D.J., Kudritzki R.P., 1997, ApJ, 474, 107
Monteverde M.I., Herrero A., Lennon D.J., 2000, ApJ, 545, 813
Najarro F., Kudritzki R.P., Hillier D.J., Lamers H.J.G.L.M., Voors R.H.M., Morris P.W., Waters L.B.F.M., 1998, ASP Conf. Ser. 131: *Properties of Hot Luminous Stars*, 131, 57
Najarro F., Puls J., et al., 2005, (in prep)
Owocki S.P., Castor J.I., Rybicki G.B., 1988, ApJ, 335, 914
Pauldrach A.W.A., Puls J., Kudritzki R.P., 1986, A&A, 164, 86
Pauldrach A.W.A., Hoffmann T.L., Lennon M., 2001, A&A, 375, 161
Puls J., et al., 1996, A&A, 305, 171
Puls J., Springmann U., Lennon, M., 2000, A&AS, 141, 23
Puls J., Urbaneja M.A., Venero R., et al., 2005, A&A, 435, 669
Repolust T., Puls J., Herrero A., 2004, A&A, 415, 349
Santolaya-Rey A.E., Puls J., Herrero A., 1997, A&A, 323, 488
Simón-Díaz S., Herrero A., Esteban C., Najarro F., 2005, A&A, in press
Trundle C., Dufton P.L., Lennon D.J., Smartt S.J., Urbaneja M.A., 2002, A&A 395, 519
Trundle C., Lennon D.J., Puls J., Dufton P.L., 2004, A&A, 417, 217
Trundle C., Lennon D.J., 2005, A&A, 434, 677
Urbaneja M.A., 2004, PhD Thesis, "Universidad de la Laguna"
Urbaneja M.A., Herrero A., Kudritzki R.P., et al., 2005a, ApJ, submitted
Urbaneja M.A., Herrero A., Bresolin F., et al., 2005b, ApJ, 622, 862
Vacca W.D., Garmany C.D., Shull J.M., 1996, ApJ, 460, 914
Venn K.A., McCarthy J.K., Lennon D.J., et al., 2000, AJ 541, 610
Vílchez J.M., Pagel B.E.J., Díaz A.I., Terlevich E., Edmunds M.G., 1988, MNRAS, 235, 633
Vink J.S., de Koter A., Lamers H.J.G.L.M., 2000, A&A, 362, 295
Vink J.S., de Koter A., Lamers H.J.G.L.M., 2001, A&A, 369, 574

The peculiar Of?p stars HD 108 and HD 191612*

Yaël Nazé [1†], Gregor Rauw[1‡], Nolan R. Walborn[2] and Ian D. Howarth[3]

[1]Institut d'Astrophysique, Université de Liège, Belgium
[2]Space Telescope Science Institute, Baltimore, USA
[3]Department of Physics and Astronomy, University College London, UK

Abstract: The Of?p spectral category was introduced by Walborn in 1972 to describe peculiar stars which possess intense emission lines of C III λλ 4647,4650,4651. Recently, two of them, HD 108 and HD 191612, were found to display spectacular line profile variations in the visible domain: these stars apparently alternate between two different spectral states (O6-O8). To discover the origin of this intriguing behaviour, a multiwavelength campaign was undertaken. In this context, the analysis of the X-ray emission is especially important since it provides crucial information for constraining the nature of these peculiar objects and testing conflicting models. We are therefore carrying out high-quality XMM-*Newton* observations of these stars and we present the results of the data obtained up to now.

1 Introduction

The Of?p category was introduced by Nolan Walborn in 1972 to describe two stars, HD 108 and HD 148937, with spectra that were slightly different from those of normal Of supergiants. Notably, they present C III lines around 4650Å with an intensity comparable to that of the neighbouring N III lines. In addition, their spectra showed sharp emission lines and some P Cygni profiles. A third star was soon added to this new class, HD 191612.

Of all Of?p stars, HD 108 is the best studied, but its observation led to conflicting results in the past. Some authors found radial velocity (RV) variations reminiscent of a binary motion, usually with a relatively short period (Hutchings 1975) although Barannikov (1999) derived a much longer period. However, other papers (e.g. Vreux & Conti 1979, Underhill 1994) reported no sign of orbital motion and rather attributed the RV and line profile variations to wind instabilities. To settle the conflicting situation, a new campaign for observing the Of?p stars was undertaken.

*Based on data collected at the Haute-Provence Observatory (France) and with the XMM-*Newton* satellite (ESA)

†Postdoctoral Researcher F.N.R.S. (Belgium)

‡Research Associate F.N.R.S. (Belgium)

"Massive Stars and High Energy Emission in OB Associations"; Proc. JENAM 2005 *Distant Worlds*, Liège (Belgium), eds. Rauw et al., p. 31-34

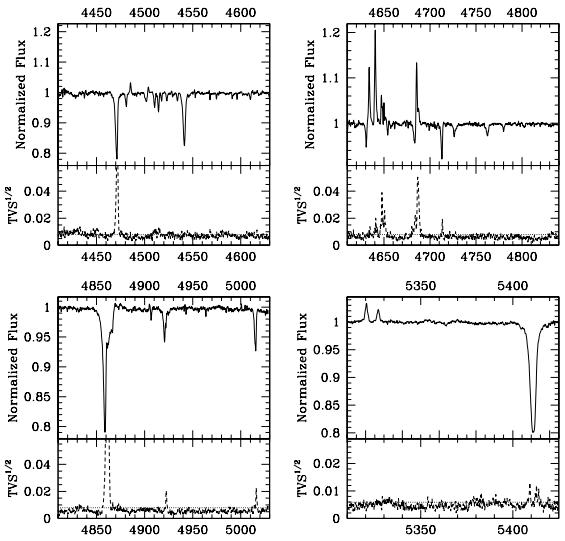

Figure 1: Mean visible spectrum of HD 191612 (top) and Time Variance Spectrum (TVS, bottom) around some key lines.

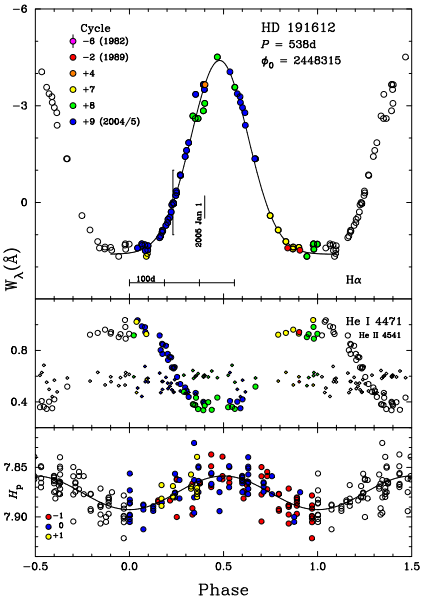

Figure 2: Variations of the EW of the Hα line (top), of the He I λ 4471 and He II λ 4542 lines (middle) and *Hipparcos* photometry of HD 191612 (bottom).

2 Observational results

2.1 Visible spectroscopy

Nazé et al. (2001) reported the first results of an ongoing monitoring of HD 108 at the Haute-Provence Observatory. The carefully measured RVs of the star were clearly incompatible with the proposed orbital solutions. In fact, they do not show any signature of orbital motion, be it on short or long term. However, when examining in detail the spectra, Nazé et al. discovered that the star underwent long-term line profile variations. The Balmer lines and the He I lines passed from emission or P Cygni profiles to absorptions. On the other hand, other emission and absorption lines were unchanged, like He II λ 4542. Since the ratio of the equivalent widths of He I λ 4471 and He II λ 4542 is used to determine the spectral type of the star, HD 108 is displaying apparent spectral type variations. After a thorough look into the literature, Nazé et al. (2001) discovered that such transitions in the H and He I line profiles had already happened in the past: the variations seem recurrent with a recurrence timescale of approximately 50-60 years. A few years later, Walborn et al. (2003) reported a very similar phenomenon in the spectrum of another Of?p star, HD 191612 (see Fig. 1), but the timescale appears much shorter, about $\sim$540 days.

Since two out of three Of?p stars are varying, Nazé (2004) tried to check the behaviour of the last member of the class, HD 148937. This star is poorly known, and only one high-resolution spectrum could be found in the literature. Compared to more recent data, no significant variations apparently occurred but if the timescale was much larger or much shorter than those of HD 108 and HD 191612, the changes would have been missed. MacConnell & Bidelman (1976) claimed that the Hβ line of HD 148937 was "filled in" while this line is now in absorption, but this does not constitute a certain clue of variation since the study relied on low-quality photographic data. On the other hand, this star is surrounded by a nebula, NGC6164-5, which is chemically enriched. It is supposed that the gas surrounding the star was ejected during a past eruption. Neither HD 108 nor HD 191612 are surrounded by such a nebula, but HD 148937 could simply be in a more advanced phase of evolution.

2.2 Photometry

Regarding HD 108, Barannikov (1999) found some magnitude and color variations in recent years: the star is becoming fainter at the same time as the emissions are decreasing. On the other hand, *Hipparcos* has observed all three Of?p stars: variability for HD 108 and HD 148937 cannot be totally excluded but the photometry of HD 191612 shows a clear modulation (Nazé 2004). The magnitude of the stars is varying with a period of approximately 540 days. Comparing with the spectroscopic results, it appears that the spectral variations and photometric changes are indeed correlated (see Fig. 2): when the star is fainter, its emission lines are minimum and the star presents a spectral type O8 (Walborn et al. 2004). This changing broad-band luminosity is not an effect of the varying emission lines themselves, since the lines are too weak to induce the large variations that are seen in the photometry.

2.3 X-ray data

To better understand these stars, we have obtained some XMM-*Newton* data. For HD 108, they were taken during Rev. 0494 and were presented in Nazé et al. (2004). To summarize, the high-resolution RGS data revealed a thermal X-ray spectrum, well fitted by a two temperature optically thin plasma (with kT_1 ∼0.2 keV and kT_2 ∼ 1 keV). Note that the iron line is present at 6.7 keV, and the star is slightly overluminous compared to the classical $L_X - L_{BOL}$ relation. Comparing to the previous detections of HD 108, by *Einstein* and *ROSAT*, we found no significant changes but these data have very large error bars and we can not exclude a small decrease in flux (less than a factor of 2).

More recently, we have undertaken a campaign to observe HD 191612 with XMM-*Newton* throughout its 540d cycle. Up to now, three datasets were taken, during Revs 0975, 0981, and 1004 - a last one will be taken at the end of this year. The observations sample the descending branch of the EW variations (see Fig. 2). A preliminary analysis shows that the X-ray spectrum of HD 191612 is very comparable to that of HD 108, with similar absorbing columns and temperatures. If we compare these new, sensitive XMM-*Newton* data with older *Einstein* observations and *ROSAT* data, we find no significant variations of the star (i.e. larger than a factor of 2). However, if we compare the XMM-*Newton* observations between one another, a small decrease of the X-ray flux, of the order of 15%, is detected although no significant changes of the other spectral parameters were found. The star thus appears slightly fainter in the visible and in the X-ray domain when the emission lines are minimum.

Finally, for HD 148937, there exist only *ROSAT* data. Taking into account the different bandpasses of *ROSAT* and XMM-*Newton*, no large differences can be found in the spectral parameters compared to HD 108 and HD 191612 (Nazé 2004).

3 Discussion and conclusions

Our ongoing observational campaign revealed many new aspects of the Of?p stars HD 108 and HD 191612. First, we have uncovered spectacular long-term variations of their visible spectra. These changes are actually recurrent, with a timescale of ∼540 days for HD 191612 and ∼50-60 years for HD 108. They are correlated with the photometric variations. In X-rays, both stars present thermal spectra with a slight overluminosity and a small decrease of the flux in phase with the visible variability. This periodicity might be linked to binarity, but since we saw no changes in the RVs, the systems would have to be seen face-on.

Several models could explain the peculiar behaviour of the Of?p stars. A first idea is that these stars are eccentric binaries containing a compact object. This compact companion would accrete matter near periastron, emitting then X-rays that are capable of altering the wind ionization structure, preventing the formation of emission lines. Unfortunately, this model has to face two important objections: first, the recent X-ray data of HD 108 and HD 191612 showed that the star is not very bright in X-rays when at or near the minimum of the emission lines; secondly, the X-rays observations further suggest a simultaneous decrease of the X-ray flux and the emission lines, whereas they should be anticorrelated in this model.

In massive stars, variations in emission lines are often related to changes of the stellar wind. Such wind variability can result from several causes, like a variable magnetic field or stellar pulsations. It can also appear when the star undergoes a peculiar evolutionary phase. Such a possibility is consistent with the fact that HD 148937 is surrounded by an enriched nebula: Of?p stars would then be precursors of the LBV state. This wind interpretation faces one major problem: the strict (and rather long-term) recurrence of the phenomenon.

Finally, we may come back to the eccentric binary interpretation, this time considering two 'normal' stars. If we compare the X-ray emission from the Of?p stars with that of other massive stars in the NGC6231 cluster (Sana et al. 2005), all Of?p stars seem overluminous (although not enough to be considered as X-ray binaries). For comparison, Sana et al. found that only colliding wind binaries deviate significantly from the $L_X - L_{BOL}$ relation. Moreover, the colliding wind interpretation is also supported by the rather high value of the second temperature fitted to the X-ray spectra. However, the exact behaviour of the Of?p stars (notably the symmetric equivalent width changes) certainly requires a rather peculiar orientation of the system.

Obviously, there are still many unanswered questions regarding the nature of the Of?p stars, but the recent data have already enabled to discard some models and to put some tight constraints on the actual nature of the stars. It is hoped that future observations will help to solve completely this mystery. However, as we have focused up to now on HD 108 and HD 191612, a last challenge merits some attention: does HD 148937 present the same behaviour as the other Of?p stars, and if yes, with what timescale?

Acknowledgements

The Liège team is greatly indebted to the F.N.R.S. for multiple assistance. This research is also supported in part by contract P5/36 "PAI" and through the PRODEX projects.

References

Barannikov A.A., 1999, Astron. Let. 25, 169
Hutchings J.B., 1975, ApJ 200, 122
Mac Connell D.J., Bidelman W.P., 1976, AJ 81, 225
Nazé Y., 2004, PhD thesis, Université de Liège
Nazé Y., Vreux J.-M., Rauw G., 2001, A&A 372, 195
Nazé Y., Rauw G., Vreux J.-M., De Becker M., 2004, A&A 417, 667
Sana H., Rauw G., Nazé Y., Gosset E., Vreux J.-M., 2005, MNRAS, submitted
Underhill A.B., 1994, ApJ 420, 869
Vreux J.-M., Conti P.S., 1979, ApJ 228, 220
Walborn N.R., Howarth I.D., Herrero A., Lennon D.J., 2003, ApJ 588, 1025
Walborn N.R., Howarth I.D., Rauw G., et al., 2004, ApJ 617, L61

A new paradigm for the X-rays from O stars *

A. M. T. Pollock [1] and A. J. J. Raassen [2,3]

[1]ESA *XMM-Newton* Science Operations Centre, ESAC, 28080 Madrid, Spain
[2]SRON, 3584 CA Utrecht, The Netherlands
[3]Astronomical Institute Anton Pannekoek, 1098 SJ Amsterdam, The Netherlands

Abstract: *XMM-Newton* observations of ζ Orionis suggest a new framework for the interpretation of the X-ray spectra of hot stars. The broad, slightly asymmetric lines all have the same velocity profile and probably originate in collisionless shocks behind which the exchange of energy between ions and electrons is so slow that electron heating does not take place, reducing the continuum. The spectrum is excited instead by protons with the randomized ion velocity dispersion accounting for the line widths. X-ray spectra in both single and binary stars are likely to be determined by the amount of post-shock electron heating: magnetically-confined plasma can evolve to high electron temperatures while in single stars this does not take place. The long mean-free path for Coulomb energy exchange suggests a minimum scale length for any structures in stellar winds, throwing into doubt the large-scale development of instability-driven shocks.

1 Shape of the X-ray lines in ζ Orionis.

The O9.7 Ib supergiant ζ Orionis is the optically brightest O star and was observed early with the *Chandra* high-energy gratings by Waldron & Cassinelli (2001), who argued that at least some of the X-rays originate very close to the stellar surface at the base of the powerful wind that is a ubiquitous feature of such hot stars. Its X-ray spectrum has proved to be typical of those seen from O stars. Miller et al. (2002) commented on the little understood broad line widths and tried to reconcile the data with the popular view that shocks developing from instabilities in the wind line-driving mechanism are responsible for generating the X-rays.

XMM-Newton (Jansen et al 2001) is ideal for observing such hot stars. The bandwidth of the Reflection Grating Spectrometer (RGS) matches perfectly that part of the X-ray spectrum in which the lines occur, extending the *Chandra* spectra beyond 25Å to the N VI lines near 29Å and C VI near 34Å. The RGS is able to resolve the lines and its high sensitivity allows the accumulation of enough statistics to study line profiles in detail. The RGS spectrum taken on 2002-09-15 is shown in Fig. 1 and shows that the broad lines continue to longer wavelengths. Where they overlap, the RGS and HETG spectra are essentially identical. In common with other O stars, the continuum is weak or absent.

*Based on observations obtained with XMM-Newton, an ESA science mission with instruments and contributions directly funded by ESA Member States and NASA

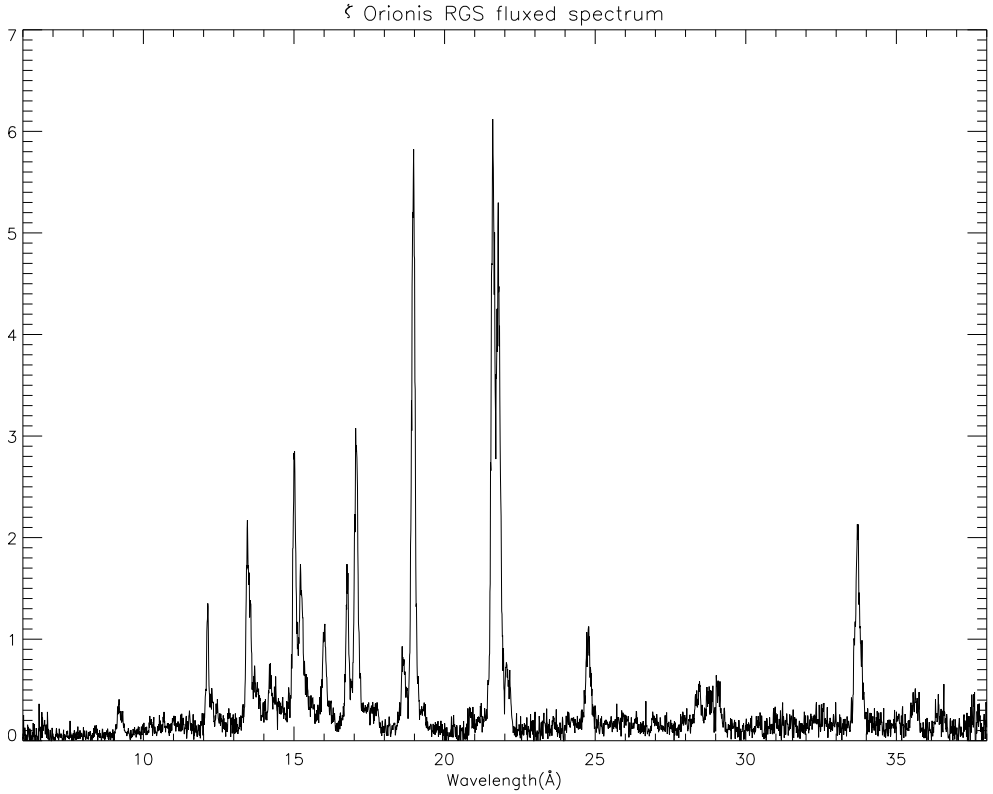

Figure 1: The RGS spectrum of ζ Orionis on 2002-09-15.

Comparison, for example, of the Lyα lines of C VI λ33.734 and Ne X λ12.132 separated by nearly a factor of 3 in wavelength shows their shapes in velocity space were very similar. In fact, we have been able to synthesize a good fit to the entire spectrum with the same velocity profile for every line using a triangular line-profile model characterized by three parameters: independent red and blue velocities where the profile goes to zero and a central velocity shift from the laboratory wavelength. The best-fit parameters reported in Table 1 were calculated for a combined fit all the available *XMM-Newton* and *Chandra* grating spectra, which were taken over two years apart but agree well both in the shapes of the lines and in overall luminosity to within a few percent. The line-profile fits show some asymmetry in ζ Orionis's lines with the line centre blue-shifted by about -300km s^{-1}. The blue and red widths are similar although the solution with blueV=redV is excluded. Both are about 70 to 80% of ζ Orionis's terminal velocity of $v_\infty = 2100$km s^{-1}.

blueV	-1585 ± 25	km s^{-1}
centralV	-303 ± 31	km s^{-1}
redV	$+1723\pm30$	km s^{-1}

Table 1: Best-fit line velocity parameters for the simultaneous fit to all the lines in *XMM-Newton* and *Chandra* grating spectra of ζ Orionis.

2 The nature of shocks in O-star winds

The general physical principles governing the development of shocks (Zel'dovich & Rayzer 2002) were considered recently by Pollock et al. (2005) for the binary-system colliding-wind X-ray shocks in WR140. Similar considerations for single hot stars lead to some interesting conclusions. An O-star wind is a plasma flow in which particle interactions are long-range Coulomb collisions that couple, for example, the small minority of UV-driven ions to the rest of the flow. In more extreme conditions, plasma shock waves show properties that result from the particularly slow character of the energy exchange between ions and electrons. The ion-ion collisional mean-free path is $l_{\rm i-i} \sim 7.0 \times 10^{18} {v_8}^4/n_{\rm i}$ cm (Spitzer 1962) where $n_{\rm i}$ is the ion density and $v = v_8 \times 1000$km s^{-1}. Close to the photosphere of ζ Orionis, where the density is high and the velocity low, $l_{\rm i-i}$ is small, but then increases rapidly with radius. At about $3R_*$ above the stellar surface in the heart of the acceleration zone, $l_{\rm i-i} \approx 0.1R_*$ while at $10R_*$, $l_{\rm i-i} \approx R_*$. If strong shocks are to develop at all then some dissipation mechanism other than collisions must operate. Collisionless shocks (e.g. Draine & McKee 1993) are probably involved in which ions are heated to high temperatures while electrons remain cold. Any subsequent equilibration takes place downstream through energy exchange between ions and electrons though, because of the large difference between their masses, this happens about a factor of 50 more slowly than ion-ion collisions, with corresponding mean-free-paths of many stellar radii. The low X-ray luminosities of O-stars show that only a small fraction of wind material is involved, the vast bulk of which remains cool. It seems likely, then, that shocked gas will not survive for long before it is mixed back with cool material and disappears from view, leaving no chance for electrons to contribute to X-ray line or continuum emission. It is further likely that the X-ray plasma is far from equilibrium.

2.1 X-ray ionization and excitation

In the absence of shock-heated electrons, protons in the immediate post-shock gas are probably responsible for exciting the X-ray spectrum. Through the shock transition, the ionization balance is unchanged although ions characteristic of the cool wind immediately find themselves in a hostile environment in which encounters take place with other ions at relative velocities roughly equal to the randomized pre-shock gas velocity, which has a well defined value of $v_\infty = 2100$ km s^{-1} in the terminal velocity regime of ζ Orionis. Protons of such velocities are an effective agent for ionization and excitation because the cross-sections depend on the relative velocity of the incident ionizing particle and that of the bound electron, whose order of magnitude is fixed by the Bohr velocity $v_{\rm Bohr} = 2188$ km s^{-1}. We suggest that it is the coincidence of this microscopic atomic value and the macroscopic terminal velocities of ζ Orionis and other O stars, that is the basic physical reason for the production of X-rays in hot stars. The X-ray spectrum should reflect the individual cross-sections of the three important processes of ionization, excitation and charge exchange between ions.

2.2 The velocity profile of the X-ray lines

Efforts made so far to account for the shape of the X-ray lines, (e.g. Ignace & Gayley 2002) have assumed that the emitting ions are moving with the majority cool gas, so that the red wing of the lines arises in material on the far side of the star flowing away from the observer. This simple assumption is hard to justify, if only because much of the ordered motion of the wind needs to be converted to heat for X-rays to be observed at all. It is more likely that the line velocity profiles simply reflect instead the line-of-sight component of the thermalized

motion of ions in the immediate post-shock gas. For a Maxwellian distribution, HWHM($v_{\rm x}$) = $\sqrt{2\ln 2(kT_{\rm S}/m)} = (\sqrt{6\ln 2}/4)v \sim 0.51v$. The observed lines in ζ Orionis are roughly consistent with this scheme, showing half-widths of about 75% of the value of $0.51v_\infty$. The small observed blue-shift of about $v_\infty/7$ is probably connected with the strong-shock post-shock bulk velocity of $v_\infty/4$.

3 Other consequences

The long Coulomb collisional mean-free-path, apart from requiring a collisionless shock transition, probably also limits the steepness of pressure gradients that can be sustained by the medium and defines a minimum size for any structures in the hot gas. In this case, it is unlikely that the microscopic instability in the line-driving mechanism will be able to steepen into the macroscopic shocks widely thought to generate O-star X-rays: the instability would soon be limited by the difficulty of transferring momentum quickly enough from the unstable driven ions to the rest of the flow, causing breakdown of the single-fluid approximation as discussed, for example, for thin hot-star winds by Springmann & Pauldrach (1992).

An inevitable consequence of the scheme proposed is the effective absence of hot electrons in an O-star wind, altering the physical basis of the plasma emission models concerned. In contrast to either ionization by electron impact or photoionization, which together account for the majority of observed X-ray plasmas, single O-star spectra may be one of the clearest examples of a protoionized plasma. The term "protoionized" seems appropriate both for the contrast with photoionized and because it describes the very earliest stages of post-shock ionization through which many plasmas are bound to pass before electrons are hot enough to take over ionization and excitation. The shock transitions themselves, though probably smaller in physical extent than those in colliding-wind flows such as WR140, obey similar jump conditions. The distinction between spectra rather lies in the post-shock relaxation layer, in the amount of equilibration that takes place between ions and electrons. If the hot plasma is confined by magnetic fields, as in WR140, for example, relaxation may take its course allowing energy to be transferred from ions to electrons, which may then excite a familiar plasma spectrum characteristic of collisional ionization equilibrium. Otherwise, in the winds of single O-stars, no electrons reach high temperatures and we observe instead the effects of the resonance between the macroscopic terminal velocity of the wind and the microscopic Bohr velocity characteristic of the electrons in bound atomic states.

References

Draine B.T., McKee C.F., 1993, ARA&A, 31, 373

Ignace R., Gayley K.G., 2002, ApJ, 568, 954

Jansen F., Lumb D., Altieri B., et al., 2001, A&A, 365, L1

Miller N.A., et al., 2002, ApJ, 577, 951

Pollock A.M.T., Corcoran M.F., Stevens I.R., Williams P.M., 2005, ApJ, 629, 482

Spitzer L.Jr., 1962, *Physics of Fully Ionized Gases*, New York: Wiley, 2nd ed.

Springmann U.W.E., Pauldrach A.W.A., 1992, A&A, 262, 515

Waldron W.L., Cassinelli, J.P., 2001, ApJ, 548, L45

Zel'dovich Ya.B., Raizer Yu.P., 2002, *Physics of Shock Waves and High-Temperature Hydrodynamic Phenomena* (Mineola, New York: Dover)

CN status of a sample of galactic OB supergiants

M. Sarta Deković and D. Kotnik-Karuza

Department of Physics, Faculty of Arts and Sciences, Rijeka, Croatia

Abstract: In our search for evidence for the CNO processed material in the atmospheres of galactic OB supergiants we measured the equivalent widths of photospheric lines in their high-resolution *IUE* spectra. A sample of 36 stars was investigated and the lines He II 1640 Å, C III 1247 Å, N IV 1718 Å and O IV 1339 Å were studied. All ions show a well-defined dependence on effective temperature. Comparison of stars with questionable CN status with normal stars gives evidence for a decrease in equivalent widths of C III and O IV lines accompanied by an increase in equivalent widths of N IV and He II lines, which leads to abundance differences.

1 Introduction

Evolutionary theories predict that some massive stars should show variations in their surface abundances indicative of CNO core-processed material being present in the photosphere. Some models (Schaller et al. 1992) imply that massive stars can evolve through blue loops, developing as main sequence-BSG-RSG-BSG stars. In that case two populations of BSG are postulated: the pre-RSG which would be chemically normal and the post-RSG which would show evidence of nucleosynthetically processed material in their atmospheres. Classical models of stellar evolution generally predict that only very massive stars with masses $\geq 60 M_{\odot}$ lose enough mass via stellar wind to show CNO enriched material, while still on the main sequence (Chiosi and Maeder 1986). Stars of lower mass show CNO processed material in their atmospheres in the later phases of their evolution, after the first dredge-up.

Recent investigations on the effect of stellar rotation on the structure and evolution of massive stars show that early atmospheric contamination can occur by mixing with the stellar interior, the contamination being more important as both, the stellar mass and the initial rotational velocity increase. This would remove the need for blue loops to explain the OBN/OBC phenomenon (Meynet and Maeder 2000).

In this work we have looked for abundance-deviations in a sample of 36 galactic OB supergiants. For some of our program stars the CN status has been estimated from optical spectra (McErlean et al. 1999; Lennon et al. 1993; Walborn 1976; Wollaert 1988; Takeda 1994; Takeda and Hidai 1995; Villamariz et al. 2002.). We have derived the CN status of the whole sample by analyzing the He, C, N and O ultraviolet lines.

▪ "Massive Stars and High Energy Emission in OB Associations"; Proc. JENAM 2005 *Distant Worlds*, Liège (Belgium), eds. Rauw et al., p. 39-42 ▪

Table1. Program stars:

No.	HD no.	Spectral type	T_{eff}/K	Name	Association	SWP	CN normal stars
1	207198	O9 Ib/II	32000		Cep OB2	25981	
2	30614	O9,5 Ia	30000	α Cam	NGC 1502	2591	
3	209975	O9,5 Ib	30000	19 Cep	Cep OB2	36503	
4	167264	O9,7 Iab	27500	15 Sgr	Sgr OB7	4368	
5	37128	B0 Ia	25000	ε Ori	Ori OB1	6727	
6	204172	B0,2 Ia	23500	69 Cyg	Cyg OB4	48946	
7	38771	B0,5 Ia	22000	κ Ori	Ori OB1	30178	
8	192422	B0,5 Ib	22000		Cyg OB1	51893	
9	213087	B0,5 Ib	22000	26 Cep	Cep OB1	2736	
10	2905	BC0,7 Ia	21000	κ Cas	Cas OB14	54038	
11	13854	B1 Iab	20000		Per OB1	2737	
12	24398	B1 Ib	20000	ζ Per	Per OB2	9685	x
13	190603	B1,5 Ia+	19000		Vul OB2	1822	
14	193183	B1,5 Ib	19000		Cyg OB1	52716	
15	13841	B1,5 Ib	19000		Per OB1	18512	
16	14143	B2 Ia	17500		Per OB1	9435	
17	14818	B2 Ia	17500	10 Per	Per OB1	9416	
18	41117	B2 Ia	17500	χ^2 Ori	Gem OB1	40669	
19	206165	B2 Ib	17500	9 Cep	Cep OB2	4406	x
20	13866	B2 Ib	17500		Per OB1	18513	x
21	31327	B2 II	17500		Aur OB1	21280	
22	198478	B2,5 Ia	16000	55 Cyg	Cyg OB7	36938	x
23	42087	B2,5 Ib	16000	3 Gem	Gem OB1	8646	
24	14134	B3 Ia	15000		Per OB1	46882	
25	53138	B3 Ia	15000	o^2 CMa	Coll 121	7193	x
26	225094	B3 Ia	15000		Cas OB5	18688	
27	36371	B4 Iab	14300	χ Aur	Aur OB1	2945	x
28	58350	B5 Ia	13500	η CMa	Coll 121	30198	x
29	164353	B5 II	13500	67 Oph	Sct OB2	4267	x
30	191243	B5 II	13500		Cyg OB3	7737	x
31	13267	B6 Ia	12900	5 Per	Per OB1	51892	x
32	12301	B7 II	12400	53 Cas		4265	x
33	34085	B8 Ia	11500	β Ori	Ori OB1	32727	
34	199478	B8 Ia	11500		NGC 6991	15552	x
35	208501	B8 Ib	11500	13 Cep	Cep OB2	4217	
36	21291	B9 Ia	10800		Cam OB1	8087	

2 Observational data

Among 36 stars from our program (Table 1) there are 12 stars to which a normal CN status has been assigned (McErlean et al. 1999, Prinja 1990, Wollaert et al. 1988 and Walborn 1976). In order to get a better mean relation for normal stars, we extended the sample of normal supergiants by adding 7 stars from Wollaert et al. (1988): HD 210809 (O9 Iab), HD 188209 (O9,5 Iab), HD 218915 (O9,5 Iab), HD 149038 (O9,7 Iab), HD 91969 (B0 Ia), HD 122879 (B0 Ia), HD 154090 (B0,7 Ia). Other stars from our sample show deviations in equivalent widths from the mean relation defined by normal supergiants as a function of their spectral type. The calibration of the effective temperature scale was adopted from Lennon et al. (1993).

3 Results

For the lines located on the shoulder of the curve of growth the deviations of equivalent widths from those of the normal supergiants, ΔlogW (Figure 3.), can be turned into logaritmic abundance deviations, ΔlogA, by multiplication with a factor 2 or larger (Wollaert et al. 1988). Thus the plot in Fig. 3 corresponds to logaritmic abundance deviations in relative units. The method allows an estimate of limit values, i.e. only lower limits for the overabundances and upper limits for the underabundances can be determined.

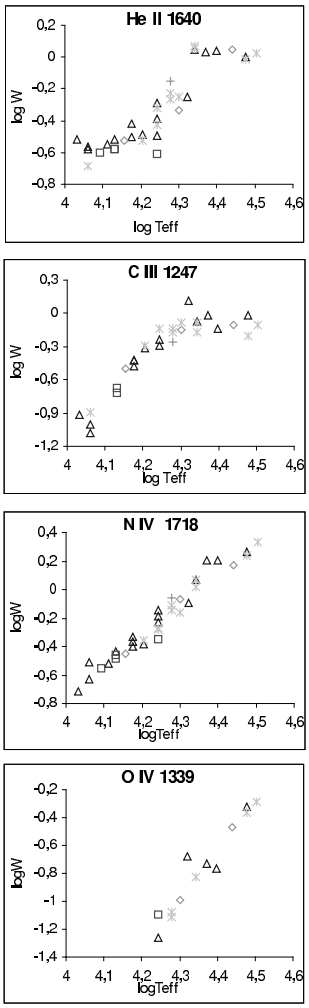

Figure 1: Equivalent widths vs. logT_{eff} for the He, C, N and O lines. The luminosities are marked by the following simbols: + Ia+, △ Ia, ◇ Iab, ∗ Ib, □ II.

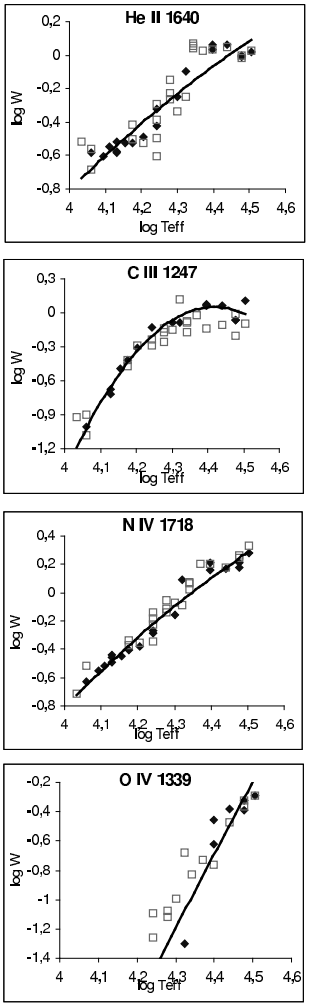

Figure 2: The solid line in the logW vs. logT_{eff} plot is defined by normal supergiants which are marked by filled diamonds, while open squares represent all other program stars.

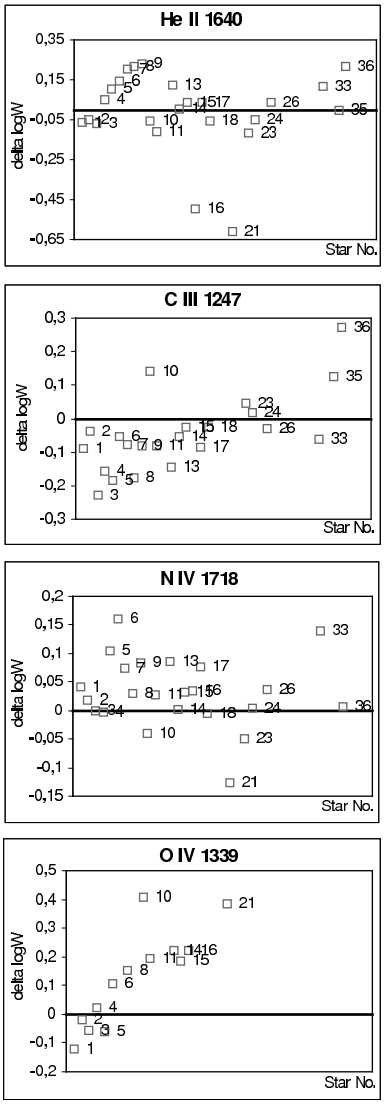

Figure 3: Deviations in equivalent widths from the mean relation defined by normal supergiants as a function of their T_{eff}. The stars are marked by numbers in agreement with assignments in Table 1.

4 Discussion

Our results show, as expected, increased helium and nitrogen abundances, accompanied by decreased carbon. Normal or moderate enrichment in nitrogen accompanied by underabundant helium observed in stars no. 1, 2, 3, 11, 24 can be explained by rotating evolutionary models: they predict that helium enrichment appeared later in the stellar atmosphere, while CNO abundance changes were already present. This might be the reason why no clear correlation between helium overabundance and CNO contamination has been found.
However, the star no. 36 gives evidence of a remarkable proportion between helium and carbon abundances, while a few other program stars show a weak correlation of helium with carbon

lines, as reported also by Lennon et al (1993).
Oxygen is showing strange overabundances in the stars no. 6, 8, 11, 14, 15, 16 which are more or less underabundant in carbon and moderatly overabundant in nitrogen. More attention should be paid to this problem, which might result from the small number of normal stars for which oxygen lines could have been measured, leading to a rather poor determination of the trend line.
One of the general predictions of the stellar evolution calculations is that the most luminous supergiants of a given spectral type should show the strongest contamination by CNO processed material, providing that they have passed through the RSG stage. Such trend is found here for the spectral type B1,5, where one Ia supergiant (No. 13) shows stronger helium and nitrogen lines and a weaker carbon line than two Ib supergiants (No. 14, 15) of the same spectral type. For the spectral type B2 we can only say that one B2 II supergiant (No. 21) shows lower helium and nitrogen lines than the three B2 Ia supergiants (No. 16, 17, 18). At B8 one Ia star (No. 33) shows stronger helium and weaker carbon line than one Ib star (No. 35). The same B8 Ia star (No. 33) shows a very strong nitrogen line, while no nitrogen line was measured in the B8 Ib (No. 35) stellar spectrum.
According to Lennon et al. (1993), it is possible that all supergiants have atmospheres enriched by CNO processed material. In our sample, only three stars (No. 10, 21, 23) are nitrogen deficient. Eight stars from the sample (No. 1, 2, 3, 10, 11, 18, 23, 24) show helium deficiency which could be explained as a result of rotational effects mentioned before.
Enhanced line strengths might confirm the presence of the CNO processed material in the atmospheres, but it does not necessarily give evidence of later stages of evolution. It could have been dredged-up during a red supergiant stage, but it also could have been mixed to the surface at an early stage of evolution because of stellar rotation. On the other hand, line strengths can be affected by atmospherical structure rather than by abundance anomalies.
The results shown here are quite preliminary. An appropriate model atmosphere in the UV would lead to a more reliable interpretation.

Acknowledgements

Our thanks are due to EAS for supporting the participation of MSD in the JENAM 2005.

References

Chiosi C., Maeder A., 1986, ARA&A, 24, 329
Lennon D.J., Dufton P.L., Fitzsimmons A., 1993, A&AS, 97, 559
Meynet G., Maeder A., 2000, A&A, 361, 101
McErlean N.D., Lennon D.J., Dufton P.L., 1999, A&A, 349, 553
Prinja R.K., 1990, MNRAS, 246, 392
Schaller G., Schaerer D., Meynet G., et al., 1992, A&AS, 96, 269
Takeda Y., 1994, PASJ, 46, 181
Takeda Y., Takada-Hidai M., 1995, PASJ, 47, 169
Villamariz M.R., Herrero A., Becker S.R., Butler, K., 2002, A&A, 388, 940
Wollaert J.P.M., Lamers H.J.G.L.M., de Jager C., 1988, A&A, 194, 197
Walborn N.R., 1976, ApJ, 205, 419

Section 2

Colliding winds and non-thermal emission

Observations of non-thermal radio emission in O-type stars

R. Blomme

Royal Observatory of Belgium, Ringlaan 3, B-1180 Brussel, Belgium

Abstract: The non-thermal radio emission of O-type stars is due to synchrotron radiation from relativistic electrons. These electrons are accelerated in shocks. Most probably, these shocks are due to colliding winds in a binary or multiple system. We present new VLA observations of the non-thermal radio emitter Cyg OB2 No. 8A, which was only recently discovered to be a binary. For this star, the radio fluxes show a good correlation with the phase in the binary period. This result is actually quite surprising because the high free-free optical depth should prevent us from detecting the synchrotron radiation emitted by the colliding-wind region. We can only explain the observations by introducing porosity in the model. We also present a complete series of archive VLA observations on the triple system HD 167971. The radio lightcurve shows a more complicated behaviour than for Cyg OB2 No. 8A: it is difficult to detect the binary period in the observations, but we found a clear variation that occurs on a $\sim$ 20-year timescale.

1 Introduction

Two distinct physical processes are responsible for the radio emission in early-type stars. First of all, there is thermal emission, which is due to free-free processes in the material of the stellar wind. All stars with an ionized wind have such thermal emission. Secondly, there is non-thermal radio emission, which is due to synchrotron radiation by relativistic electrons. It is this second process that links radio emission to high-energy astrophysics. Typically, one needs electrons with energies of 100 MeV in a 0.1 G magnetic field to have a peak synchrotron radio flux at 6 cm. Electrons attain such high energies by scattering around a shock: due to the first-order Fermi mechanism part of the shock energy is transferred to the electrons (Bell 1978).

It was believed for some time that wind-embedded shocks in single O stars were responsible for the relativistic electrons (Chen & White 1994). However, Van Loo et al. (2005, see also Van Loo, these proceedings) showed that the shocks in the outer wind are not strong enough to explain the observed dependence of the non-thermal flux on wavelength. Therefore all non-thermal radio-emitting O stars are most probably binaries, where the synchrotron emission is caused by the two shocks on either side of the colliding-wind region.

We studied the radio fluxes of two non-thermal sources which are known O-type binaries: Cyg OB2 No. 8A and HD 167971.

"Massive Stars and High Energy Emission in OB Associations"; Proc. JENAM 2005 *Distant Worlds*, Liège (Belgium), eds. Rauw et al., p. 45-48

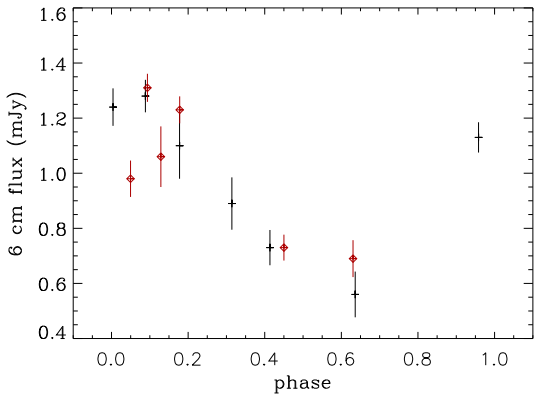

Figure 1: VLA 6 cm fluxes of Cyg OB2 No. 8A, plotted as a function of phase, based on the spectroscopic 21.908 d period. The two different symbols and colours indicate results from two orbits.

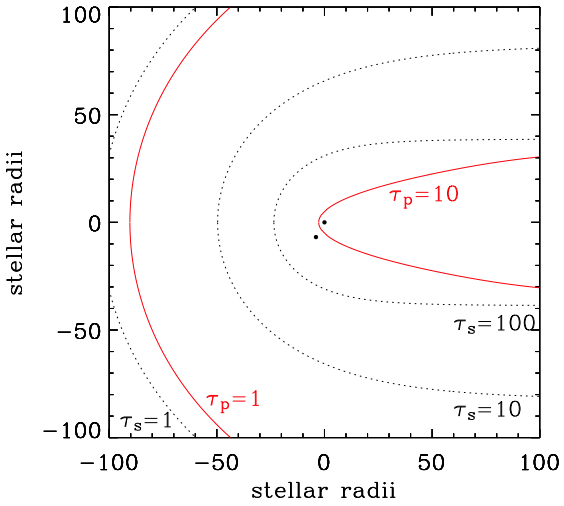

Figure 2: Contour lines of constant optical depth (at 6 cm), for an observer situated to the left. The dotted lines represent the $\tau = 1$, 10 and 100 contours of a smooth wind. The solid line shows contours for $\tau = 1$ and 10 of a wind where porosity was included. The two dots near the centre represent the binary components.

2 Cyg OB2 No. 8A

Cyg OB2 No. 8A was for a long time thought to be a single star, until De Becker et al. (2004) provided spectroscopic evidence that it is a binary, with an orbital period of 21.908 days. The binary consists of an O 6 + O 5.5 star, probably a supergiant and a giant.

We obtained 6 cm radio observations using the NRAO Very Large Array[1] (VLA) during February - March 2005. The measured fluxes show excellent phase-locking when folded with the spectroscopic period (Fig. 1).

This highly interesting result is, however, difficult to explain theoretically. The high free-free optical depth creates a 'radio photosphere', which should block the synchrotron radiation emitted by the colliding-wind region and therefore no phase-locked variation should be seen. Calculations of the optical depth show that the colliding-wind region should be well inside the $\tau = 100$ surface (Fig. 2). Neither can we explain the observations by assuming that the relativistic electrons escape from the colliding-wind region and become detectable once they are outside the radio photosphere: because of inverse Compton scattering, these electrons will quickly lose their energy.

Clumping might be considered as a possible solution to this problem. There are many indicators of clumping in stellar winds, but we mention just two. Kramer et al. (2003) introduce it to explain why the X-ray lines are formed so close to the stellar surface and Bouret et al. (2005) require it in their non-LTE modelling to obtain a better fit for the P Cygni profiles of

[1]The National Radio Astronomy Observatory is a facility of the National Science Foundation operated under cooperative agreement by Associated Universities, Inc.

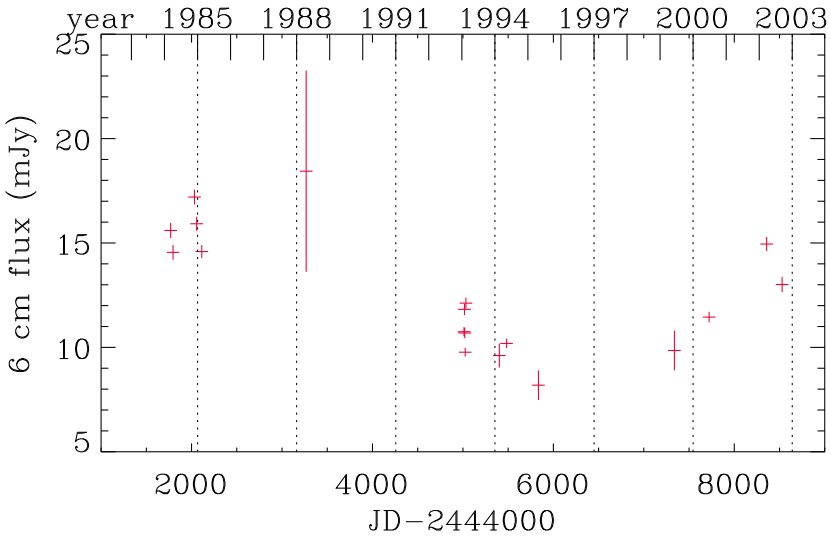

Figure 3: VLA 6 cm radio light curve of HD 167971.

HD 190429. Using the Abbott et al. (1981) formula for clumping does not solve the problem however: the surfaces where a certain optical depth is reached are the same for a clumped wind as for a smooth one, provided we require that the resulting radio flux is the same.

Porosity (e.g., Owocki et al. 2004) does provide a way out. Contrary to the clumping formalism, porosity allows the clumps to become optically thick. It is therefore possible to introduce a porosity-law (as a function of distance) that substantially reduces the optical depth, while still providing the same radio flux. Fig. 2 compares a smooth wind model to one that includes porosity. The (somewhat arbitrary) porosity model shown in Fig. 2 uses a clumping factor of 4.0 and clump-size that starts at 0.1 R_* at the stellar surface and increases outward, proportionally with distance. One component of the binary is now well outside the $\tau = 10$ surface, making it much more likely that we will detect at least some of the synchrotron emission.

3 HD 167971

Leitherer et al. (1987) discovered that HD 167971 is a triple system, consisting of a 3.3213-day period eclipsing binary and a third component, which may, or may not, be gravitationally bound to the binary. The binary is of spectral type O 5-8 V + O 5-8 V, the third component is probably an O 8 supergiant.

We obtained VLA observations of HD 167971 and complemented those with VLA archive observations. The resulting radio lightcurve at 6 cm is shown in Fig. 3. There are clear variations on a long timescale (of order 20 years). Superimposed on that are variations on a shorter timescale. We checked whether these short-term variations were related to the 3.3-day optical period, but this turned out not to be the case.

Using a porosity model (as for Cyg OB2 No. 8A) shows that we should have been able to see the 3.3-day variations due to the colliding-wind region between the two stars of the eclipsing binary. The fact we do not detect them could be due to the third component somehow blocking the radio flux. Or, more probably, it shows that the idea of porosity should not be pushed too far: there could be differences between supergiants and main-sequence stars. This would tie in well with other observations that show that clumping is usually needed in supergiants, but less so in main sequence stars.

4 Conclusions

Non-thermal radio emission is due to synchrotron radiation emitted in the colliding-wind region of a binary. Because the synchrotron radiation has to traverse the free-free radio absorption region of at least one of the two stars, one would expect to detect the non-thermal emission only for long-period binaries: only when the components are at a large enough separation will the colliding-wind region be outside the radio photosphere.

Surprisingly, the 21.9-day period of Cyg OB2 No. 8A is already sufficiently long for us to detect synchrotron emission from the colliding-wind region. It does not seem possible to explain this quantitatively with a smooth or clumped wind; rather a wind with porosity needs to be applied. The HD 167971 observations, on the other hand, caution us not to push this porosity idea too far, as for this system the 3.3-day period is not detected in the data.

The introduction of porosity will reduce the mass-loss rates that are traditionally derived from radio observations. This conclusion is of course highly relevant for models of stellar and Galactic evolution.

Acknowledgements

This research was done in collaboration with S. Van Loo (University of Leeds), M. C. Runacres (Vrije Universiteit Brussel), G. Rauw and M. De Becker (Université de Liège).

References

Abbott D.C., Bieging J.H., Churchwell E., 1981, ApJ, 250, 645
Bell A.R., 1978, MNRAS, 182, 147
Bouret J.-C., Lanz T., Hillier D.J., 2005, A&A, 438, 301
Chen W., White R.L., 1994, Ap&SS, 221, 259
De Becker M., Rauw G., Manfroid J., 2004, A&A, 424, L39
Kramer R.H., Cohen D.H., Owocki S.P., 2003, ApJ, 592, 532
Leitherer C., Forbes D., Gilmore A.C., et al., 1987, A&A, 185, 121
Owocki S.P., Gayley K.G., Shaviv N.J., 2004, ApJ, 616, 525
Van Loo S., Runacres M.C., Blomme R., 2005, submitted to A&A

Radio emission from colliding-wind binaries: observations and models

S. M. Dougherty [1], J.M. Pittard[2] and E.P. O'Connor[1,3]

[1]National Research Council, Herzberg Institute of Astrophysics, DRAO, Penticton, Canada
[2]School of Physics and Astonomy, U. Leeds, Leeds, UK
[3]Physics Dept., U. Prince Edward Island, Charlottetown, PEI., Canada

Abstract: We have developed radiative transfer models of the radio emission from colliding-wind binaries (CWB) based on a hydrodynamical treatment of the wind-collision region (WCR). The archetype of CWB systems is the 7.9-yr period binary WR140, which exhibits dramatic variations at radio wavelengths. High-resolution radio observations of WR140 permit a determination of several system parameters, particularly orbit inclination and distance, that are essential for any models of this system. A model fit to data at orbital phase 0.9 is shown, and some short comings of our model described.

1 What are colliding-wind binaries?

Observations of WR+O binary systems such as WR140 (Williams et al. 1990; White & Becker, Dougherty et al. 2005), WR146 (Dougherty et al. 1996, 2000; O'Connor et al., these proceedings) and WR147 (Williams et al. 1997) reveal synchrotron emission arising from relativistic electrons accelerated where the massive stellar winds of the binary companions collide - the WCR. There is strong evidence that all WR stars (Dougherty & Williams 2000), and now many O stars (van Loo et al., 2005, and references therein), that exhibit non-thermal emission are binary systems. It is widely accepted that the electrons are accelerated by diffusive shock acceleration (DSA), and CWB systems present a unique laboratory for investigating particle acceleration since they provide higher mass, radiation and magnetic field energy densities than in supernova remnants, which have been widely used for such work.

2 Models of radio emission in CWBs

To date, models of the radio emission from these systems have been based largely on highly simplified models. As a first step toward more realistic models, we have developed models of the radio emission based on 2D axis-symmetric hydrodynamical models of the stellar winds and the WCR. The temperature and density on the hydrodynamical grid (Fig. 1) are used to calculate the free-free emission and absorption from each grid cell. We assume the electrons are accelerated at the shocks bounding the WCR by DSA, and then advected out of the system

"Massive Stars and High Energy Emission in OB Associations"; Proc. JENAM 2005 *Distant Worlds*, Liège (Belgium), eds. Rauw et al., p. 49-52

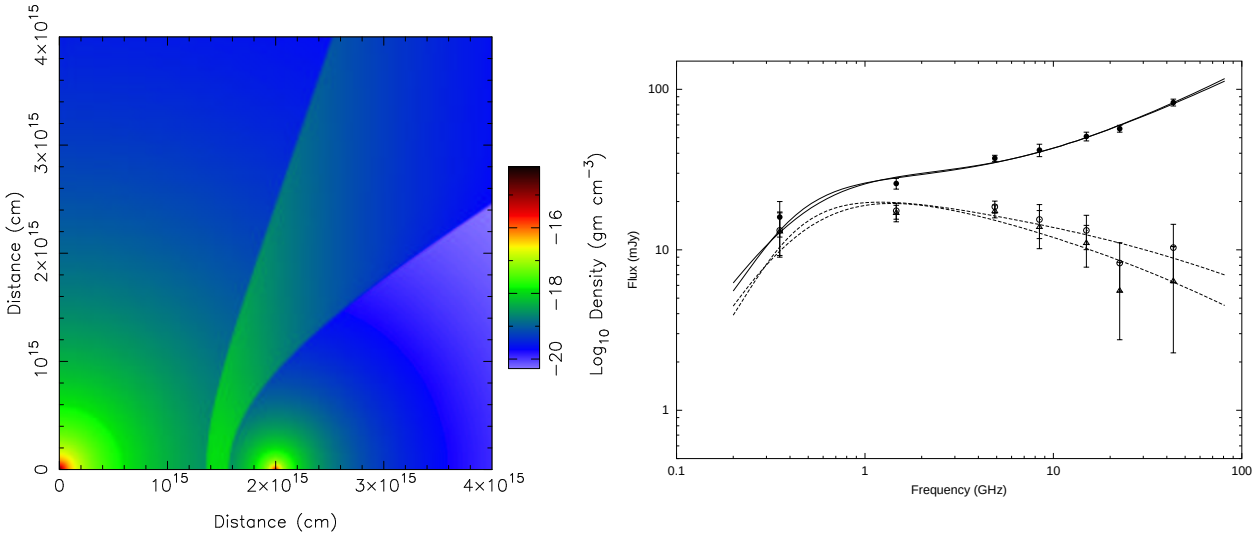

Figure 1: Left: Density distribution of a model CWB. The WR star is at (0,0) and the O star companion at (0,2 × 10^{15}) cm. Right: Models of the radio spectrum of WR147. The total (solid) and synchrotron (dashed) emission are shown for two possible models.

in the post-shock flow. At the shocks, the energy distribution of the relativistic electrons is specified by a power-law i.e. $n(\gamma) \propto \gamma^{-p}$. This spectrum evolves away from a simple power law as the electrons cool via several processes, including inverse-Compton and Coulombic cooling. The models take all these effects into account, including the impact of Razin effect. The synchrotron emission and self-absorption from each cell within the WCR are then calculated from the local energy distribution of non-thermal electrons. For more details see Dougherty et al. (2003) and Pittard et al. (2005).

We have applied these models to observations of WR147 (Fig. 1) and WR146 (see O'Connor et al., these proceedings) with some success. The models of WR147 are not as well constrained by the available data as those from WR146. O'Connor et al. (these proceedings) point out that models of WR146 would be much better if the spectra steepened at high frequencies, and if the WCR emission was less extended. We continue to investigate these issues.

3 Observations and models of WR140

The development of more realistic models of the radio emission from CWBs was motivated, in part, by the difficulties earlier work had with modelling the radio variations observed in WR140 (Williams et al., 1990; White & Becker, 1995). In spite of the wealth of multi-frequency observations of WR140, a number of critical system parameters are either unknown (e.g. system inclination), or weakly constrained (e.g. distance and luminosity class of the companion). Recent radio observations now provide these key constraints.

3.1 Modelling constraints from observations

A 24-epoch campaign of VLBA observations of WR140 was carried out between orbital phase 0.7 and 0.9. An arc of emission is observed, resembling the bow-shaped morphology expected for the WCR (Fig. 2). This arc rotates from "pointing" NW to W as the orbit progresses (Fig. 3) which, in conjunction with the observed separation and position angle of the two stellar components at orbital phase 0.3 (Monnier et al. 2004), leads to a solution for the orbit

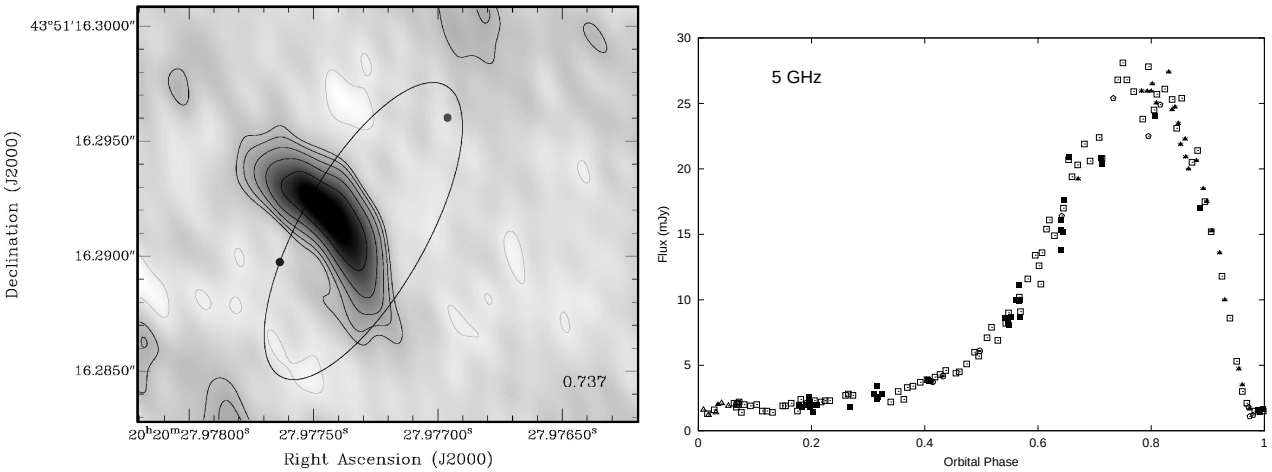

Figure 2: Radio observations of WR 140. Left: 8.4-GHz VLBA observation at orbital phase 0.737, with the deduced orbit superimposed. Right: 5-GHz flux as a function of orbital phase from orbit cycles between 1978-1985 (pentagons), 1985-1993 (squares), 1993-2001 (triangles), and the current cycle 2000-2007 (circles). Open symbols are from the VLA, and solid symbols from the WSRT.

inclination of $122\pm5^\circ$ and the orbit semi-major axis of 9.0 ± 0.5 mas. Using the $a \sin i$ derived by Marchenko et al. (2003), we can derive a distance of 1.85 ± 0.16 kpc to WR 140. This represents the first distance derived for CWB systems *independent* of stellar parameters, and together with the optical luminosity of the system implies the O star is a supergiant. In addition, total flux measurements from the VLA (Fig. 2) show that the radio variations from WR 140 are very closely the same from one orbit to the next, pointing strongly toward emission, absorption and cooling mechanisms that are controlled largely by the orbital motion (Dougherty et al. 2005).

3.2 Modelling the radio emission from WR140

Using these new system parameters, we have applied our new radiative transfer models to the spectrum of WR 140 in order to investigate the emission and absorption processes that govern the radio variations. At orbital phase 0.9, an excellent fit to the spectrum is possible (Fig. 3). The free-free flux is negligible compared to the synchrotron flux, which suffers a large amount of free-free absorption by the unshocked O-star wind, as anticipated at this orbital phase since the bulk of the WCR is "hidden" behind the photospheric radius of the O-star wind. The low frequency turnover in this model is due to the Razin effect. Similar fits can be determined for the spectrum at phase 0.8. However, we have difficulty at earlier orbital phases (~ 0.4) if the low frequency turnover is the result of the Razin effect, largely due to the low value of magnetic field strength that is required, and the commensurate extremely high acceleration efficiency that is implied. We are continuing to explore these models.

The manner in which the non-thermal radio emission is calculated gives both the spatial distribution of the magnetic field strength, the intrinsic radio synchrotron luminosity, and the population and distribution of non-thermal electrons. These can provide a robust estimate of the high energy emission from CWBs, which is very relevant given the current and planned high-energy observatories (see Pittard, these proceedings).

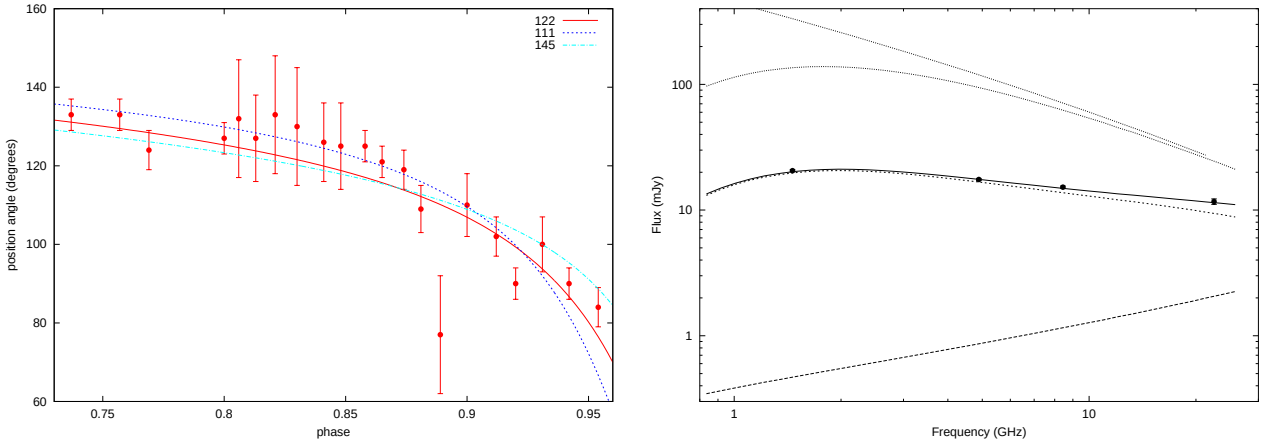

Figure 3: Left: The rotation of the WCR in WR140 as a function of phase, deduced from VLBA observations. Curves derived from known orbital parameters and three inclinations are shown, including the best-fit of 122°. Right: The spectrum of WR140 at phase 0.9. The observations are the solid circles. Various emission components from the model are shown - free-free (long-dashed), synchrotron flux (short-dashed), intrinsic synchrotron flux (dotted), and total flux (solid). The top curve shows the intrinsic synchrotron spectrum without the Razin effect.

Acknowledgments

This work was supported by the National Research Council of Canada, and the University of Prince Edward Island Co-op programme. JMP is supported by a University Research Fellowship of the Royal Society, and SMD acknowledges gratefully funding from the School of Physics and Astronomy during a visit to Leeds.

References

Dougherty S.M., Beasley A.J., Claussen M.J., Zauderer B.A., Bolingbroke N.J., 2005, ApJ, 623, 447

Dougherty S.M., Pittard J.M., Kasian L., Coker R.F., Williams P.M., Lloyd H.M., 2003, A&A, 409, 217

Dougherty S.M., Williams P.M., 2000, MNRAS, 319, 1005

Dougherty S.M., Williams P.M., Pollacco D.L., 2000, MNRAS, 316, 143

Dougherty S.M., Williams P.M., van der Hucht K.A., Bode M.F., Davis R.J., 1996, MNRAS, 280, 963

Marchenko S.V., et al., 2003, ApJ, 596, 1295

Monnier J.D., et al., 2004, ApJ, 602, L57

Pittard J.M., Dougherty S.M., Coker R., O'Connor E.P., Bolingbroke N.J., 2005, A&A, submitted

White R.L., Becker R.H., 1995, ApJ, 451, 352

Williams P.M., Dougherty S.M., Davis R.J., van der Hucht K.A., Bode M.F., Setia Gunawan D.Y.A., 1997, MNRAS, 289, 10

Williams P.M., van der Hucht K.A., Pollock A.M.T., Florkowski D.R., van der Woerd H., Wamsteker W.M., 1990, MNRAS, 243, 662

van Loo S., Runacres M.C., Blomme R., 2005, A&A, 433, 313

The *XMM-Newton* view of Plaskett's star and its surroundings

N. Linder and G. Rauw*

Institut d'Astrophysique et de Géophysique, Université de Liège, Belgium

Abstract: *XMM* data of Plaskett's star (HD 47129) are used in order to analyse its X-ray spectrum and variability and hence to derive further constraints on the wind interaction in this early-type binary (O6 I + O7.5 I) system. Combining the information provided by the EPIC and RGS instruments, we find that the X-ray spectrum of Plaskett's star is dominated by thermal plasma at lower energies, whereas the higher energy part (> 3 keV) could probably best be represented by a featureless power law component since we do not detect a significant Fe-K line. Our tests also suggest that an overabundance in nitrogen by a factor ~ 6 might be indicated to best represent the RGS spectrum. On the other hand, 71 X-ray sources have been detected in Plaskett's star field of view and most of them have counterparts in near-IR colours that are consistent with slightly reddened main-sequence objects. Actually, a sizeable fraction of the X-ray sources in the EPIC images could be either foreground or background sources with no direct connection to HD 47129.

1 Introduction

HD 47129 has first been studied by J.S. Plaskett in 1922. For this reason, HD 47129 is commonly referred to as Plaskett's star. The star is actually a spectroscopic binary system and it is believed to belong to the Mon OB2 association (at a distance of 1.5 kpc).
The first spectrum was obtained in 1921 and allowed Plaskett to assign an O5e spectral type. The spectrum of the fainter component (the secondary) appeared to be similar to the primary's one, but weaker and more diffuse. As no variations in the brightness of this system were observed, the lack of photometric eclipses renders the determination of the orbital inclination rather difficult. Plaskett estimated the diameters of the stars to be 20 and 18 $R_\odot$ and their separation to be about 128.5 $R_\odot$. Then the maximum possible inclination would be 73°, which leads to masses of 86 and 72 $M_\odot$ for the primary and secondary respectively, corresponding to the most massive stars in a binary known at that time.

Bagnuolo et al. (1992) analysed *IUE* data and found a mass ratio $q = 0.847 \pm 0.12$ (the secondary being more massive than the primary). Assuming an inclination of 70°, the mass of the primary would then be equal to 42.5 $M_\odot$, and the mass of the secondary would be equal to 51.0 $M_\odot$. These authors used a tomographic technique to separate the spectra of the two

*Research Associate FNRS, Belgium

	M/$M_\odot$	Spectral type	T_{eff} [K]	log L/$L_\odot$	R/$R_\odot$	$Vsini$ [km/s]
Primary	42.2	O7.5 I	35,100	5.80	21.5	75
Secondary	51.0	O6 I	38,400	5.57-5.94	13.8-21.1	310

Table 1: Characteristics of Plaskett's star (Bagnuolo et al. 1992)

components of the system and found spectral types of O7.5 I and O6 for the primary and for the secondary, respectively.

XMM data of Plaskett's star are used here in order to analyse its X-ray spectrum and variability and hence to derive further constraints on the wind interaction in this binary system. The observation was made on 16th March 2003 for a total exposure time of 21.621 ks. The thick filter was used to reject optical light, and the operating mode was the full window mode for all three EPIC instruments.

2 Spectral analysis

The spectra were fitted with various models using the *xspec* software. We tested several combinations of absorbed optically thin thermal plasma (`mekal`) and powerlaw models. The choice of these model components is motivated by the fact that the X-ray emission of massive stars can (to first approximation at least) be represented by an optically thin thermal plasma (e.g. Rauw et al. 2002, De Becker et al. 2004). The power law component is added to account for a possible inverse Compton tail that could be produced by relativistic electrons accelerated in the wind collision zone. In all combinations, the interstellar absorption along the line of sight of Plaskett's star was frozen at a column density of hydrogen equal to 0.15×10^{22} cm^{-2} (Diplas & Savage 1994). The statistically best fit to the EPIC data was achieved for a model `ISM`$*$[`mekal`$+$(`wabs`$*$`mekal`)$+$(`wabs`$*$`powerlaw`)] (see Fig. 1(a)). The softer mekal component

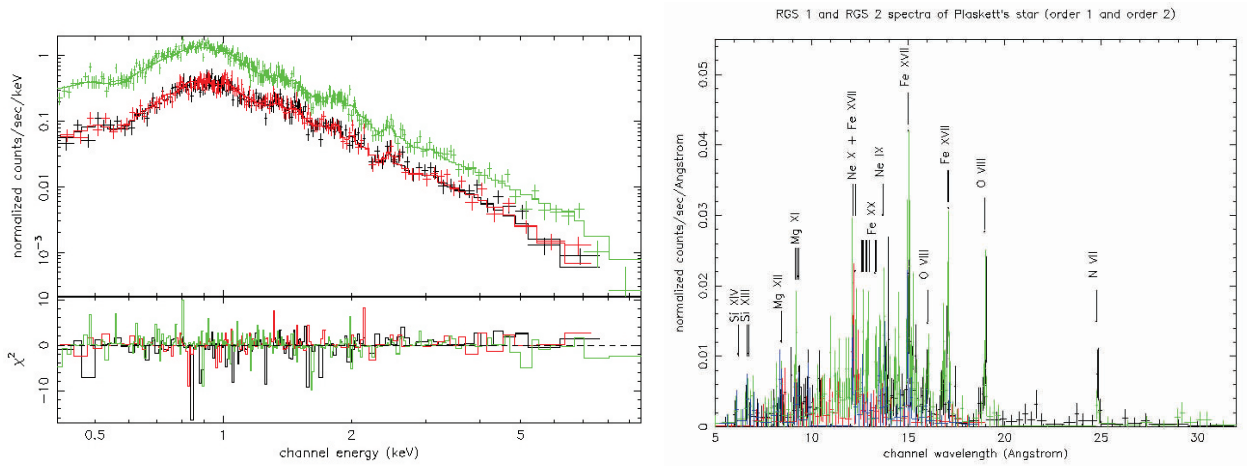

(a) (b)

Figure 1: (a) EPIC spectra of Plaskett's star from 0.4 kev to 10 keV along with the best fit model. MOS 1 is in black, MOS 2 in red and PN in green. (b) RGS spectra of Plaskett's star. The first order of RGS 1 is in black, and its second order is in red. The first order of RGS 2 is in green, and the second order in blue.

of this model has a temperature of 0.64 keV, quite typical of the intrinsic X-ray emission of O-type stars. The other mekal component has a temperature of 1.25 keV. Although it is harder than expected for shocks intrinsic to the winds, this value is not as extreme as the temperature seen for several other colliding wind binaries. Finally, the power law component has a photon index of 2.6. This value is quite large, but is reminiscent of the results obtained for other O-star binaries (e.g. HD 159176, De Becker et al. 2004).

The N VII Lyα line at 24.8 Å is quite intense in the RGS spectra (see Fig. 1(b)) despite the large ISM absorption. This prompted us to test also models with a variable nitrogen abundance. When only EPIC data are fitted, no improvement is observed and the nitrogen tends to disappear. Actually, the power law component with $\gamma \sim 2.6$ seems to account for the bump at 0.5 keV in the EPIC spectra. On the other hand, for all models tested, when only the RGS data are fitted, the fit yields a nitrogen overabundance by a factor ~ 6 compared to solar. With its superior spectral resolution, the RGS allows us to see that the 0.5 keV feature is actually due to N VII line emission rather than continuum. This suggests that, if a power law component is indeed present in the X-ray spectrum of HD 47129, it is probably not as steep as indicated by the EPIC fits.

3 Surroundings of Plaskett's star

71 serendipitous sources have been detected in Plaskett's star field of view. Among these sources, only a fraction corresponds to known objects. The positions of these X-ray sources have been compared to three existing catalogues in order to determine whether they have a counterpart at other wavelengths: the GSC (Guide Star Catalogue), USNO (United States Naval Observatory) and 2MASS (Two MicronsAll Sky Survey). 37 sources have at least one counterpart in each of the three catalogues, and for 32 of them this counterpart is unique. On the other hand, there are 25 sources for which no counterpart could be found in any of the three catalogues.

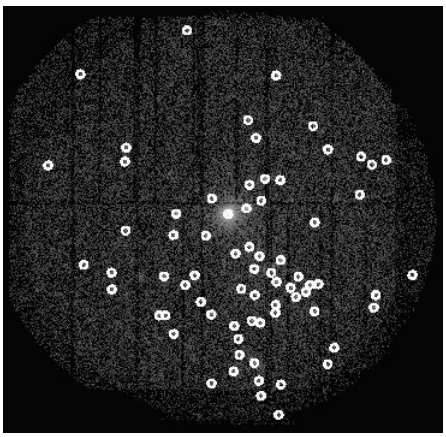

Figure 2: Detection of 71 secondary sources in the EPIC field of view around Plaskett's star.

The open cluster NGC 2244, situated in the Rosette Nebula, forms the nucleus of the Mon OB2 association. Plaskett's star lies at an angular distance of 107 arcmin from the core of NGC 2244. Assuming that Plaskett's star is situated at the same distance from Earth as NGC 2244 (1.5 kpc, Berghöfer & Christian 2002), they are separated by at least 46.7 pc, which means that HD 47129 is too far from the cluster to belong to it. Furthermore, the peculiar

velocity of the star is rather low, making it unlikely that the binary formed in the cluster and was ejected through subsequent dynamical interactions.
On statistical grounds, a sizeable fraction of the X-ray sources in the field of view could be either foreground or background sources. On the other hand, Berghöfer & Christian (2002) found an important number of X-ray bright pre-main sequence stars in NGC 2244. Although HD 47129 is probably not a member of NGC 2244, one could nevertheless expect a priori that a fraction of the X-ray sources near the star might be pre-main sequence objects. However, there is no clear excess of X-ray sources that could reveal the presence of a sizeable population of low-mass pre-main sequence stars in the surroundings of Plaskett's star.
This fact is confirmed by the $J - H$ vs. $H - K$ diagram derived from the 2MASS data and shown on Fig. 3. The classical T Tauri stars have circumstellar disks that produce an infrared excess and they are thus mostly found towards the right of the reddening band (Meyer et al. 1997). We can see on Fig. 3 that only one source of Plaskett's star field is actually a good candidate for a classical T Tauri star.

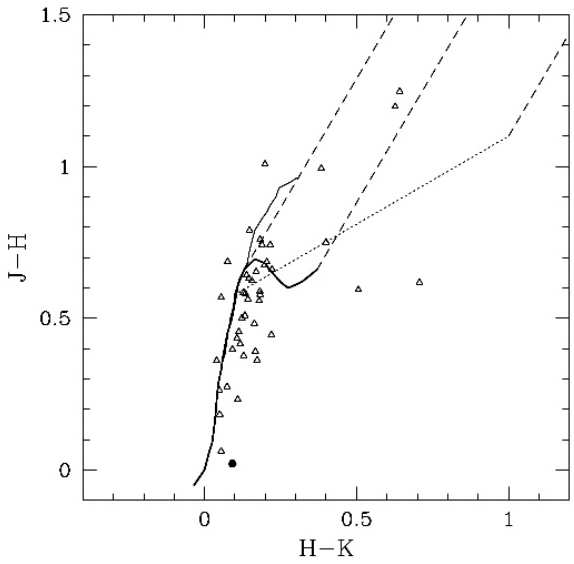

Figure 3: JHK colour-colour diagram of the 2MASS counterparts of the X-ray sources in the EPIC field of view around HD 47129. The solid bold line yields the intrinsic near-IR colours of main sequence stars while the other solid line is the locus of unreddened giants. The dotted straight line yields the locus of dereddened colours of classical T Tauri stars, whereas the dashed lines form the reddening band for normal dwarf stellar photospheres. Plaskett's star is indicated by a filled circle.

References

Bagnuolo W.G., Gies D.R., Wiggs M.S., 1992, ApJ, 385, 708
Berghöfer T.W., Christian D.J., 2002, A&A, 384, 890
De Becker M., Rauw G., Pittard J.M., et al., 2004, A&A, 416, 221
Diplas A., Savage B.D., 1994, ApJS, 93, 211
Meyer M.R., Calvet N., Hillenbrand L.A., 1997, AJ, 114, 288
Rauw G., Blomme R., Waldron W.L., et al., 2002a, A&A, 394, 993

Non-thermal X-ray and gamma-ray emission from the colliding wind binary WR 140

J. M. Pittard [1] and S. M. Dougherty [2]

[1]School of Physics and Astronomy, The University of Leeds, Leeds, UK
[2]National Research Council, Herzberg Institute of Astrophysics, DRAO, Penticton, Canada

Abstract: WR 140 is the archetype long-period colliding wind binary (CWB) system, and is well known for dramatic variations in its synchrotron emission during its 7.9-yr, highly eccentric orbit. This emission is thought to arise from relativistic electrons accelerated at the global shocks bounding the wind-collision region (WCR). The presence of non-thermal electrons and ions should also give rise to X-ray and γ-ray emission from several separate mechanisms, including inverse-Compton cooling, relativistic bremsstrahlung, and pion decay. We describe new calculations of this emission and make some preliminary predictions for the new generation of gamma-ray observatories. We determine that WR 140 will likely require several Megaseconds of observation before detection with INTEGRAL, but should be a reasonably strong source for GLAST.

1 Introduction

CWB systems are an important laboratory for investigating the underlying physics of particle acceleration since they provide access to higher mass, radiation and magnetic field energy densities than in supernova remnants, which have been widely used for such work. High-resolution observations (e.g., Williams et al. 1997; Dougherty et al. 2000, 2005) show that the particle acceleration site is where the massive stellar winds collide - the WCR. In addition to synchrotron radio emission, these non-thermal particles should give rise to X-ray and γ-ray emission from several separate mechanisms, including inverse-Compton (IC) cooling, relativistic bremsstrahlung, and pion decay, though definitive evidence for such emission does not yet exist. The advent of new and forthcoming observatories (INTEGRAL, GLAST and VERITAS) will dramatically improve the chance of detecting these systems, and in this paper we make new predictions for the expected flux from WR 140.

Previous predictions of the IC emission have been based on the assumption that the ratio of the luminosity from IC scattering to the synchrotron luminosity is equal to the ratio of the photon energy density, $U_{\rm ph}$, to the magnetic field energy density, $U_{\rm B}$:

$$\frac{L_{\rm ic}}{L_{\rm sync}} = \frac{U_{\rm ph}}{U_{\rm B}}. \quad (1)$$

However, the use of this equation is rather unsatisfactory for a number of reasons. For example, $L_{\rm sync}$ is typically set to the *observed* synchrotron luminosity, whereas free-free absorption by

the extended wind envelopes can be significant (see Pittard et al. 2005). In such cases the intrinsic synchrotron luminosity, and thus the non-thermal X-ray and γ-ray luminosity, will be underestimated. The predictive power of Eq. 1 is also greatly undermined by the fact that the magnetic field strength in the WCR of CWB systems is generally not known with any certainty. Since $U_{\rm B} \propto B^2$, small changes in the estimated value of B can lead to large changes in $L_{\rm ic}$ (see Fig. 3 in Benaglia & Romero 2003).

A more robust estimate of the IC emission from CWB systems can be acquired from model fits to radio data, where the population and spatial distribution of non-thermal electrons is determined (see Dougherty et al. 2003 and Pittard et al. 2005). A key improvement in these papers over earlier modelling of the radio emission from CWB systems is the use of a hydrodynamical model to describe the stellar winds and WCR. The free-free emission and absorption coefficients are determined from the local temperature and density values on the hydrodynamic grid. Particle acceleration at the shocks bounding the WCR creates a population of non-thermal particles with a power-law energy distribution (i.e. $n(\gamma) \propto \gamma^{-p}$, where γ is the Lorentz factor) - as these advect downstream IC cooling modifies the energy distribution of non-thermal electrons. Since the population of non-thermal particles is not determined from first principles, their energy density is normalized to some fraction ($\zeta_{\rm rel,e}$ and $\zeta_{\rm rel,i}$ for the electrons and ions, respectively) of the thermal energy density ($U_{\rm th}$) at the shocks. For the non-thermal electrons, IC cooling reduces this fraction below $\zeta_{\rm rel,e}$ in the downstream flow. Similarly, the magnetic field energy density is normalized by setting $U_{\rm B} = \zeta_{\rm B} U_{\rm th}$. When modelling specific systems, $\zeta_{\rm B}$ and $\zeta_{\rm rel,e}$ are chosen to best match the observed radio emission. Predictions for the IC and relativistic bremsstrahlung emission then follow since these arise from the same non-thermal relativistic electrons which are responsible for the synchrotron radio emission.

2 The high energy non-thermal emission

In our current calculations we assume that IC scattering is isotropic and takes place in the Thomson regime. Since the average photon energy of an early-type star, $h\nu_* \sim 10$ eV, Lorentz factors of order $10 - 10^4$ are sufficient to produce IC X-ray and γ-ray radiation. The resulting emission has a spectral shape which is identical to the synchrotron emission at radio frequencies. Bremsstrahlung radiation at γ-ray energies is emitted from relativistic electrons since photons of comparable energy to that of the emitting particle can be produced. Finally, it is possible to obtain γ-ray emission from hadronic collisions involving non-thermal ions, through the decay of neutral pions, e.g., $p+p \rightarrow \pi^0+X$, $\pi^0 \rightarrow \gamma+\gamma$. The pion decay process yields information on the population of non-thermal nucleons, in contrast to the IC and bremsstrahlung processes where the emission is dependent on the population of non-thermal electrons. We conservatively set the energy density ratio of non-thermal ions to electrons, $\zeta_{\rm rel,i}/\zeta_{\rm rel,e}$, to 20. Further background to the calculations can be found in Pittard & Dougherty (2006).

3 Models of WR 140

We apply our model to WR 140, the archetype of long-period CWB systems. It consists of a WC7 star and an O4-5 star in a highly elliptical orbit ($e \approx 0.88$), and in the context of the present paper is most noteable for its possible association with an EGRET source, lying on the outskirts of the positional error box of 3EG J2022+4317 (Romero et al. 1999). We adopt the orbital parameters and mass-loss rates determined by Dougherty et al. (2005), but allow the mass-loss rate of the O star (and thus the wind momentum ratio η) to vary, as this

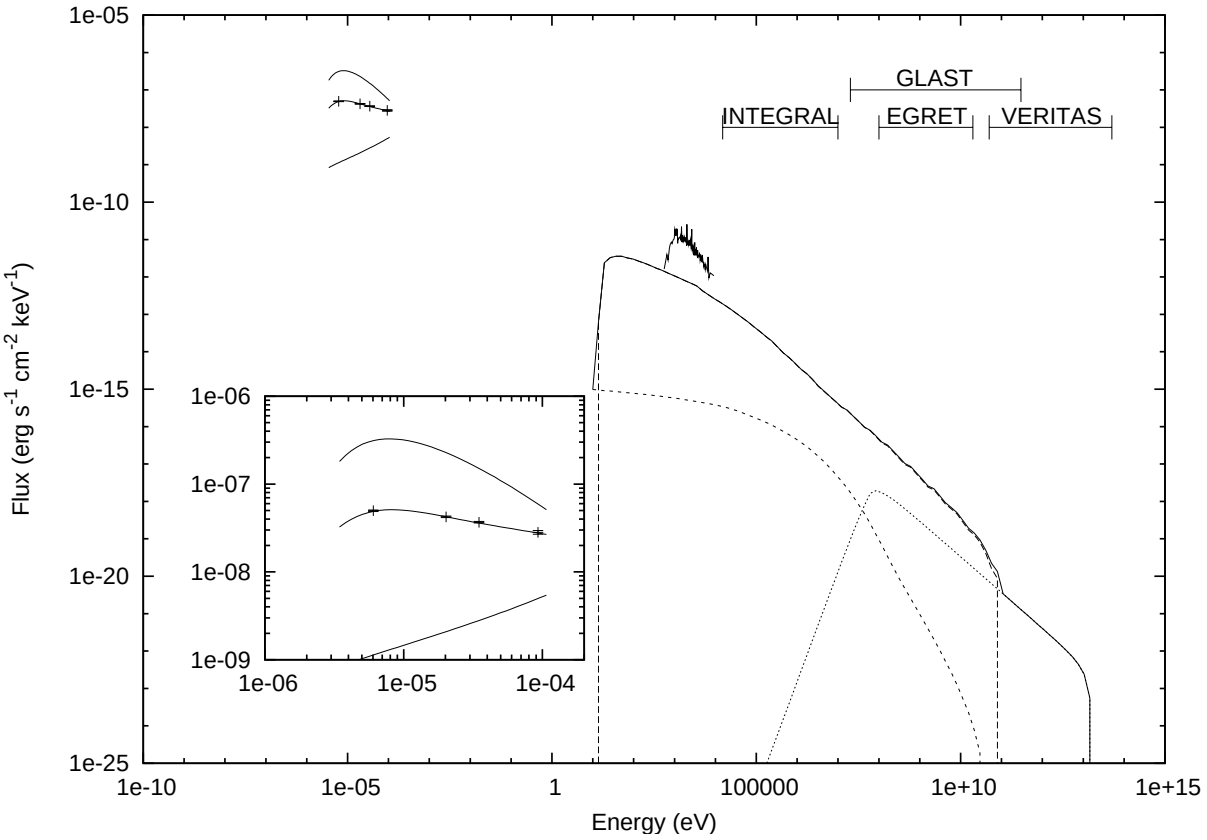

Figure 1: The radio, and non-thermal UV, X-ray and γ-ray emission calculated from our model of WR 140 at $\phi = 0.9$, together with the observed radio and X-ray flux. The model radio data that we show indicate the thermal free-free flux (displayed below the data points), the *intrinsic* synchrotron flux (displayed above the data points), and the total observed emission. This region is expanded in the inset. The IC (long dash), relativistic bremsstrahlung (short dash), and pion decay (dotted) emission are shown as separate components, and their sum is also displayed (solid). No absorption has been included in the calculation of the high-energy emission. We also show the observed X-ray spectrum obtained at $\phi = 0.84$ with *ASCA* (dataset 27022010, observed on 1999-10-22). It is reassuring that the IC flux predicted from our model is less than the observed X-ray flux.

parameter is not well determined. The system distance is assumed to be 1.85 kpc. Further details on the modelling can be found in Pittard & Dougherty (2006) and Dougherty et al. (these proceedings).

Given the wealth of observational data which now exists for WR 140, we have concentrated on obtaining a reasonable spectral fit to the radio data at a specific orbital phase, namely $\phi = 0.9$. Fig. 1 shows the resulting fit where it is clear that the intrinsic synchrotron emission suffers significant free-free absorption by the extended circumbinary envelope. A key point is that the large ratio between the intrinsic and observed synchrotron emission implies that the IC luminosity predicted using Eq. 1 will be substantially underestimated.

The high energy emission resulting from the radio fit is also shown in Fig. 1. The IC emission dominates for photon energies less than 50 GeV, while the emission from pion decay reaches energies up to 15 TeV. The relativistic bremsstrahlung emission is a minor contributor to the total non-thermal flux, and does not dominate at any energy. A gradual steepening of the IC spectrum occurs between $10^2 - 10^6$ eV. The lack of a clearly defined spectral break reflects the

fact that the break frequency is spatially dependent, and so is smoothed out once the flux is integerated over the entire WCR (Pittard et al. 2005).

The total photon flux in the 100 MeV - 20 GeV EGRET band from our model is 3×10^{-8} ph s^{-1} cm^{-2}, which is an order of magnitude below the flux detected from 3EG J2022+4317 during the December 1992 observation at $\phi = 0.97$. The different phases prevent a direct comparison, but we expect that the IC emission will increase between $\phi = 0.9 - 0.97$ as the stellar separation more than halves. Considering the limitations of the present model, this level of agreement is satisfactory. We predict a photon flux in the 15 keV-10 MeV sensitivity range of the IBIS instrument onboard INTEGRAL of 1.4×10^{-4} ph s^{-1} cm^{-2}, which is likely to require an exposure time greater than 3 Msec for a 5σ detection. The predicted 20 MeV-300 GeV photon flux is 1.4×10^{-7} ph s^{-1} cm^{-2}, and thus WR 140 should be fairly easily detected by GLAST. Our flux predictions are approximately 7 times lower than those made by Benaglia & Romero (2003) - this is partly due to the greater distance which we assume for WR 140.

4 Conclusions

We have presented predictions of the high energy non-thermal flux from WR 140. We find that a long observation will be required for detection of WR 140 with INTEGRAL, but it should be a reasonably strong source in the GLAST energy band. The current neglect of two-photon pair production prevents us from making predictions for the flux in the sensitivity range of VERITAS, a Cherenkov air shower telescope array. However, we expect that this absorption mechanism will significantly attenuate the emission in the TeV range and suggest that other CWB systems which are wider and less distant (e.g., WR 146 and WR 147) may be better targets at these energies. Improved high energy data will drive the development of theoretical models which include anisotropic IC emission and two-photon pair production, and will allow a much more detailed comparison between observations and predictions.

Acknowledgements

JMP gratefully acknowledges funding from the Royal Society.

References

Benaglia P., Romero G.E., 2003, A&A, 399, 1121

Dougherty S.M., Beasley A.J., Claussen M.J., Zauderer B.A., Bolingbroke N.J., 2005, ApJ, 623, 447

Dougherty S.M., Pittard J.M., Kasian L., Coker R.F., Williams P.M., Lloyd H.M., 2003, A&A, 409, 217

Dougherty S.M., Williams P.M., Pollacco D.L., 2000, MNRAS, 316, 143

Pittard J.M., Dougherty S.M., Coker R.F., Bolingbroke N.J., O'Connor E., 2005, A&A, submitted

Pittard J.M., Dougherty S.M., 2006, MNRAS, submitted

Romero G.E., Benaglia P., Torres D.F., 1999, A&A, 348, 868

Williams P.M., Dougherty S.M., Davis R.J., van der Hucht K.A., Bode M.F., Setia Gunawan D.Y.A., 1997, MNRAS, 289, 10

Can single O stars produce non-thermal radio emission? Or are they binaries?

S. Van Loo [1, 2]

[1] Royal Observatory of Belgium, Belgium
[2] School of Physics and Astronomy, University of Leeds, UK

Abstract: We present qualitative models for the non-thermal radio emission of single O stars, in terms of synchrotron emission by wind-embedded shocks. When we include the fact that shocks weaken as they move out with the wind, as predicted by time-dependent hydrodynamical simulations, these models produce a radio spectrum with a positive slope (as function of frequency), in contradiction with the observed negative slope. We conclude that non-thermal radio emission cannot originate from wind-embedded shocks, and is likely to be caused by a wind-colliding shock. A radio light curve analysis of two non-thermal O stars that are generally assumed to be single supports this conclusion.

1 Introduction

Many O stars are observable at radio frequencies, due to free-free emission from the circumstellar ionised gas. The emergent *thermal* radio spectrum is of the form $F_\nu \propto \nu^{+0.6}$, where the power +0.6 is referred to as the spectral index. However, a significant fraction of the brightest O stars have a radio spectrum that differs strongly from thermal wind emission (Bieging et al. 1989). Instead of the characteristic positive index, the radio spectrum has a negative spectral index, i.e. the flux decreases as a function of frequency. This *non-thermal* radio emission is synchrotron radiation from relativistic electrons gyrating in a magnetic field (White 1985). These synchrotron-emitting electrons are accelerated to relativistic energies by the first-order Fermi mechanism at shocks (Bell 1978).

A fundamental question regarding non-thermal radio emission is its correlation with binarity. For Wolf-Rayet stars, the evolutionary descendants of O stars, this link is already well established, i.e. a binary component is a prerequisite for non-thermal radio emission (Dougherty & Williams 2000). For binaries, the shocks needed for the acceleration of the electrons arise where two stellar winds collide (Eichler & Usov 1993). The situation is less clear for the O stars. Roughly two thirds of the non-thermal O stars are confirmed binary or multiple systems. For the other stars, binarity has not been established. In these single stars, shocks are generated by the line-deshadowing instability of the radiative driving mechanism (Owocki et al. 1988).

"Massive Stars and High Energy Emission in OB Associations"; Proc. JENAM 2005 *Distant Worlds*, Liège (Belgium), eds. Rauw et al., p. 61-64

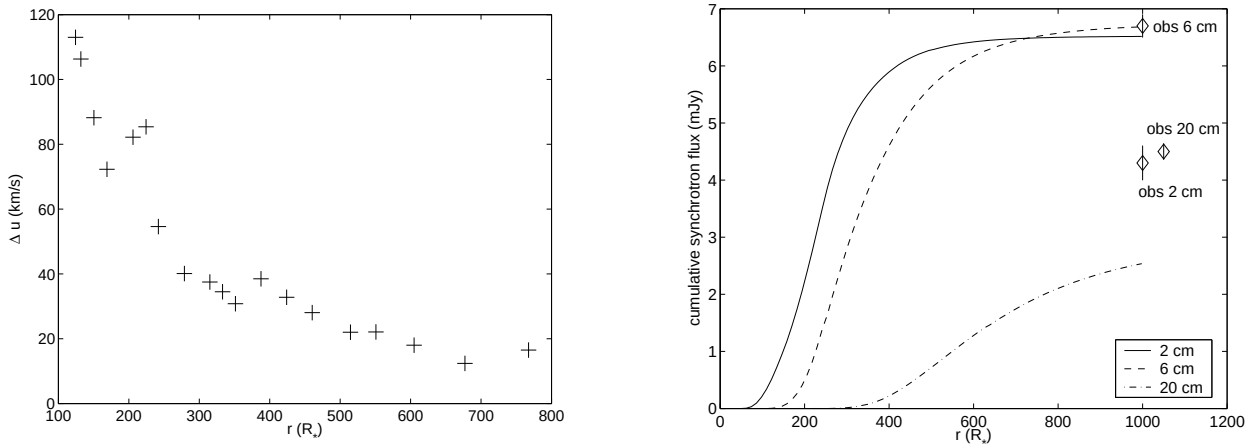

Figure 1: (a) *left panel*: The shock velocity jump (plus signs) of a typical strong shock in the periodic box model of Runacres & Owocki (2005), as function of radius. (b) *Right panel*: Emergent synchrotron fluxes due to all shocks between the stellar surface and a position r in the wind, at 2 cm (solid line), 6 cm (dashed) and 20 cm (dash-dotted). The diamonds are the observed synchrotron fluxes of Cyg OB2 No. 9 and also the error bar is given.

2 Synchrotron models for single stars

Electrons are accelerated at a shock by the first-order Fermi acceleration mechanism (Bell 1978). By crossing the shock front many times, an electron can be accelerated to relativistic energies. Once the electron leaves the shock front, the acceleration ceases and cooling mechanisms - such as inverse Compton scattering and adiabatic cooling (e.g. Chen 1992) - will reduce its energy. The synchrotron-emitting electrons cannot travel far from the shock front before being completely thermalised. Therefore the synchrotron emission is limited to narrow layers behind a shock.

Van Loo et al. (2005a) showed that the synchrotron flux F_ν produced by a single shock is proportional to Δu^3, where Δu is the velocity jump across the shock. The dependence of the synchrotron emission on the compression ratio χ of the shock is more complicated, but the flux also increases with χ. This means that the shocks with the highest χ and Δu dominate the synchrotron emission. Therefore, the distribution and strength of instability-generated shocks has important consequences for the results of our synchrotron models.

Time-dependent hydrodynamical simulations show that a hot-star wind is filled with shocks out to very large distances in the wind (e.g. Runacres & Owocki 2005). In Fig. 1a we show the shock velocity jump of a typical strong shock as a function of radius. The shocks are strongest close to the star, and gradually weaken as they move outward with the flow. As the flux is a strongly increasing function of the shock velocity jump (i.e. $F_\nu \propto \Delta u^3$), this means that the synchrotron emission declines rapidly as a function of radius.

Due to the large free-free opacity of the wind at radio wavelengths, only photons produced at large distances can be observed. All the photons emitted too close to the star are absorbed. By analogy we call the radius of unit optical depth at e.g. 2 cm the *radio photosphere* at that wavelength. Due to the wavelength-squared dependence of the free-free opacity, the size of the radio photosphere increases with wavelength. For the non-thermal emitter Cyg OB2 No. 9, the radio photosphere at 2 cm is 90 R_* and 190 R_* at 6 cm.

The emergent flux is determined by the interaction between the non-thermal emission and the thermal absorption. Let us concentrate on the flux produced at 2 and 6 cm. Due to the free-free absorption, the synchrotron emission at 2 and 6 cm is produced in different regions of

the wind. For Cyg OB2 No. 9, the 2 cm photons are absorbed within 90 R_* of the star, while at 6 cm the photons are absorbed up to 190 R_* (see Fig. 1b). Thus the inner-wind shocks contribute more to the flux at 2 cm than at 6 cm. Recall that these inner-wind shocks also produce more emission. It is then difficult to produce much more 6 cm flux than 2 cm flux (see Fig. 1b). Adding the contribution by free-free emission of the wind, the emergent radio spectrum has a positive spectral index, contrary to the observations (Van Loo et al. 2005b).

We have investigated some possibilities by which we can reconcile the results of the hydrodynamical simulations with the observed non-thermal emission. We find that the observations can only be reproduced by counteracting the rapid radial decrease of the synchrotron emission. As the emission is directly proportional to the shock velocity jump, a natural way to get a slower decline is to assume a weaker radial dependence of Δu. Numerical simulations show that, to reproduce the non-thermal spectrum, the shock velocity jump must be nearly constant between 100 and 1 000 R_*. However, it is highly unlikely that the shock strength is constant over such large distances.

We also examined the effect of re-acceleration - the main mechanism by which previous authors (Chen 1992) were able to reproduce the observed non-thermal spectra. These authors included the ad-hoc shock model of Lucy (1982) in their synchrotron models. In the Lucy model, relativistic electrons can travel from one shock to another before being thermalised. Relativistic electrons are then accelerated in subsequent shocks, leading to a larger population of relativistic electrons in the outer wind. Thus re-acceleration substantially slows down the decrease of the synchrotron emission. However, in time-dependent hydrodynamical simulations (e.g. Runacres & Owocki 2005), shocks always occur in pairs at either side of a dense shell. Electrons can then only encounter a single shock before being trapped in a shell. Consequently, re-acceleration is highly unlikely in a instability-generated shock structure and of no importance in our models (Van Loo et al. 2005b).

Based on the models, we conclude that the observed emission is probably not from wind-embedded shocks associated with the line-deshadowing instability.

3 Synchrotron model for binary stars

In the previous section we showed that the observed non-thermal emission cannot be produced in the wind of a single star. As all non-thermal Wolf-Rayet stars appear to be in a binary system, the most likely alternative is that, in non-thermal O stars, the emission is also produced in a wind-collision shock associated with a binary or multiple system.

In the simplest case of wind-collision system, i.e. a binary, the radio flux changes are due to changes in the orbit (e.g. WR 140). This means that the flux variations are repeatable from period to period. In the radio light curve of Cyg OB2 No. 9 (a star currently believed to be single), we find an unambiguous period of $\sim$ 2.4 yr (see Fig. 2). A similar result is found for HD 168112 (also believed to be single), where we find a period of 1.4 yr (Blomme et al. 2005).

How the period from the radio light curve relates to an orbital period is yet unclear. For WR 140, the best studied wind-collision binary, the radio period is identical to the orbital period (White & Becker 1995). However, this is not true for Cyg OB2 No. 5. Although the orbital period of the O-star binary Cyg OB2 No.5 is only 6.6 days, the radio flux changes over a period of the order of years (Miralles et al. 1994). A solution was offered when high-resolution radio imaging revealed a secondary source in this system, i.e. a wind-collision region where the O-binary wind collides with a nearby B star (Contreras et al 1999). However, the observed flux changes are predominantly due to the binary and are not coming from the wind-collision region (Dougherty, pers. comm.). Therefore, the fact that a period is found in the radio light

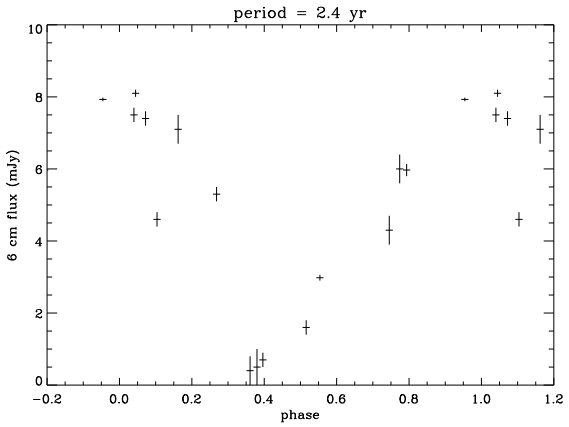

Figure 2: The 6 cm radio fluxes of Cyg OB2 No. 9, folded with a 2.4 yr period (Van Loo 2005). Note that some observations are plotted twice. Phase 0.0 was arbitrarily set at 1 Jan 1980.

curves of Cyg OB2 No. 9 and HD 168112 is only an indication that these stars are binaries.

4 Conclusions

We found that the observed non-thermal radio spectra cannot be produced by instability-generated shocks associated with a chaotic, unstable wind. The most likely alternative is synchrotron emission from shocks associated with colliding winds. All non-thermal O stars should thus be members of a binary or multiple system. Additional observations (radio monitoring, interferometry, radio imaging, etc ...) are necessary to confirm this hypothesis.

References

Bell A.R., 1978, MNRAS, 182, 147
Bieging J.H., Abbott D.C., Churchwell E.B., 1989, ApJ, 340, 518
Blomme R., Van Loo S., De Becker M., et al., 2005, A&A, 436, 1033
Chen W., 1992, PhD Thesis John Hopkins Univ., Baltimore, MD
Contreras M.E., Rodriguez L.F., Tapia M., et al., 1997, ApJ, 488, 153
Dougherty S.M., Williams, P.M., 2000, MNRAS, 319, 1005
Eichler D., Usov V., 1993, ApJ, 402, 271
Lucy L.B., 1982, ApJ, 255, 286
Miralles M.P., Rodriguez L.F., Tapia M., et al., 1994, A&A, 282, 547
Owocki S.P., Castor J.I., Rybicki G.B., 1988, ApJ, 335, 914
Runacres M.C., Owocki S.P., 2005, A&A, 429, 323
Van Loo S., 2005, PhD Thesis K.U. Leuven, Belgium
Van Loo S., Runacres M.C., Blomme R., 2005a, A&A, 433, 313
Van Loo S., Runacres M.C., Blomme R., 2005b, submitted to A&A
White R.L., 1985, ApJ, 289, 698
White R.L., Becker R.H., 1995, ApJ, 451, 352

Are WC9 Wolf-Rayet stars in colliding-wind binaries?*

P. M. Williams [1], K. A. van der Hucht [2,3] and G. Rauw [4†]

[1]Institute for Astronomy, University of Edinburgh, United Kingdom
[2]SRON Netherlands Institute for Space Research, Utrecht, The Netherlands
[3]Astronomical Institute Anton Pannekoek, University of Amsterdam. The Netherlands
[4]University of Liège, Astrophysics Institute, Belgium

Abstract: We present results from a spectroscopic search for massive companions to dust-making Galactic WC9 stars as a step to testing the paradigm that dust formation in these systems requires colliding winds to produce over densities. We find evidence for OB companions to the WC9 stars WR 59 and WR 65, but not WR 121 or WR 117. We identify lines of N III-V and possibly N II in the spectrum of WR 88, one of the few Galactic WC9 stars which do not make circumstellar dust, and suggest that WR 88 is a transitional WN–WC9 object and less evolved than the other WC9 stars. On the other hand, the possible identification of a strong emission line at 4176Å in the spectrum of WR 117 with Ne I suggests that this star is more evolved than other WC9 stars studied.

1 Wolf-Rayet dust formation and binarity

Infrared observations over the last 30+ years have shown that WC-type Wolf-Rayet stars make dust, but the mechanism for this is still not understood. Studies have shown that dust formation by WR stars requires that their winds contain regions of significantly higher density. These can be provided by shocks in colliding stellar winds (Usov 1991) if the WR stars are members of massive binary systems. Observational support for this process comes from the infrared light curve of the episodic WC7+O5 dust-maker WR 140, which makes dust very briefly during periastron passage when the pre-shock wind density is highest (Williams 1999), and from the rotating 'pinwheels' of heated dust formed by the persistent dust-makers WR 104 (Tuthill, Monnier & Danchi 1999) and WR 98a (Monnier, Tuthill & Danchi 2000), which are considered to be binaries observed at low inclination angle. The presence of heated dust around most WC9 stars then prompts the question: are all dust-making WC9 stars colliding-wind binaries? As a step to answering this question, we observed (Williams & van der Hucht 2000, Paper I) a selection of WC9 stars with the 1.9-m telescope at the SAAO and found absorption lines attributable to companions to the WC9 stars in the spectra of WR 104 and WR 69. We also

*Based on data collected at the European Southern Observatory (La Silla, Chile)
†Research Associate FNRS (Belgium)

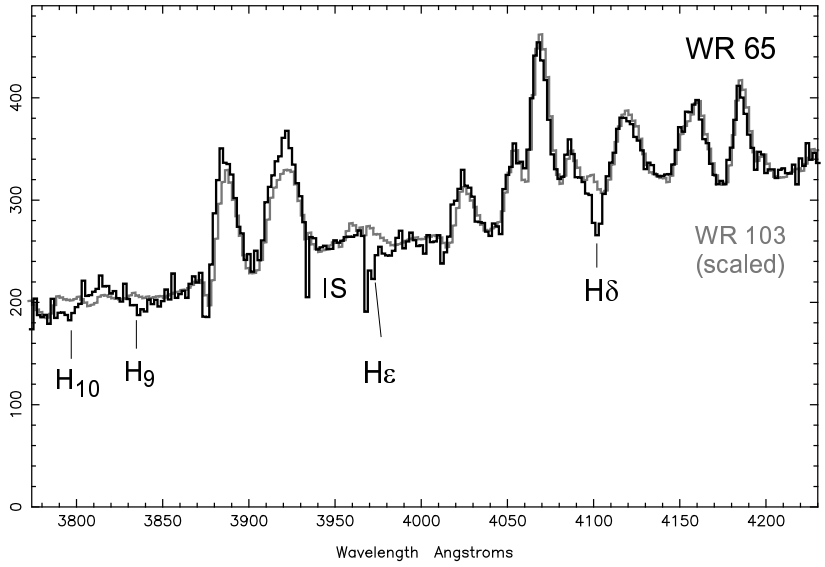

Figure 1: The spectrum of WR 65 compared with that of WR 103 (grey), scaled to match that of WR 65. Balmer lines H_{10}, H_9, Hϵ (in the wing of interstellar Ca II H) and Hδ are clearly visible in WR 65.

found spectroscopic differences between two non-dusty WC9 stars and the dusty stars in our sample, suggesting a compositional difference having a bearing on dust formation.

Here we report a follow-up of that study, based on medium-dispersion ($\sim$ 1Å) spectra observed with EMMI on the ESO NTT in 2001 June. We used Grating 3 at two settings, centred near 4000Å ('violet') and 4150Å ('blue'), to search for Hγ and higher-n Balmer and He I absorption lines indicative of OB companions. For our candidates, we included the WC9 stars noted as having diluted emission-line spectra in the VIIth Catalogue (van der Hucht 2001). Because Hγ and Hδ lie close to emission lines, we found that Hϵ and H_9, which are located in clearer regions of the spectrum, were good diagnostics despite their relative weakness.

We discovered Balmer absorption lines in our EMMI spectra of WR 59 and WR 65, but not in those of WR 121 or WR 117. The 'violet' spectrum of WR 65 is shown in Fig. 1, where it is compared with the spectrum of WR 103, a well-observed, 'typical' WC9 star. The 'blue' spectrum showed Hγ absorption. Our spectra of WR 59 are similar to those of WR 65, but also show weak absorption on top of the 4025Å He I + He II and 4472Å He I profiles, and also possibly He I at 4387Å. From the apparent absence of He I absorption in WR 65, its companion may be of earlier subtype than that in WR 59 but further work, using synthetic composite spectra, is needed to estimate strengths of He II lines to classify the companions. Together with Paper I, we have spectroscopic companions to 4/11 WC9 systems observed. Our results suggest we should detect any OB companions at least as luminous as the WC9 stars. The three WC9 stars with known luminosities have $-4.16 \geq M_v \geq -4.97$ (VIIth Catalogue), so there could still be undetected main-sequence OB companions.

Confirmation that the absorption lines do come from a companion require observation of RV shifts attributable to orbital motion. We re-observed WR 69, found to have a companion in our SAAO spectroscopy, and found that there was indeed a relative shift in RVs (absorption – emission) between SAAO and ESO observations, making this star a prime candidate for an orbital analysis.

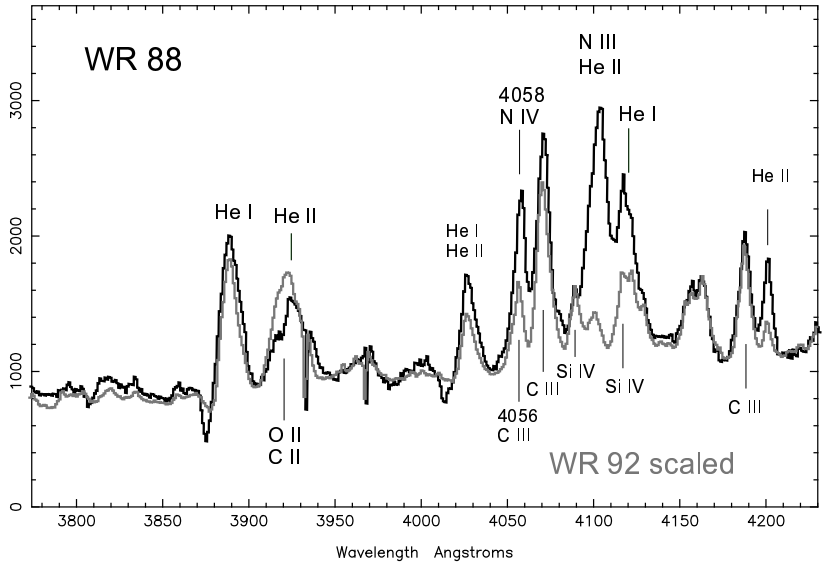

Figure 2: Part of the spectrum of WR 88, compared with that of another dust-free WC9 star, WR 92 (grey), scaled to match the C III lines in WR 88. From comparison of the He II lines, we believe most of the 4101Å line comes from another ion, which we suggest is N III, while from comparison of the C III lines, we suggest that N IV is a major contributor to the line at 4058Å.

2 Spectral diversity: an evolutionary sequence?

We observed in Paper I that the spectra of two WC9 stars (WR 81 and WR 92), which had never (in 20+ years of IR photometry) shown dust emission, differed from the other WC9 stars in having weaker O II (relative to C II), and stronger He II lines, suggesting a compositional difference. Previously, Torres & Conti (1984) had found that the spectrum of the dust-free WC9 star WR 88 differed from those of the other WC9 stars in having stronger He II and weaker C II lines. We re-observed WR 88 with EMMI to see if its O II/C II ratio resembled those of WR 81 and WR 92 in being lower than in dust-forming WC9 stars. Our spectra of WR 88 (the 'violet' spectrum is compared with that of WR 92 in Fig. 2) confirmed the strengths of the lines at 4101Å and 4200Å but other He II lines, e.g. those near 3968Å and 3923Å, are not stronger. We deduce that most of the 4101Å feature in WR 88 must come from another ion, for which we propose multiplet 1 of N III. Multiplet 6 of N III could contribute to He II line at 4200Å and we observe multiplet 17 at 4379Å in our 'blue' spectrum. The 4650Å C III line is stronger and broader in WR 88 and does not have the P-Cygni absorption component seen in WR 92, possibly due to the strong N III 4640Å multiplet. We confirm the identification of the 4603Å line with N V as we also see the 4619Å line of the same multiplet. As shown in Fig. 2, WR 88 appears to have N IV 4058Å blended with C III 4056Å, which is much weaker in WR 92.

We examined the 10-Å resolution spectra of WR 88 and WR 92 in the Torres & Massey (1987) atlas and observed other differences, e.g. the presence in WR 88 of the N IV 5200Å and 7117Å and N V 4933-45Å lines seen in WN stars (cf. Hamann, Koesterke & Wessolowski 1995). We may also be seeing some N II lines in WR 88, but this needs confirmation with higher resolution spectroscopy.

We conclude that WR 88 either has a WN companion or is of a previously unobserved transitional WN–WC9 type, and prefer the latter alternative since the N lines have comparable widths to the C lines, suggesting formation in the same wind. This would make WR 88 less evolved than WR 92 and WR 81, and even less evolved than the dust-making WC9 stars.

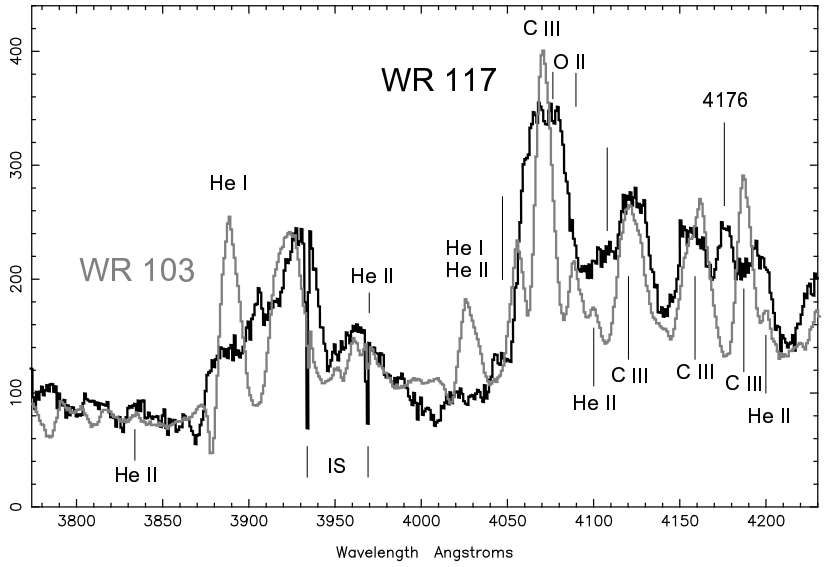

Figure 3: Spectrum of WR 117, compared with that of WR 103 (grey). Note the weakness of the He I lines in WR 117, and the line at 4176Å.

While WR 88, WR 92 and WR 81 appear to be less evolved than most of the WC9 stars, we found one star to be apparently more evolved: WR 117. We had time to observe only a 'violet' spectrum (Fig. 3), which appears to be significantly different from that of WR 103. The lines in WR 117 are broader than in WR 103, but comparisons with another broad-lined WC9 star, WR 53 (Paper I), and the WC8 star WR 135 (Torres & Massey), show similar differences. The feature at 4176Å does not appear to coincide with ions usually seen in WR stars, and we identify it with the $2p^5(^2P^o_{3/2})3p$–$2p^5(^2P^o_{3/2})8d$ array of Ne I (van Hoof 1999). We urgently need spectroscopy in the red to confirm the presence of Ne I, which would make WR 117 more evolved than other WC9 stars. The apparent evolutionary sequence exemplified by WR 88 → (WR 81, WR 92) → (WR 103 etc) → WR 117 needs to be tested by full spectroscopic analyses.

References

Hamann W.-R., Koesterke L., Wessolowski U., 1995, A&AS, 113, 459
Monnier J.D., Tuthill P.G., Danchi W.C., 1999, ApJ, 525, L97
Torres A.V., Massey P., 1987, ApJS, 65, 459
Torres A.V., Conti P.S., 1984, ApJ, 280, 181
Tuthill P.G., Monnier J.D., & Danchi W.C., 1999, Nature, 398, 486
Usov V.V., 1991, MNRAS, 252, 49
van der Hucht K.A., 2001, New Astron. Revs, 45, 135 (VIIth Catalogue)
van Hoof P., 1999, The Atomic Line List v2.04, `http://www.pa.uky.edu/~peter/atomic/`
Williams, P.M. 1999, in *Wolf-Rayet Phenomena in Massive Stars and Starburst Galaxies*, Proc. IAU Symp. 193, K.A. van der Hucht, G. Koenigsberger & P.R.J. Eenens (eds), San Francisco, ASP, p. 267
Williams P.M., van der Hucht K.A., 2000, MNRAS, 314, 23 (Paper I)

X-ray analysis of the close binary system FO 15

J.F. Albacete Colombo* and G. Micela

INAF - Osservatorio Astronomico di Palermo, Piazza del Parlamento 1, Palermo, Italy.

Abstract: We analyse the *XMM-Newton* observations of the close massive (O5V((f))+O9.5V) FO 15 binary system. X-ray spectra are described by a combination of absorption models WABS (N_H^{ISM}) and ABSORI (N_H^{wind}) with two absorbed thermal (APEC) models (kT_1=0.22±0.01 and kT_2=1.43±0.40 keV) plus a non-thermal Power-Law (PO) model (Γ=1.50±0.46). Observed emission lines from high ionization states of N, O, Ca, Si, Ne and Fe are produced by thermal plasma temperatures according to those obtained from our X-ray spectral fit model. The hard thermal component comes from the colliding wind region (CWR) of the primary stellar wind onto the secondary surface. We find L_x/L_{bol} is about 9.0×10^{-7} in excess with respect to the relation of single O-type stars, likely due to the CWR of the system. We estimate that CWR gas reaches the radiative limit, and mostly emits absorbed soft X-ray photons, while hard X-ray photons come from the inner part of the CWR throughout Inverse Compton (IC) scattering processes. Finally, we confirm the existence of short-term variability which seems to be related to radiative gas at the outer zones of the CWR, since the variability is only present in the soft X-ray band, while the hard X-ray emission remains constant.

1 Introduction

Most of X-ray emission from single O- and early B-type stars display a soft thermal spectrum ($kT \sim 0.2$-0.9 keV), as well as an X-ray luminosity (L_x) level approximately scaling with bolometric luminosity (L_{bol}) following a proportionality ratio of $\sim 2\times10^{-7}$ (Berghöfer et al. 1997). However, massive binaries often display an additional X-ray luminosity compared to suspected single stars of the same spectral type and luminosity classes (Chlebowski & Garmany 1991). Such an excess is usually attributed to the presence of a colliding wind region (CWR), making the X-ray domain adequate to study the CW phenomena in binary systems. Here we present the X-ray analysis of the close (P_{orb} =1.41358 days) massive binary FO 15 (O5V((f)) + O9.5V) (Niemela et al. 2005) of the Carina nebula (NGC 3372).

2 X-ray observations

The Carina Nebula field was observed with *XMM-Newton* in ten separate revolutions. Observations were centered at η Carina or at WR 25 position, leading at the FO 15 positions to off-axis values of 8.45 and 10.1 arcmin, respectively. However, some EPIC observations appear

* *e-mail:* facundo@astropa.unipa.it

to have CCD gaps and bad columns, that lie close to the centre of the source PSF, yielding unreliable spectral fits. We then performed our spectral analysis using data sets 0112580601 (Rev #115), 0112560101 (Rev.#283) and 0112560301 (Rev,#285). Data were not affected by high level of soft proton background.

3 Spectral analysis

3.1 Getting the spectra

All extracted spectra were acquired in the 0.4 to 10 keV energy range. We use a 30 arcsec radius to extract individual PN and MOS pulse-height source and background spectra, which include almost 90% of the encircled energy by the local PSF. We also constructed the corresponding redistribution matrices (RMF) and ancillary response (ARF) files. The source spectra were binned to reach 2,4 and 9 counts per channel and fit in a simultaneous way to improve the source spectrum statistics.

3.2 Choosing absorption and emission models

In order to obtain the most significant model for the X-ray emission of the FO 15, we choose the Rev.#115, where the source appears brighter.

Figure 1: FO 15 PN spectra from observations in Rev. #115, #283 and #285, respectively.

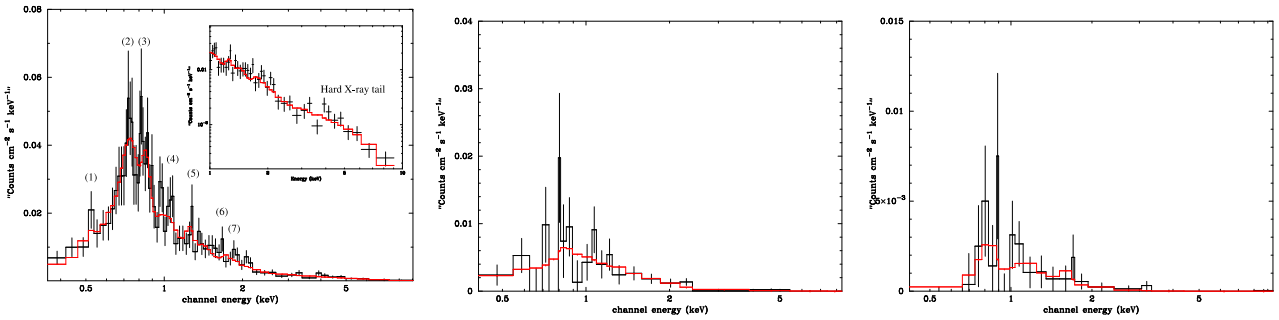

Note: the solid line shows the best fit model. X-ray emission changes by more than a factor 6 between them, suggesting some kind of phase-locked variability (see discussion in section 3.3). In the left figure we indicate identified emission lines and their identification are presented in an electronic version (see http://www.astropa.unipa.it/∼facundo/proceedings/Table1.pdf)

We have adopted a "warm" absorber model (Waldron 1984) produced by: *i)* "hot" absorption model related to ionized hydrogen column density stellar wind, and *ii)* "cold" absorption model produced by a neutral hydrogen column, this last fixed at $N_H = 0.62 \times 10^{22}$ cm^{-2} (Shull & van Steenberg 1985). We assumed solar abundances throughout our fitting procedures.
We first fit single PO as well as single thermal models, in both cases without success. We then tried a 2T thermal model obtaining an overall reduction of the χ^2_ν test, but this model was unable to fit data above 3 keV (see Fig. 1-left). As a consequence, we used and adopted a three component model, consisting in two APEC thermal models (kT_1=0.22±0.01 and kT_2=1.43±0.40 keV) plus another PO component (Γ=1.50±0.46). We discuss the origin of the hard X-ray non-thermal emission in section 3.4.
Absorbed and un-absorbed X-ray fluxes are 1.91×10^{-13} and 15.8×10^{-13} erg cm^{-2} s^{-1} (L_x =

9.5×10^{32} erg s^{-1} assuming a distance of 2250 pc), giving a luminosity ratio $L_x/L_{bol} \approx 9.0 \times 10^{-7}$ which is about 4 times greater than accepted estimates for O-type stars.

3.3 X-ray spectral variability

The system has a circular orbit, thus an explanation of the observed X-ray flux variability, such as that observed in Fig 1, is the change of the absorption column density along the line of sight as a function of the orbital phase.

Adopting system and stellar parameters from Niemela et al. (2005), we calculated on-axis momentum balance (η) of the system of 0.05 (see equation 1-left). Then the equal-momentum stagnation point (X^0_{cwr}) is about 14.3 $R_\odot$, where the total binary separation is only 20 $R_\odot$, being on-axis primary wind literally shocked onto the secondary photosphere.

Because of the short period of the system (P=1.41 days), radiation fields of the companions indeed disturb the acceleration of the winds with the *inhibition effect* (Stevens & Pollock 1994), and/or produces *braking effect* (Gayley et al 1997). Thus, the primary stellar wind (v^{wind}_{cwr}) at the CWR does not reach velocities greater than 1000 km s^{-1}. The angular component of the stellar wind is at least 370 km s^{-1}, about 40% of the v^{wind}_{cwr}. Then Coriolis forces result in a substantial distortion of the CWR geometry, being 2D symmetry broken. Furthermore, the off-axis wind-wind collision has smaller $v_\perp$, thus the post shock temperature is lower (between 10^6 to 10^7 K), and the gas is confined to a thermal thin sheet. X-rays emitted from this "thin" region are absorbed by the "cool" wind of the secondary. Following Stevens et al. (1992), we calculated the thermodynamical condition of the gas using equation 1-right.

$$\eta_o = \frac{\dot{M}_2\, v_2}{\dot{M}_1\, v_1} \qquad\qquad \chi_{rad} = \frac{t_{cool}}{t_{esc}} \approx \frac{v_8^4\, d_7}{\dot{M}_{-7}} \qquad (1)$$

At the on-axis CWR we found $\chi_{rad} \approx 0.25$, while off-axis values are even lower $\chi_{rad} \approx 0.11$. Such radiative CWR successfully explain the observed emission lines (Fig. 1), which require plasmas temperatures between 1.0 to 15 MK. This fact agrees with our two temperature model, where soft emission (kT_1=0.22 keV) is produced by instability driven wind shock models of the primary and secondary components, meanwhile hard thermal emission (kT_2=1.4 keV) is related to the CWR plasma.

However, our thermal model partially fit some emission lines, being the excesses produced likely by a combination of three effects: *A)* non solar abundances, *B)* non-thermal equilibrium emission lines; and *C)* the intense UV radiation field of O type stars induces a strong enhancement of inter-combination lines (i) and decrement of the forbidden (f) component (Porquet et al. 2001). Unfortunately, the low resolution of the EPIC spectra makes them unreliable to address these subjects.

3.4 The origin of hard X-ray photons

Thermal hard X-ray photons (energies above 3 keV) are produced in strong wind-wind collisions where the shock compression ratio (χ) is about 4, and the particle energy distribution follows $N(E) \propto E^{-n}$ being $n=(\chi+2)/(\chi-1)=2$ (White & Chen 1995). On the contrary, in close hot massive binaries wind-wind shocks are weaker ($\chi<4$ - $n>2$), producing a steeper particle energy distribution (to lower energies). In hot luminous stars, with thermal plasma greater than 10^7 K ($kT>0.9$ keV), inverse Compton (IC) cooling becomes more important than collisional cooling, thus reducing the energy available for thermal X-ray emission. Then the competition between

IC losses and shock acceleration processes fix the highest energy of the electrons.
In the vicinity of the shock region, as well as near the secondary surface, the magnetic field (B) should not be discarded. Following White & Chen (1995) approximation, and according to wind-photosphere shock velocity of $v_8^{sh}<1$ ($10^8\,cm\,s^{-1}$), a CWR distance from secondary of $r_{AU}\approx 0.002$ AU, a luminosity $L=10^5\,L_\odot$ and a typical magnetic field of $B\approx$ 100 Gauss, we calculated the maximum energy of the electrons at the CWR, *after* IC scattering and *before* IC, which are about 170 MeV and 44 keV, respectively. This difference ($\Delta E_e^{max}=E_e^{in}-E_e^{out}$) is high enough to produce a large relativistic electron population to rise up UV photons ($\sim$0.01 - 0.07 keV) to hard X-ray photons (>3.0 keV) by means of IC scattering processes.

4 Short-term variability

We study the existence of short-term variability in FO 15 using the longest observation (Rev. # 115) We extracted background corrected light curves using 4 different bin-sizes of 250, 500, 750 and 1000 sec. The statistical significance of variability were calculated as the ratio of two theoretical χ^2 distributions, that follows the Snedecor F-distribution with $\nu_1 = 1$ and $\nu_2 = N_{bins}$-n-2 degree of freedom. By the fitting of a 4^{th} degree polynomial function we confirm with $P(F_\chi) > 95\%$ the existence of variability at time scales of hours, and with amplitude of 25% of the total X-ray emission of FO 15 ($\Delta F_x^0 \sim 3.8\times10^{-13}$ erg s^{-1} cm^{-2}).
We also investigate the spectral behavior of short-term variability, and we extracted light-curves for Total- (T_x: 0.2- 10. keV), Soft- (S_x: 0.2-1.2 keV) and Hard- (H_x: 1.2-10.0 keV) energy bands, as well as we compute the hardness ratio of such variability. The observed X-ray variability is dominated mostly by soft X-ray emission $(\sigma/< cr >)_{soft}=0.35$, while hard energies remain roughly constant $(\sigma/< cr >)_{hard}=0.21$. Therefore, the observed short-term X-ray variability is related to dynamical instabilities along the CWR, where strong radiative cooling occurs.

Acknowledgments

J.F.A.C acknowledges support by the Marie Curie Fellowship Contract No. MTKD-CT-2004-002769 (*The Influence of Stellar High Energy Radiation on Planetary Atmospheres*).

References

Berghöfer T., Schmitt J.H.M.M., 1994, Ap&SS, 221, 309
Chen W., 1992, PhD Thesis, Johns Hopkins University
Chlebowski T., Garmany C.D., 1991, ApJ, 368, 241
Gayley K.G., Owocki S.P., Cranmer S.R., 1997, ApJ, 475, 786
Niemela V., Morrell N., Barbá R., Albacete Colombo J.F., Orellana M., 2005, in prep.
O'Toole S.J., Jordan S., Friedrich S., Heber U., 2005, A&A, 437, 227
Porquet D., Mewe R., Raassen A., Kaastra J., Dubau J., 2001, ASPC, 234, 144
Shull J.M., van Steenberg M.E., 1985, AJ, 298, 268
Stevens I.R., Pollock A.M.T., 1994, MNRAS, 269, 226
Waldron W.L., 1984, AJ, 282, 256
White R., Chen W., 1995, IAUS, 163, 438

Evidence for phase-locked X-ray variations from the colliding wind massive binary Cyg OB2 #8A*

Michaël De Becker† and Gregor Rauw‡

Institut d'Astrophysique et de Géophysique, Université de Liège, Belgium

Abstract: We report on preliminary results of a multi-observatory investigation of the X-ray emission from the massive colliding wind binary Cyg OB2 #8A (O6If + O5.5III(f)). On the basis of our new *XMM-Newton*-EPIC observations, along with archive *ASCA*-SIS and *ROSAT*-PSPC data, we show strong evidence for a significant phase-locked variability of the X-ray emission from Cyg OB2 #8A with the period of 21.9 days determined by De Becker et al. (2004). These results lend further support to the colliding wind scenario that was already suggested by optical data (De Becker & Rauw 2005). We briefly discuss the behaviour of the X-ray emission from this binary system as a function of phase in the context of the colliding wind scenario.

1 Introduction

Cyg OB2 #8A is a binary system with a period of about 21.9 days, and an eccentricity of 0.24 (De Becker et al. 2004). Optical data strongly suggest that the winds of the two stars (O6If + O5.5III(f)) interact (De Becker & Rauw 2005). Another particularity of this system is that it is known to be a non-thermal radio emitter displaying a phase-locked modulation of its radio flux (see Ronny Blomme's contribution, this conference). These variations lend further support to the idea that binarity is a necessary condition to observe non-thermal radio emission from massive stars (see Sven Van Loo's contribution). This system is also expected to give rise to modulations of its X-ray emission correlated with its orbital motion. For this reason, we investigated its X-ray behaviour using new *XMM-Newton* and archive *ASCA* and *ROSAT* data.

2 Data description and analysis

2.1 *XMM-Newton*-EPIC

We obtained 4 pointings (~ 20 ks each) centered on Cyg OB2 #8A with a time separation of about 10 days (end of 2004). A significant soft protons contamination of the fourth observation

*Based on data obtained with *XMM-Newton*.

†e-mail: debecker@astro.ulg.ac.be

‡Research Associate FNRS (Belgium)

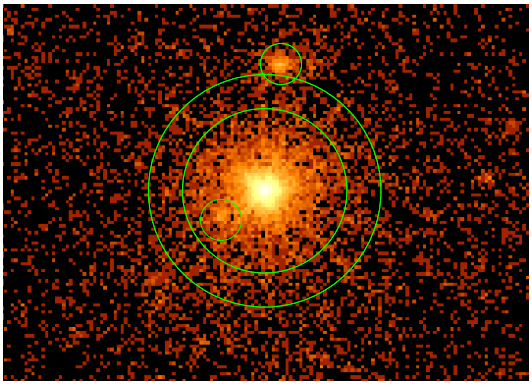

Figure 1: EPIC-MOS1 X-ray image of Cyg OB2 #8A. The source (inner circle) and background (annulus) regions are shown. Close point sources were rejected from the source and background regions (small circles). The North is up and the East is on the left.

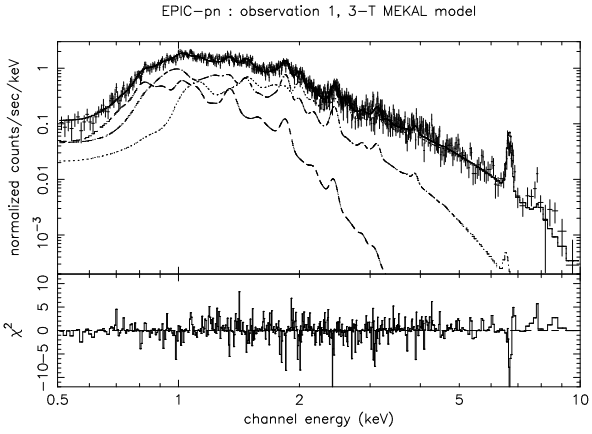

Figure 2: EPIC-pn spectrum of Cyg OB2 #8A for Obs. 1. The spectrum is fitted with a three-component thermal model, including ISM (neutral) and local (ionized) absorption components. The typical plasma temperatures are about 3, 9, and 20 MK respectively for the three emission components. The strong Fe K blend at about 6.7 keV argues in favor of the thermal nature of the hard part of the spectrum (see De Becker et al. 2005).

reduced its effective duration to ~ 10 ks but Cyg OB2 #8A is bright enough in X-rays to produce a high quality EPIC spectrum in only 10 ks. No significant pile-up was detected despite of the brightness of our target. The spectrum of Cyg OB2 #8A was extracted within a 60 arcsec radius circular region, and the background events were selected within an annulus centered on the source (see Fig.1).

Good quality spectra were obtained and analysed with the XSPEC software (see Fig. 2 for EPIC-pn). Best-fits were obtained using a three-component thermal model (`mekal` model, see Kaastra 1992). The results we obtained for the four observations were very consistent, with a slight variation of the temperature of the hard component (for details, see De Becker et al. 2005). The presence of a thermal component with a very high characteristic temperature (~ 20 MK), the very high X-ray luminosity (about a factor 10 overluminous as compared to that expected for a single star of identical L_{bol}), and the strong variability of the X-ray flux (see Sect. 3 and 4) argue strongly in favor of a colliding wind scenario.

2.2 *ASCA*-SIS

The Cyg OB2 region was observed with the *ASCA* satellite in April 1993 (Kitamoto & Mukai 1996), with an exposure time of ~ 30 ks. We retrieved the data and analysed them with the XSELECT package to obtain spectra between 0.5 and 10.0 keV and derive an X-ray luminosity for Cyg OB2 #8A. The characteristic temperatures derived for a 3-T model are similar to those obtained for *XMM-Newton* data.

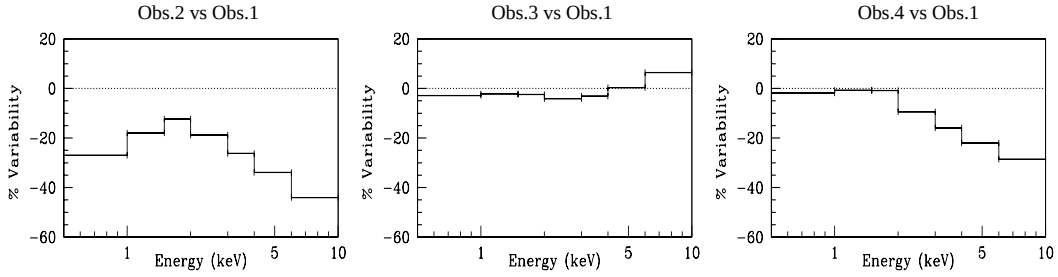

Figure 3: Relative X-ray variability of Cyg OB2 #8A between 0.5 and 10.0 keV as observed with EPIC-pn. The fluxes in all energy bands were determined on the basis of the 3-T thermal model. A negative (resp. positive) value of the percentage stands for a decrease (resp. increase) of the flux of an observation (2, 3, or 4) as compared to the first one.

2.3 *ROSAT*-PSPC

Two ROSAT observations of Cyg OB2 #8A were found in the archives: (i) one from 1991 April 21, and (ii) one resulting from a series of pointings executed between 1993 April 29 and 1993 May 5. The 1993 data set was split into its four individual main exposures of about 3-4 ks each. All spectra were fitted with thermal models. We obtained characteristic plasma temperatures of about 6-7 MK.

3 Variations from *XMM-Newton* data

On the basis of the best-fit 3-T model, we estimated the X-ray fluxes in several energy bands, between 0.5 and 10.0 keV. We used the first observation as a reference, and we compared the fluxes obtained in all energy bands to evaluate the variability level (see Fig. 3). On the basis of these results, the variability can be discussed in the context of the colliding wind scenario. Accordingly, the X-ray flux can vary for two main reasons:

- a variation of the absorption along the line of sight (mainly in the soft part of the EPIC spectrum).
- the eccentricity, likely to cause the physical conditions of the collision zone to change with orbital phase (mainly the hard part of the spectrum).

From Obs. 1 to Obs. 2, the X-ray fluxes decrease in all energy bands. This can be explained by the fact that we compare fluxes obtained respectively close to apastron and periastron ((i)absorption increases, and (ii) the separation decreases, leading to a lower pre-shock temperature). No significant differences are observed between Obs. 1 and Obs. 3. This is not unexpected as they fall at similar orbital phases (see Fig. 4). Obs. 4 presents a strong decrease of the X-ray flux in the hard part of the spectrum. However, the soft part remains steady as compared to Obs. 1. This suggests that the absorption conditions are similar during Obs. 1 and Obs. 4. Identical trends are observed either with fluxes or count rates, for EPIC-MOS and EPIC-pn, therefore lending strong support to these results.

4 Phase-locked variations

We first folded the 3-T model obtained for the first *XMM-Newton* observation with the response matrices of the *ASCA*-SIS and *ROSAT*-PSPC instruments, and we determined the count rate

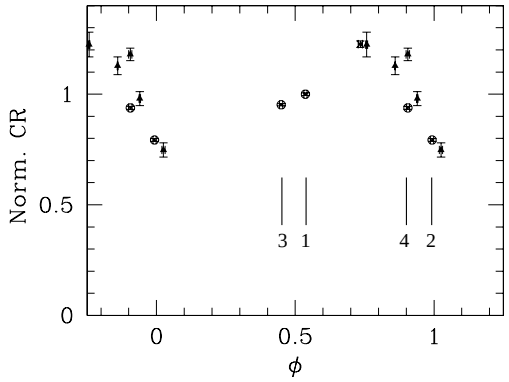

Figure 4: Phase folded X-ray light curve of Cyg OB2 #8A. The equivalent normalized count rates of *XMM-Newton*-EPIC (open circles), *ASCA*-SIS (cross) and *ROSAT*-PSPC (filled triangles) are plotted. According to the ephemeris determined by De Becker et al. (2004), apastron and periastron fall respectively at phases 0.5 and 0.0. The four *XMM-Newton* points are individually labelled (see De Becker et al. 2005).

of the faked spectra. We then compared the observed count rates to the faked ones, and normalized them relative to that of the first *XMM-Newton* observation. We finally folded all the count rates with the ephemeris determined by De Becker et al. (2004) and we obtained the X-ray light curve plotted in Fig. 4, where the count rate of the first *XMM-Newton* observation is equal to 1. The reasonable agreement between the counts rates obtained with the various instruments at different epochs strongly argues in favor of a phase-locked variability on the orbital period of 21.908 days determined by De Becker et al. (2004).

5 Summary and conclusions

On the basis of four new *XMM-Newton* observations and of archive *ASCA* and *ROSAT* data, we investigated the properties of the X-ray emission of Cyg OB2 #8A. The spectrum between 0.5 and 10.0 keV is fitted with a three-component thermal model, with characteristic plasma temperatures of about 3, 9 and 20 MK.

We detected a significant variability ($\sim 20\%$) of the X-ray flux, and our multi-observatory investigation shows clearly that the variations are phase-locked. These results provide strong evidence that the X-ray emission from Cyg OB2 #8A is strongly dominated by the colliding wind interaction.

Acknowledgements

This research is supported in part by contract PAI P5/36 (Belgian Federal Science Policy Office) and through the PRODEX XMM/INTEGRAL contract.

References

De Becker M., Rauw G., 2005, in *Massive Stars in Interacting Binaries*, eds A.F.J. Moffat & N. St-Louis, in press

De Becker M., Rauw G., Manfroid J., 2004, A&A, 424, L39

De Becker M., et al., 2005, MNRAS, in preparation

Kaastra J.S., 1992, *An X-ray spectral code for optically thin plasmas*, Internal SRON-Leiden Report

Kitamoto S., Mukai K., 1996, PASJ, 48, 813

Preliminary results of an observational campaign aiming at the study of the binary system LSS3074 *

E. Gosset[1†], G. Rauw[1†], J. Manfroid[1‡], E. Antokhina[2],
I.R. Stevens[3] and H. Sana[1§]

[1] Institut d'Astrophysique, Université de Liège,
Allée du 6 Août, 17, Bat.B5c, B-4000 Liège, Belgium
[2] Sternberg Astronomical Institute, Moscow State University,
Universitetkii pr., 13, 119899 Moscow, Russia
[3] School of Physics and Astronomy, University of Birmingham,
Edgbaston, B15 2TT Birmingham, Great Britain

Abstract: We present preliminary results of an observational campaign aiming at the study of the binary system LSS3074. A new lightcurve clearly indicates that the system is in contact. Recent spectroscopy broadly confirms the previous results and the rather low masses of both components (O4f$^+$ and O6-7:(f):). We further analyse an XMM-*Newton* observation of the object that indicates a rather hard X-ray spectrum. This is partly due to the high interstellar extinction towards the object but also to the high plasma temperature (k$T \sim$ 1.2-1.3 keV).

1 Introduction

LSS3074 is a short-period (P$\sim$2.18 days) spectroscopic binary system situated in the Coalsack region. Being classified O4f$^+$ + O6-7:(f):, it is a very interesting target since it harbours one of the very few known O4f$^+$ stars. These objects are rare since they probably represent a short-lived transition phase in the evolution of massive O-type stars before they become Wolf-Rayet stars. An accurate determination of the mass is thus of the utmost importance. A first orbital solution was presented by Morrell and Niemela (1990) leading to rather low minimum masses around 8-9 solar masses. The first light curve was presented by Haefner et al. (1994) but they did not achieve a good phase coverage. Nevertheless, they proposed an inclination of the order of 50°-55°. Such an inclination suggests masses in the range 17-21 solar masses which remains

*Based on data collected at the Cerro Tololo Inter-American Observatory and at the European Southern Observatory (La Silla, Chile) as well as with the XMM-*Newton* Observatory, an ESA Science Mission with instruments and contributions directly funded by ESA Member States and by the USA (NASA).

†FNRS Research Associate (Belgium)

‡FNRS Research Director (Belgium)

§FNRS Research Fellow (Belgium)

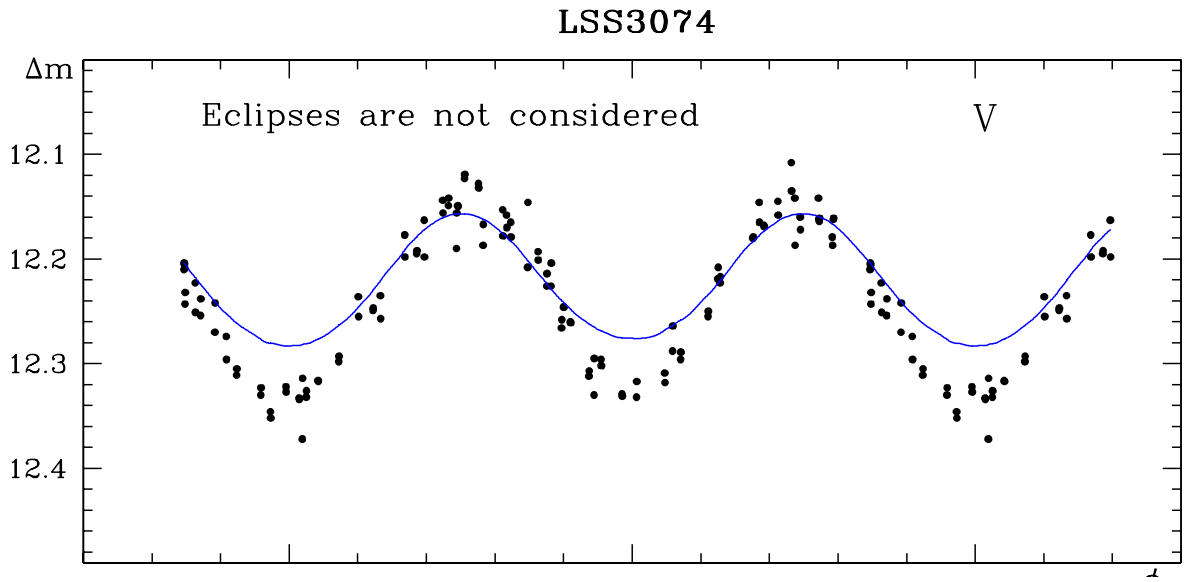

Figure 1: The observed instrumental V lightcurve (dots) of LSS3074 and the theoretical lightcurve (continuous line) of a similar system exhibiting pure ellipsoidal variations but no eclipse at all. Phase 0.0 corresponds to conjunction with the primary in front.

rather low. We acquired new photometry and new spectroscopy of the system and we also observed it with the XMM-*Newton* observatory. We describe here the preliminary results of this campaign.

2 Spectroscopy

Several spectra of LSS3074 were acquired at the Cerro Tololo Inter-American Observatory and at the European Southern Observatory at La Silla in Chile. The spectrum of LSS3074 is characterized by He I and He II absorption lines and is also marked by strong interstellar lines (Ca II, Na I, DIBs). A few lines exhibit strong emission (Hα, He II λ 4686, N III $\lambda\lambda$ 4634-4640, He I λ 5876). Weaker lines are also present in emission (Si IV $\lambda\lambda$ 4088-4116-6668, N IV λ 4058). Careful measurements of the positions of the absorption lines of the primary and secondary stars led to a new set of radial velocities. We derived a new standard orbital solution confirming the low value of the minimum masses. The total ($a \sin i$) amounts to some 19.1 solar radii. The primary O4f^{+} turns out to be the less massive star. It is interesting to notice that the radial velocity variations of the nitrogen emission lines follow the primary orbital movement.

3 Photometry

LSS3074 was monitored over two 15-day runs separated by 20 days without observation. The images were acquired with the Yale 1m telescope at Cerro Tololo equipped with the ANDICAM instrument. The daily rate corresponds to two or three well separated measurements per night. The photometry was performed in the Johnson *BVRI* system. In all the bandpasses, the lightcurves of LSS3074 are almost perfectly sinusoidal with an amplitude of about 0.18-0.20 mag., the two minima being essentially equal. This amplitude is rather difficult to explain by pure ellipsoidal variations of the system. In Fig. 1, we exhibit the V lightcurve and the

predicted amplitude of the variations due to the ellipsoidality of the components. It is necessary to invoke eclipses to explain the observed minima. The sinusoidality of the lightcurve linked to the necessity for the presence of eclipses rather suggests that the eclipse is large in phase to the point that the system must be in contact. From the fit of the lightcurve, an inclination of roughly 55° is derived and thus absolute masses of 16 and 19.3 solar masses for the primary and the secondary, respectively.

4 X-ray observation

LSS3074 was observed with the XMM-*Newton* observatory in August 2001. The exposure time for the EPIC-pn instrument was 22.8 ks. The EPIC field of view for the LSS3074 observation contains the low-mass X-ray binary (LMXB) XB1323–619 (see e.g. Boirin et al. 2005) which is outstanding in the image (see Fig. 2). LSS3074 is detected as a mildly hard source: it is the star at the centre of the field.

We have extracted the EPIC-pn spectrum of LSS3074. It is rather well-fitted with a one temperature optically thin plasma model of the `mekal` type: the derived temperature is kT = 1.29 keV. A two temperature fit gives kT_1 = 0.10 keV and kT_2 = 1.23 keV thus confirming the 1.2 keV component. The source appears hard due to a combination of this rather high temperature and of a rather large absorbing column. The fitted models correspond to an ISM corrected flux $f_X^{\rm unabs} = 9 \times 10^{-14}$ erg cm^{-2} s^{-1} in the range 0.5-5.0 keV.

5 Conclusion

LSS3074 turns out to be a very interesting object whose evolution could have been heavily influenced by its binarity. The origin of its X-ray emission needs further study. All the details about the present campaign and the related results will appear in a future paper.

Acknowledgements

The Belgian authors are greatly indebted towards the Fonds National de la Recherche Scientifique for multiple support. They further acknowledge support from the PRODEX XMM and Integral projects as well as from the contracts P4/05 and P5/36 'Pôle d'Attraction Interuniversitaire' (Belgium). EA benefited from a support by the Russian Foundation for Basic Research (project No 02-02-17524) and by the Russian LSS (project No 388.2003.2)

References

Boirin L., Méndez M., Diaz Trigo M., Parmar A.N., Kaastra J.S., 2005, A&A, 436, 195
Haefner R., Simon K.P., Fiedler A., 1994, IBVS, 3969, 1
Morrell N.I., Niemela V.S., 1990, in *Properties of hot luminous stars*, A.S.P. Conf. Ser., 7, 57

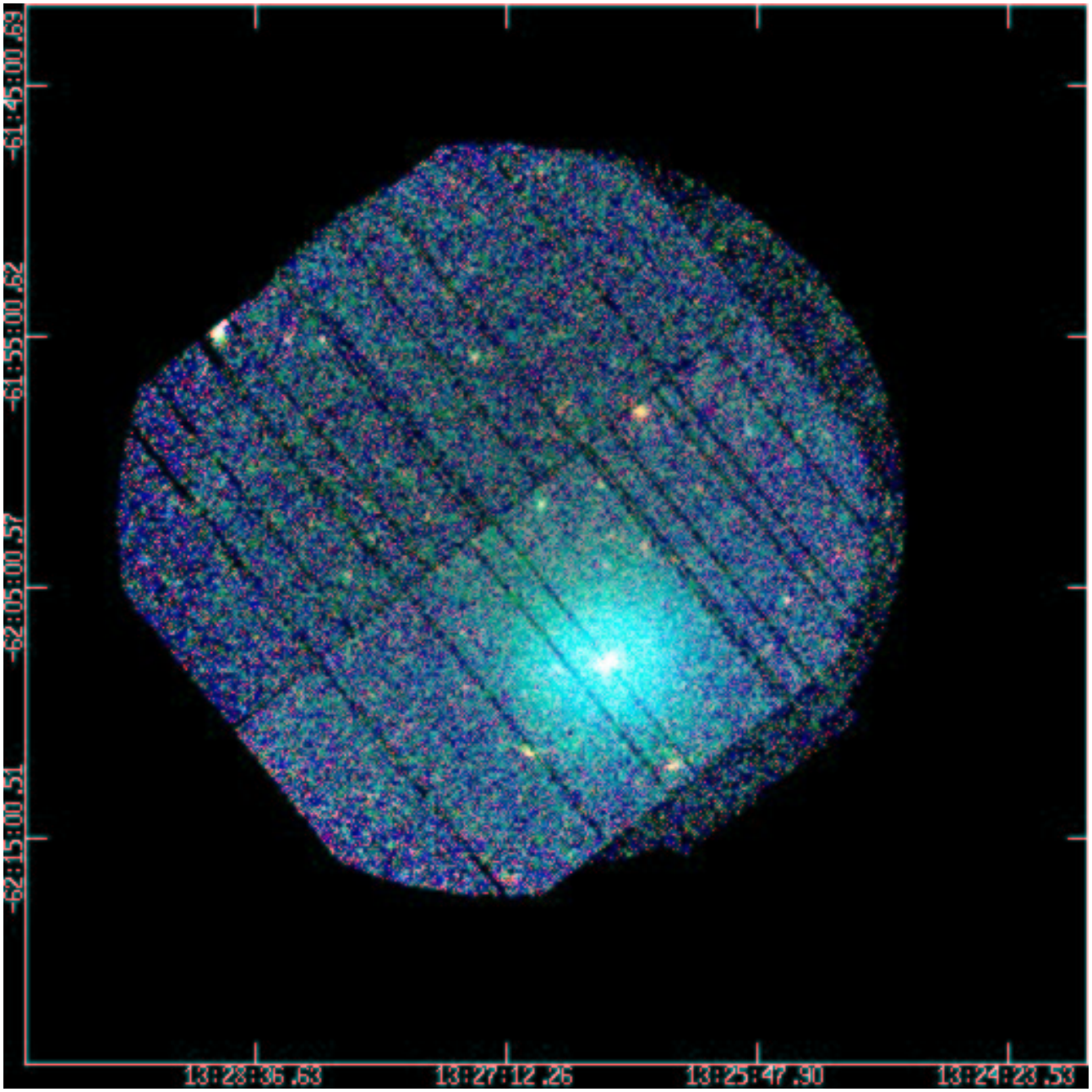

Figure 2: Combined EPIC-MOS1, EPIC-MOS2 and EPIC-pn image in the 0.5-8.0 keV band. The LMXB star is outstanding. LSS3074 is the star at the centre of the field.

The colliding winds of WR 146: seeing the works

E. P. O'Connor [1,2], S. M. Dougherty [2], J. M. Pittard[3] and P. M. Williams[4]

[1]Physics Dept., U. Prince Edward Island, Charlottetown, PEI., Canada
[2]National Research Council, Herzberg Institute of Astrophysics, DRAO., Penticton, Canada
[3]School of Physics and Astonomy, U. Leeds, Leeds, UK
[4]Institute for Astronomy, U. Edinburgh, Scotland, UK

Abstract: WR146 is a WC6+O8 colliding-wind binary (CWB) system with thermal emission from the stellar winds of the two stars, and bright non-thermal emission from the wind-collision region (WCR) where the winds collide. We present high resolution radio observations from 1.4 to 43 GHz that give one of the best quality radio spectra of any CWB to date. Observations at 22 GHz now span 8 years, and reveal the proper motion of the system, allowing comparison of multi-epoch data. VLBI observations show the location of the WCR relative to the stellar components, from which the wind momentum ratio can be shown to be $\eta = 0.06 \pm 0.15$. The radio spectrum and the spatial distribution of emission are modelled, and we determine the contribution of both stellar winds and the WCR to the observed emission. We show that our current models fail to account for the high frequency spectrum of WR146, and also produce too much emission far from the stagnation point of the wind collision.

1 Observations

On 2004 October 1, WR 146 was observed at 1.4, 4.8, 8.3, 15, and 43 GHz with the highest-resolution configuration of the Very Large Array (VLA) in conjunction with the Pie Town antenna of the Very Large Baseline Array (VLBA). Two components are observed at 15, 22, and 43 GHz. At 43 GHz, the two sources are separated by 152 ± 2 mas (Fig. 1 - left). The northern component (N) has a predominately synchrotron spectrum at almost all frequencies, except at 43 GHz where it is a combination of emission from the WCR and the O star stellar wind (see Fig. 3). The southern source (S) has a thermal spectrum and we identify this as the wind from the WC6 star (Dougherty et al. 1996, 2000), which STIS spectroscopy confirms is the spectral type of the southern component.

WR146 was also observed at 4.9 GHz using the European VLBI Network (EVN) and the MERLIN array in the UK on 2001 February 12. The EVN observation shows a bow-shaped arc of emission (Fig. 1 - centre), with a brightness temperature of 10^7 K, which we identify as the WCR. Such a shape is consistent with the WCR "wrapping" around the star with the lower wind momentum, the northern O star (e.g. see Eichler & Usov 1993, Dougherty et al. 2003). The EVN observations indicate the WR and O star are south and north of the WCR, consistent

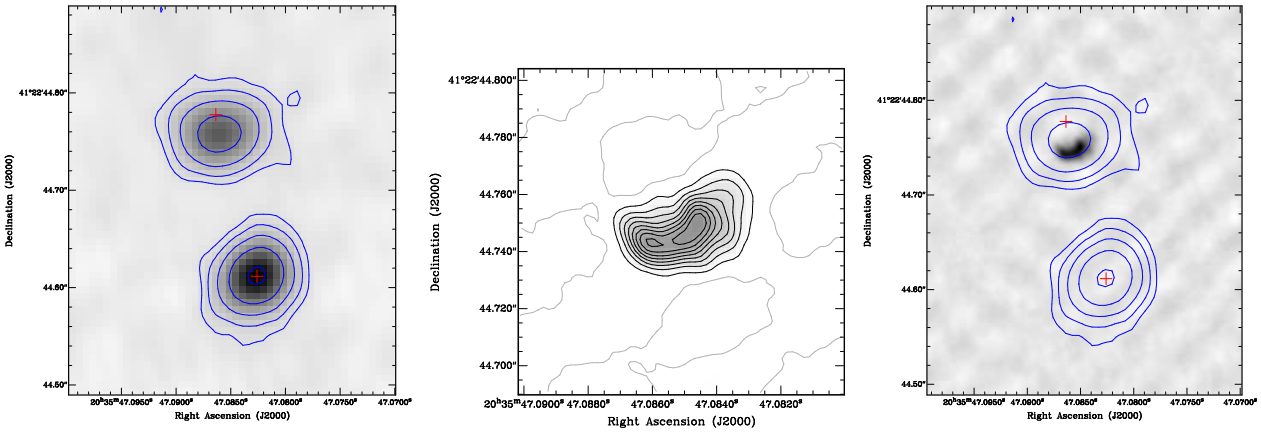

Figure 1: (Left) WR146 with VLA+PT at 43 GHz, with resolution of 30 mas. Two sources are clearly observed, with a separation of 152 ± 2 mas. (Centre) EVN observation at 5 GHz with resolution of 9 mas. A bow-shaped region is observed as expected for a WCR. (Right) An overlay of the VLA 43 GHz (contours) with the EVN (greyscale) 5-GHz emission shown. The proper motion of the source between the observations has been taken into account. The stellar positions are marked, as deduced from HST observations, with a separation of 168 mas.

with previous suggestions (Dougherty et al. 1996, 2000; Lépine et al. 2001). MERLIN also detects only the WCR.

2 Proper motion

In order to align correctly radio images of any stellar source obtained at widely separated epochs it is necessary to know the proper motion of the source. In addition to the VLA observations from 2004, WR 146 was also observed at 22 GHz with the VLA on 1996 October 26 and 1999 August 26. Each of these observations was phase-referenced using the same quasar, J2007+404, and the change in the relative position of WR 146 and J2007+404 can be determined over the 8 years of observations. A weighted regression fit to the relative positions of WR146 leads to a proper motion of $\mu_\alpha = -3.65 \pm 0.17$ and $\mu_\delta = -6.46 \pm 0.40$ mas yr^{-1}.

3 Component separation and wind-momentum ratio

By observing the relative position of the stars and the WCR (located around the stagnation point of the two stellar winds), we can determine the wind-momentum ratio η. After taking account of the proper motion, a comparison of the EVN and VLA observations reveal the position of the WCR relative to the WR star, with a separation of 135 ± 6 mas. From Niemela et al. (1998), the HST observed a separation of 168 ± 31 mas between the WR and O stars. Taking the uncertainty of the location of the stagnation point as the half-width of the WCR as detected by the EVN, we find $\eta = 0.06 \pm 0.15$. The bulk of the error is due to the uncertainty of the stellar separation ($\pm$31 mas).

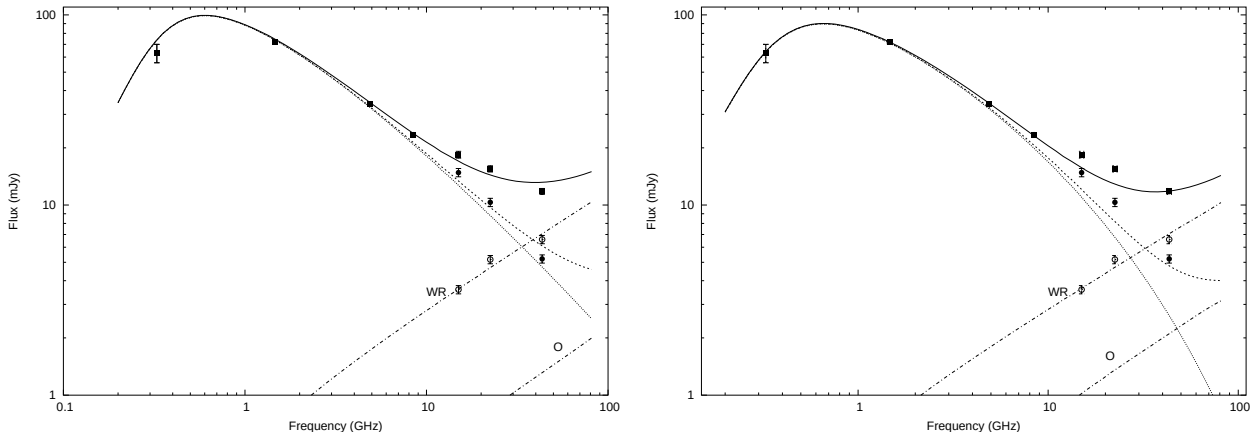

Figure 2: Comparison of observations and two model spectra of WR146. Solid squares mark the total flux from N+S (327 MHz datum from Taylor et al. (1996)), solid circles the flux from N and open circles that from S. Best-fit models of the emission from component N (synchrotron - dotted; thermal - lower dot-dashed; synchrotron+thermal - dashed) and the thermal emission from S (higher dot-dashed) are shown. The total flux from N+S is shown by the solid line. The two models presented are where the high frequency synchrotron spectrum is determined by IC cooling (left) or the high energy cutoff of the shock accelerated electrons (right).

4 Modelling the spectrum

We have modelled the radio emission from WR 146 using a hydro-dynamical model of the density and pressure distribution of a colliding-wind system and solving the radiative transfer equation for thermal and magneto-bremsstrahlung emission and absorption, as well accounting for the Razin effect, inverse-Compton (IC) and Coulomb cooling (Dougherty et al. 2003, Pittard et al. 2005). The model successfully recovers the total flux up to 8.3 GHz. At higher frequencies the fit is less convincing, due to a poor model of component N. Either the 43-GHz flux is overestimated or the 15 and 22-GHz fluxes are underestimated (see Fig. 2). These problems can be resolved if the synchrotron spectrum steepens around ~ 22 GHz.

5 Simulated observations

Using the model parameters derived from the spectrum we can generate synthetic images of WR146, using the AIPS routine UVCON. This allows us to "observe" our model (Fig. 3), and impose constraints on the model from the spatial distribution of the model emission. The similarities between the synthetic images and the observations is remarkable, particularly at 43 GHz. Clearly, the 43-GHz emission is a combination of O-star stellar wind and WCR emission - its peak is not located at either the contact discontinuity or the stellar position, but between them. Comparison with Fig. 1 (left) suggests the emission from N is too extended, both E-W and N-S. The EVN model image also reveals the spatial distribution of the model emission is too wide. We conclude that the model produces too much emission far from the stagnation point of the WCR. Our models also show that deducing the location of the stagnation point from observations is complicated by the relative brightness of the WR and O-star shocked plasma in the WCR.

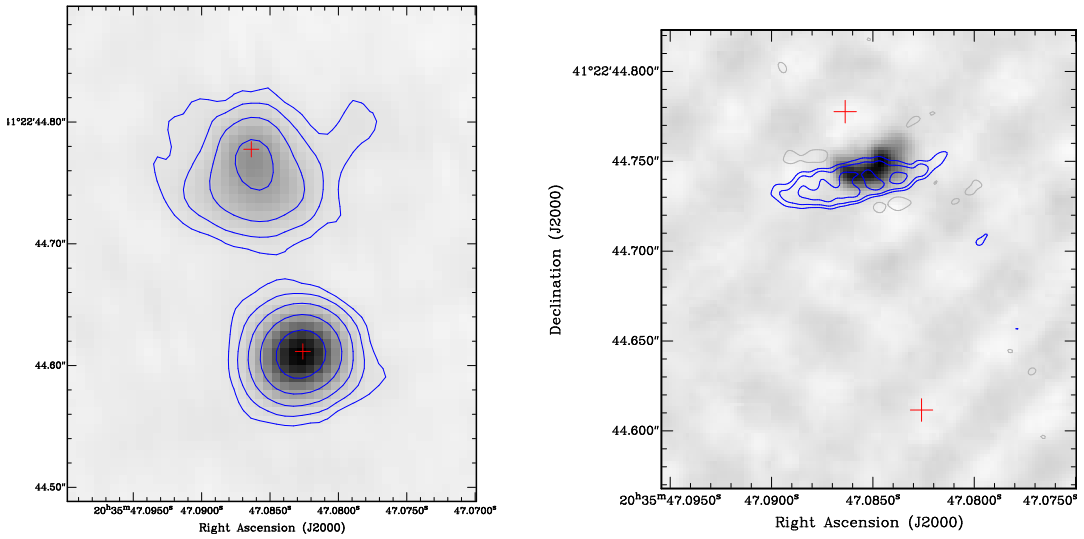

Figure 3: Simulated observations of WR146 at 43 GHz with the VLA+PT (left), and at 4.9 GHz with the EVN (right). The input 43-GHz model is based on the model from Fig. 2 (right), and the EVN model from Fig. 2 (left). The crosses mark the relative location of the two stars as determined by HST observations . Compare the left-hand figure to Fig. 1 (left). The EVN observation and simulated data are superimposed for a clear comparison.

Acknowledgments

This work was supported by the National Research Council of Canada, and the University of Prince Edward Island Co-op programme. JMP acknowledges gratefully funding from the Royal Society. The observations were obtained from the Very Large Array, operated by the National Radio Astronomy Observatory, and the MERLIN array, operated by the University of Manchester on behalf of PPARC. The European VLBI Network is a joint facility of European, Chinese, South African and other radio astronomy institutes funded by their national research councils.

References

Dougherty S.M., Beasley A.J., Claussen M.J., Zauderer B.A., Bolingbroke N.J., 2005, ApJ, 623, 447

Dougherty S.M., Pittard J.M., Kasian L., Coker R.F., Williams P.M., Lloyd H.M., 2003, A&A, 409, 217

Dougherty S.M., Williams P.M., Pollacco D.L., 2000, MNRAS, 316, 143

Dougherty S.M., Williams P.M., van der Hucht K.A., Bode M.F., Davis R.J., 1996, MNRAS, 280, 963

Eichler D., Usov V., 1993, ApJ, 402, 271

Lépine S., Wallace D., Shara M.M., Moffat A.F.J., Niemela V.S., 2001, AJ, 122, 3407

Niemela V.S., Shara M.M., Wallace D.J., Zurek D.R., Moffat A.F.J., 1998, AJ, 115, 2047

Pittard J.M., Dougherty S.M., Coker R., O'Connor E., Bolingbroke N.J., 2005, A&A, submitted

Taylor A.R., Goss W.M., Coleman P.H., van Leeuwen J., Wallace B.J., 1996, ApJS, 107, 239

On the multiplicity of the non-thermal radio emitters 9 Sgr and HD 168112*

Gregor Rauw[1†], Hugues Sana[1‡], Eric Gosset[1†], Michaël De Becker[1], Julia Arias[2], Nidia Morrell[3], Philippe Eenens[4] and David Stickland[5]

[1]Institut d'Astrophysique, Université de Liège, Belgium
[2]Facultad de Ciencias Astronómicas y Geofísicas, Universidad Nacional de La Plata, Argentina
[3]Las Campanas Observatory, The Carnegie Observatories, La Serena, Chile
[4]Departamento de Astronomia, Universidad de Guanajuato, Mexico
[5]Rutherford Appleton Laboratory, Chilton, UK

Abstract: We discuss the first results of our ongoing optical spectroscopic monitoring campaign of the two O-type stars 9 Sgr and HD 168112. Both objects display a non-thermal radio emission and were considered as single stars. Based on a large set of high-resolution spectra, we find that 9 Sgr is clearly an eccentric SB2 binary with an orbital period of several years. On the other hand, no evidence for radial velocity variations attributable to binary motion is found in our spectra of HD 168112.

1 Introduction

One of the most intriguing features of early-type stars is the non-thermal radio emission that is observed for some of them. This emission is interpreted as synchrotron radiation, implying that the winds of these stars harbour a population of relativistic electrons. The most likely acceleration sites of these relativistic electrons are hydrodynamic shocks. Such shocks are known to exist at the interface between the stellar winds of the components of early-type binary systems and over the last few years, it has become more and more obvious that many of the non-thermal radio emitters are indeed binary systems (Dougherty & Williams 2000 and references therein; see also Van Loo, these proceedings).

Over the last few years, we have been investigating the multi-wavelength (radio, optical, X-ray and γ-ray) properties of a sample of non-thermal radio emitting O-type stars (see e.g. Rauw et al. 2002, De Becker et al. 2004a, 2004b, 2005, Blomme et al. 2005). Some of our targets (9 Sgr, HD 168112, Cyg OB2 #8a) were previously considered as single stars. We therefore initiated a spectroscopic monitoring of these stars, to uncover yet unknown binary systems.

*Based on data collected at the European Southern Observatory (La Silla, Chile), the Complejo Astronómico El Leoncito (Argentina) and the Observatorio Astronómico Nacional of San Pedro Mártir (Mexico)
†Research Associate FNRS (Belgium)
‡Research Fellow FNRS (Belgium)

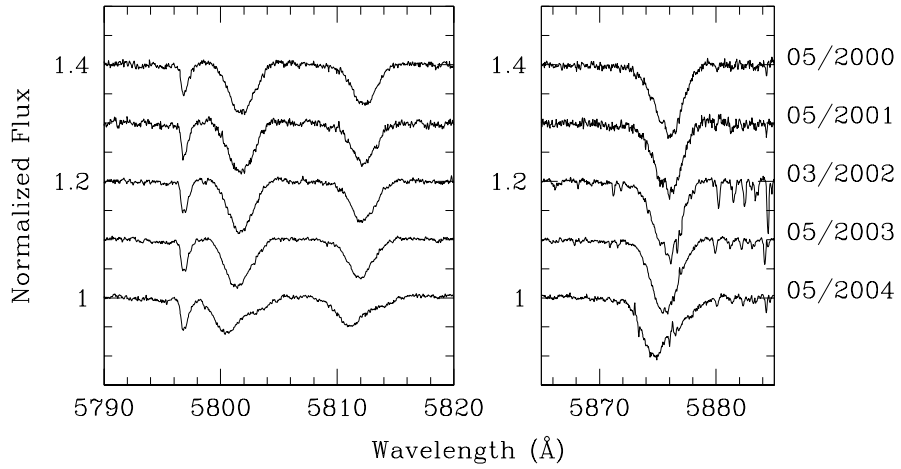

Figure 1: Variations of the C IV $\lambda\lambda$ 5801, 5812 and He I λ 5876 line profiles in the FEROS spectra of 9 Sgr.

A first result of this campaign was presented by De Becker et al. (2004b) who showed that Cyg OB2 #8a is in fact an eccentric spectroscopic binary system with a period of 21.9 days. Here, we discuss preliminary results for 9 Sgr and HD 168112.

2 9 Sgr

In the course of our ongoing monitoring campaign of the O4 V((f$^+$)) star 9 Sgr, we have gathered a total of 31 spectra with the FEROS echelle spectrograph (R = 48000). The data were obtained between 1999 and 2002 at the ESO 1.5 m and since 2003 at the 2.2 m telescopes at La Silla (Chile). In addition, one spectrum was taken with the EMMI instrument in echelle mode (R = 7700) at the New Technology Telescope (La Silla) in 2002. The data taken in 2004 reveal a clear SB2 signature in the C IV $\lambda\lambda$ 5801, 5812 and He I λ 5876 lines: the core of these lines is clearly shifted towards the blue, whilst the red wing shows the presence of a fainter secondary component (see Fig. 1). The ESO data are complemented by 5 spectra obtained in 1995 with the REOSC echelle spectrograph (R = 15000) at CASLEO. Despite their rather low signal to noise ratio, these data play a crucial role since they reveal an SB2 signature similar to that observed in 2004 and to the one already observed in 1987 by Fullerton (1990).

To measure the radial velocities of the two components of 9 Sgr, we have first applied a simultaneous fit of two Gaussians to the spectra obtained during 2004 i.e. near maximum separation. For the other spectra, we have measured the radial velocity (RV) of the line core. The latter values most likely reflect the primary RVs. As a next step, we then applied the spectral disentangling method of González & Levato (2005) to separate the spectra of the primary and secondary component and to determine the RVs. In this approach, we have used the primary RVs derived hereabove as the starting values of the iterative procedure. The results are shown in Fig. 2. Note that secondary RVs obtained when the RV separation is small are quite uncertain. Our results indicate that 9 Sgr is most probably an eccentric SB2 binary system with an orbital period of order 8 – 9 years.

The disentangled spectra of the primary and secondary components yield a brightness ratio of about 4 ± 1 ($\Delta m_V \simeq 1.5 \pm 0.3$) from the ratio of the EWs of the C IV and He I absorptions.

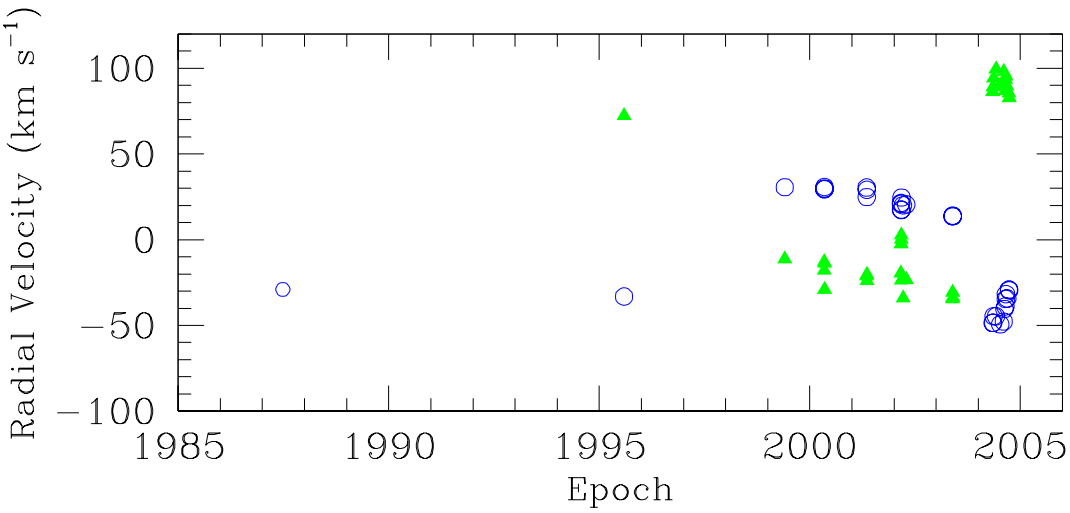

Figure 2: Radial velocities of 9 Sgr as determined using the González & Levato (2005) disentangling method (except for the first observation taken from Fullerton 1990). Open circles and filled triangles indicate the RVs of the primary and secondary components respectively. All RVs were obtained from the C IV $\lambda\lambda$ 5801, 5812 and He I λ 5876 lines.

3 HD 168112

In addition to the data discussed by De Becker et al. (2004a), we have obtained 15 new FEROS spectra spread over six months in 2004. This brings the total number of our echelle spectra of HD 168112 to 25 spanning a total time interval of 1233 days. Our present time series allows us to investigate variations on time scales from a few days to about 10 months as well as from about 1.5 to 4 years. Due to the sampling, periods shorter than one day, between about 10 and 15 months or longer than about 4 years are not well constrained by our data.

We have measured the heliocentric RVs of the strongest absorption lines in our spectra. The RVs of individual lines show little evidence for variability. The 1-σ dispersions range from 1.6 km s^{-1} for the He II λ 5412 line to 6.5 km s^{-1} for He II λ 4686, the latter line being probably affected by wind variations. We averaged the RVs of the Hγ, Hβ, He II $\lambda\lambda$ 4200, 4542, 4686, 5412; He I λ 5876 and C IV $\lambda\lambda$ 5801, 5812 lines. The results are shown in Fig. 3. No obvious trend is apparent on the RV data. The 1-σ dispersion amounts to 3.3 km s^{-1}.

For the time scales covered by our data, we assume that the amplitude of RV variations K is less than $2 \times \sigma = 6.6$ km s^{-1}. Using Kepler's law for a binary system of eccentricity e, period P, mass ratio $q = m1/m2$ yields

$$K = \frac{\sin i}{\sqrt{1-e^2}} \left(\frac{2\,\pi\,G\,m_1}{P\,q\,(1+q)^2} \right)^{1/3}$$

Assuming a mass of 50 M$_\odot$ for the O5.5 III(f$^+$) star in HD 168112, we focus on three different values of the mass ratio: $q = 1$, $q = 5$ (corresponding roughly to a B2 V secondary) and $q = 10$ ($\sim$ B6 V secondary). Some results are illustrated in Table 1 below. This table provides the largest acceptable inclination that can be accommodated within our upper limit on K, as well as the probability to have such a low inclination for a random distribution of orbital inclinations.

Of particular interest are the values for $P = 500$ days in Table 1. Indeed, this corresponds roughly to the 1.4 year period suggested by Blomme et al. (2005) to match both the radio and X-ray light curve. We see that in order to have a colliding wind interaction (which probably

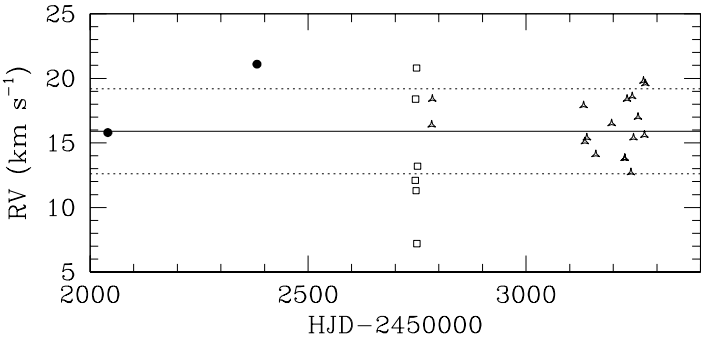

Figure 3: Average RVs of 9 absorption lines in the spectrum of HD 168112. Different symbols stand for data obtained with different instruments. The solid and dotted lines yield the mean as well as the mean ± 1-σ respectively.

requires $q \leq 5$) for such a period, the inclination would have to be less than about 20°. Using Kepler's law and assuming a 1.4 year orbital period, we estimate that $a > 4.61$ AU, which at a distance of 2 kpc yields an angular separation of > 2.3 mas, which should make the companion detectable with the VLTI. A no detection would be a serious challenge for the binary scenario for non-thermal radio emission in O-type stars.

Table 1: Upper limits on the orbital inclination if HD 168112 were a binary with $e = 0$ for different values of P and q. Also indicated is the probability that i be lower than $i_{\rm lim}$ assuming a random distribution of orbital directions in space.

P	10 days			100 days			500 days			1000 days		
q	1	5	10	1	5	10	1	5	10	1	5	10
$i_{\rm lim}(^\circ)$	1.6	5.9	11.1	3.6	12.7	24.6	6.1	22.1	45.4	7.7	28.4	63.7
$p(i \leq i_{\rm lim})(\%)$	0.04	0.5	1.9	0.2	2.5	9.1	0.6	7.4	29.7	0.9	12.0	55.7

Acknowledgements

The Liège team is greatly indebted to the F.N.R.S. for multiple assistance. This research is also supported in part by contract P5/36 "PAI" and through the PRODEX projects.

References

Blomme R., Van Loo S., De Becker M., et al., 2005, A&A, 436, 1033
De Becker M., Rauw G., Blomme R., et al., 2004a, A&A, 420, 1061
De Becker M., Rauw G., Manfroid J., 2004b, A&A, 424, L39
De Becker M., Rauw G., Blomme R., et al., 2005, A&A, 437, 1029
Dougherty S.M., Williams P.M., 2000, MNRAS, 319, 1005
Fullerton A.W., 1990, PhD thesis, University of Toronto
González J.F., Levato H., 2005, A&A, in press
Rauw G., Blomme R., Waldron W.L., et al., 2002, A&A, 394, 993

CPD −41°7742: an unusual wind interaction*

H. Sana[1†], E. Gosset[1‡], G. Rauw[1‡], E. Antokhina[2], P. Royer[3], J. Manfroid[1§] and J.-M. Vreux[1]

[1]Institut d'Astrophysique et de Géophysique, Liège University, Allée du 6 Août 17, Bat. B5c, B-4000 Liège, Belgium

[2]Sternberg Astronomical Institute, Moscow State University, Universitetskii pr., 13, 119899 Moscow, Russia

[3]Instituut voor Sterrenkunde, Katholieke Universiteit Leuven, Celestijnenlaan 200 B, B-3001 Leuven, Belgium

Abstract: We summarize the results of a multiwavelength observing campaign on the massive eclipsing binary CPD −41°7742, another remarkable object in the young open cluster NGC 6231. Our campaign relies on high resolution echelle spectroscopy, narrow-band optical photometry, and *XMM-Newton* X-ray observations. Combined with the spectroscopic analysis, the light curve analysis provides a direct measurement of the masses and sizes of the system components. However, the most outstanding results come from the *XMM-Newton* observations. Our 180 ks campaign towards NGC 6231, and CPD −41°7742, provides an unprecedented phase coverage of such a close early-type binary. The EPIC-MOS light curves almost fully cover the 2.4 day period of the system and the brightness of the object is sufficient to yield a time resolution as tight as 1 ks. The X-ray flux presents clear variations along the orbit, that we interpret as the signature of an unusual wind interaction. We indeed expect that, in this O+B system, the dominant primary wind crashes into the secondary surface, leading to a wind-photosphere interaction. As a strong support to our interpretation, we provide a geometrical model that associates an extra X-ray emission to the secondary inner surface. Though quite simple, the present model matches the main features of the X-ray light curve.

1 Introduction

CPD −41°7742 is an SB2 eclipsing binary with a period $P \approx 2.44$d. In Sana et al. (2005a), we analyse its optical light curve and, combining these new constraints with those obtained from the spectroscopy (Sana et al. 2003), we derive the absolute orbital and physical parameters of the system. In particular, we show that CPD −41°7742 is most probably formed by an O9V and a B1V star. In the present

*Based on data collected at the European Southern Observatory (La Silla, Chile) and with *XMM-Newton*, an ESA Science Mission with instruments and contributions directly funded by ESA Member States and by the USA (NASA).

†FNRS Research Fellow (Belgium)

‡FNRS Research Associate (Belgium)

§FNRS Research Director (Belgium)

"Massive Stars and High Energy Emission in OB Associations"; Proc. JENAM 2005 *Distant Worlds*, Liège (Belgium), eds. Rauw et al., p. 89-92

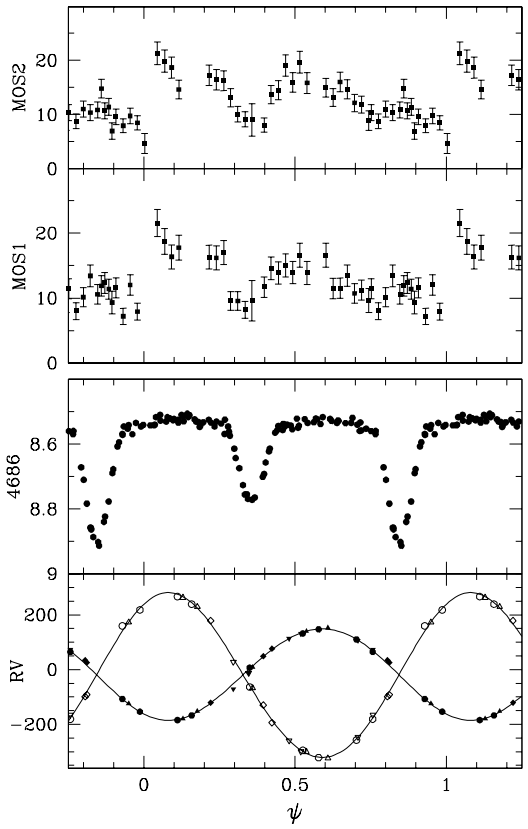

Figure 1: From bottom to top: RV curves (in km s^{-1}), optical light curve (in mag, at $\sim \lambda 4686$Å) and *XMM-Newton* EPIC-MOS1 and MOS2 (in 10^{-3} cts s^{-1}) X-ray light curves of CPD $-41°7742$. The bin size of the X-ray curves is 1 ks.

contribution, we summarize the analysis of the *XMM-Newton* EPIC-MOS X-ray light curve. The details of our observing campaign and of our analysis are to be found in Sana et al. (2005a).

2 An unprecedented X-ray light curve

In Sept. 2001, the young open cluster NGC 6231 has been the target of a 180 ks monitoring campaign with *XMM-Newton* (Sana et al. 2005b). These X-ray observations yielded an almost complete coverage of the CPD $-41°7742$ orbital cycle. The brightness of the object was further sufficient to obtain a time resolution as tight as 1 ks. Briefly, *XMM-Newton* revealed a clearly variable, though complex, X-ray light curve (Fig. 1). In particular, we observed an X-ray eclipse (at $\phi \approx 0.35$) almost perfectly synchronized with the secondary eclipse in the optical light curve (Fig. 1). This suggests the presence of an additional localized X-ray component associated with the secondary inner surface.

3 An unusual wind interaction

In CPD $-41°7742$, the winds from the two components are strongly off balance and no ram pressure equilibrium can be sustained on the binary axis. As a consequence, the overwhelming O-type primary wind most probably crashes into the B-type secondary surface. In this scenario,

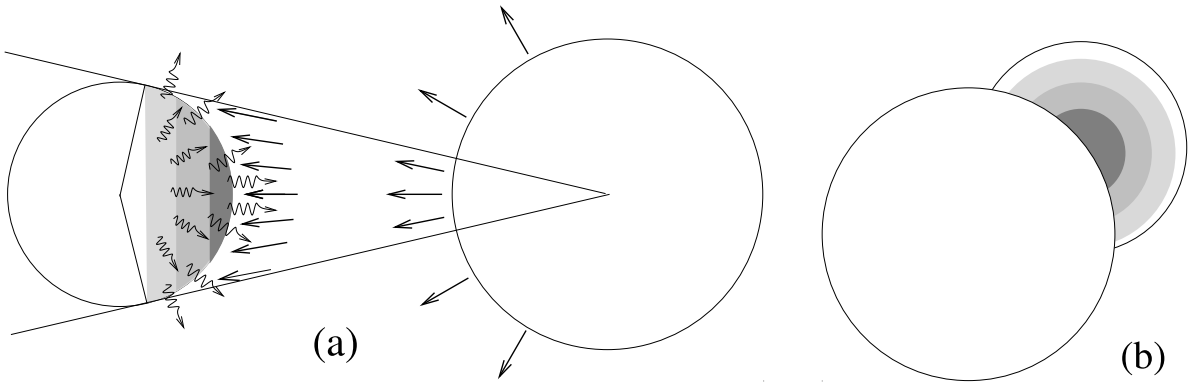

Figure 2: Schematic view of our geometric interaction model. **(a)** A view from above the orbital plane: the secondary star intercepts a small fraction of the primary wind, of which part of the kinetic energy is turned into heat. **(b)** A similar view along the line of sight. The different degrees of shading of the secondary surface represent the different X-ray emissivities, these latter being larger closer to the system axis.

the extra X-ray emission component produced by the wind interaction is naturally associated with the secondary inner surface (Fig. 2).

3.1 A wind-photosphere interaction model

To test our interpretation of the CPD−41°7742 X-ray light curve, we built a simple phenomenological model based on the following assumptions:

- **Ingredients:** 3-D geometry, spherically symmetric stars and winds, circular orbit, accelerated winds ($\beta = 1$ velocity law), neglect of the influence of the orbital motion, fully radiative shock (immediate cooling)

- **Fixed parameters:** geometry (sizes, separation, inclination), constrained from the SB2E orbital solution; wind parameters ($\dot{M}$ and v_∞), derived from the mass loss recipes of Vink et al. (2001)

- **Free parameter:** amplitude of the emissivity (or, equivalently, efficiency of the cooling)

To compare the *predictions* of our model with the observed X-ray light curve, we separate the signal into a constant emission threshold and a variable component with which we confront the modelled light curve. As seen from Fig. 3, our simple model reproduces to the first order the modulations of the X-ray flux of CPD−41°7742. In particular, the width of the X-ray *eclipse* is well rendered.

3.2 Final remark

We can not rule out that radiative braking (Gayley et al. 1997) be strong enough to alter the wind-photosphere interaction, resulting in a wind-wind interaction structure instead. However, the latter should still be located close to the secondary surface. Briefly, even if braking occurs, we still expect similar modulations of the X-ray flux.

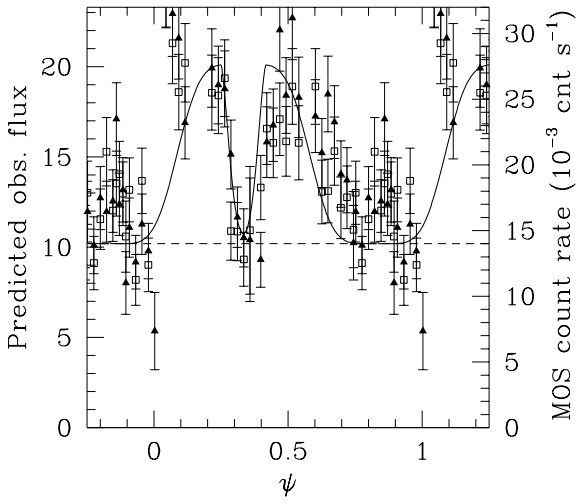

Figure 3: EPIC-MOS X-ray light curves. The thick line indicates the contribution of the wind interaction component computed from our geometrical model. The amplitude of the predicted variations has been arbitrarily scaled to the data.

4 Conclusions

Our *XMM-Newton* campaign almost fully covered the orbital cycle of the early-type binary CPD−41°7742 and yielded an unprecedented X-ray light curve of such a close system. The clear modulations of the X-ray flux are interpreted as the signature of a wind interaction, though of a particular kind: the overwhelming primary wind crashes into the secondary star, producing an extra X-ray component associated with the secondary inner surface. It is the first time that such a wind-photosphere interaction is unveiled from the observational point of view. Finally, the case of CPD−41°7742 outlines the need for phase-resolved observations of close early-type binary systems, that provide a phase-coverage as good as possible. It is only thanks to the unprecedented quality of the EPIC-MOS X-ray light curve of CPD−41°7742 that we could unveil the unusual wind interaction happening in this system.

Acknowledgements

The Liège team acknowledges support from the PRODEX XMM and Integral Projects, as well as contracts P4/05 and P5/36 'Pôle d'Attraction Interuniversitaire' (Belgium). EA acknowledges support from the Russian Foundation for Basic Research (project No 02-02-17524) and the Russian LSS (project No 388.2003.2).

References

Gayley K.G., Owocki S.P., Cranmer S.R., 1997, ApJ, 475, 786
Sana H., Hensberge H., Rauw G., Gosset E., 2003, A&A, 405, 1063
Sana H., Antokhina E., Royer P., Manfroid J., Gosset E., Rauw G., Vreux J.-M., 2005a, A&A, 441, 213
Sana H., Gosset E., Rauw G., Sung H., Vreux J.-M., 2005b, A&A, in press
Vink J.S., de Koter A., Lamers H.J.G.L.M., 2001, A&A, 369, 574

Section 3

High-energy emission

from young open clusters

Energetic processes and nonthermal emission of starforming complexes

A.M. Bykov

A.F.Ioffe Institute for Physics and Technology, St.Petersburg, Russia, 194021

Abstract: We discuss models of energetic particle acceleration, interactions and nonthermal emission in active starforming regions at different stages of their evolution. Powerful stellar winds and supernova explosions with intense energy release in the form of strong shock waves can convert a sizeable part of the kinetic energy release into energetic particles. The starforming regions are argued as a favorable site of energetic particle acceleration and could be efficient sources of nonthermal emission.

1 Introduction

The star-forming regions (SFRs) in galaxies are generically associated with molecular clouds and contain a variety of energetic outflows at different stages of massive star evolution from protostellar accreting objects through fast winds of massive OB or WR stars to the most energetic supernova events. Energetic outflow events with fast shocks in a dense ambient medium should result in a rapid conversion of kinetic power into emission. Here we shall discuss two different phenomena of SFR activity — a class of hard non-thermal emission sources due to supernova remnant (SNR) shell interactions with a fast wind of a massive star and a process of magnetic field generation in superbubbles related with energetic particle acceleration by shocks.

Young massive star formation occurs in massive molecular clouds. A gravitational collapse of a giant molecular cloud can result in a formation of several groups of massive O and B stars considered as an OB-association. The distance between two neighboring stars in the groups could be less than 10 pc. The compact groups are the favorable sites of some new type of high energy sources produced by shocks and winds.

A substantial amount of massive stars are binaries. Colliding winds in early type binaries were suggested (e.g. Eichler & Usov 1993) as possible strong sources of nonthermal particles and emission. Indeed, nonthermal radio emission was observed from WR type stars in binary systems (Dougherty & Williams 2000; Rauw 2004).

A region where an expanding shell of a SNR interacts with a fast powerful wind of a young massive star (or a star cluster) contains a converging MHD flow. Hydrodynamic simulations of SNR — wind collisions carried out by Velázques, Koenigsberger & Raga (2003) illustrate the basic properties of the multi-shock flow during the collision. Even before a direct collision a converging flow will exist between the fast stellar wind and the expanding supernova ejecta. The converging flow in a diffusive medium (particle diffusion coefficient $\kappa_{\rm i}(\gamma)$ depends on the Lorentz factor γ) is argued to be a plausible site for GeV–TeV regime lepton acceleration.

"Massive Stars and High Energy Emission in OB Associations"; Proc. JENAM 2005 *Distant Worlds*, Liège (Belgium), eds. Rauw et al., p. 95-98

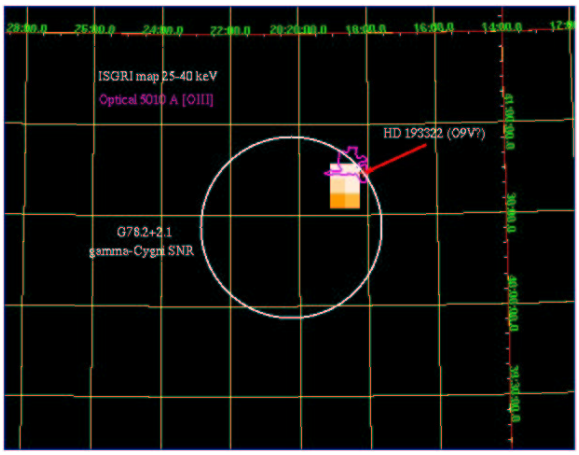

Figure 1: *INTEGRAL ISGRI* 25-40 keV image of γ-Cygni SNR (Bykov et al. 2004). Optical [OIII] 5010 Å line contour (solid line) from Mavromatakis (2003). The SNR border (radio) is roughly indicated by the large solid circle. The arrow points to the position of the O9V star HD 193322 (20:18:07,+40:43:55). All maps are made for J2000. The source may originate from the SNR-O star wind interaction.

A kinetic model without nonlinear back-reaction effect predicts efficient particle acceleration between converging flows (of velocities u_1 and u_2) with the acceleration time

$$\tau_a(\gamma) \approx \frac{3}{u_1+u_2}\int_{\gamma_0}^{\gamma}\left(\frac{\kappa_1(\gamma)}{u_1}+\frac{\kappa_2(\gamma)}{u_2}\right)\frac{d\gamma}{\gamma} \qquad (1)$$

and a hard spectrum of electrons at the TeV energy regime inside the converging flow

$$N_i(z,\gamma,t) = \frac{N_0(\gamma_0,\gamma_m)}{\gamma}\cdot H(\gamma-\gamma_0)\cdot H(t-\tau_a(\gamma))\cdot\exp(-u_{\rm i}\cdot|z|/\kappa_{\rm i}(\gamma)), \qquad (2)$$

where γ_m is the maximal Lorentz factor, and $H(x)$ is the standard Heaviside step function.

Synchrotron emission of the TeV electrons may have a very hard spectrum with a photon index ~ 1 and a spectral break in between keV and MeV photon energies for extended SNRs. Because of that hard spectrum of accelerated electrons the mechanism provides a high efficiency of conversion of SNR shell — fast wind kinetic luminosity into hard X-rays and γ-rays. The efficiency of synchrotron emission in hard X-rays is high. The X-ray luminosity may exceed 0.001 of the kinetic power of the shocks. In Fig.1 we show a hard X-ray emission clump detected with *INTEGRAL-ISGRI* in a region containing γ-Cyg SNR and the stellar wind of the O9V star HD 193322. The hard X-ray source can be explained in this scenario. The new type of hard X-ray sources may be rather common in star forming regions. The Galactic center region could contain such kind of objects. The sources are promising candidates for observations with H.E.S.S. and other TeV telescopes.

2 Non-thermal phenomena in superbubbles

At intermediate stages of OB association evolution (after a few million years) the kinetic energy release within the bubble created by a stellar association may reach a few times 10^{38} erg s^{-1} due to intense stellar winds and multiple SN explosions. The process is accompanied by formation of shocks, large scale flows and broad spectra of MHD fluctuations in a tenuous plasma with frozen-in magnetic fields. Vortex electric fields generated by the large scale motions of highly conductive plasma with shocks result in a non-equilibrial distribution of the charged nuclei. Non-linear models of temporal evolution of particle distribution function accounting for the feedback effect of the accelerated particles on the shock turbulence inside the superbubble were constructed by Bykov (2001). The models demonstrated a high efficiency of the conversion of

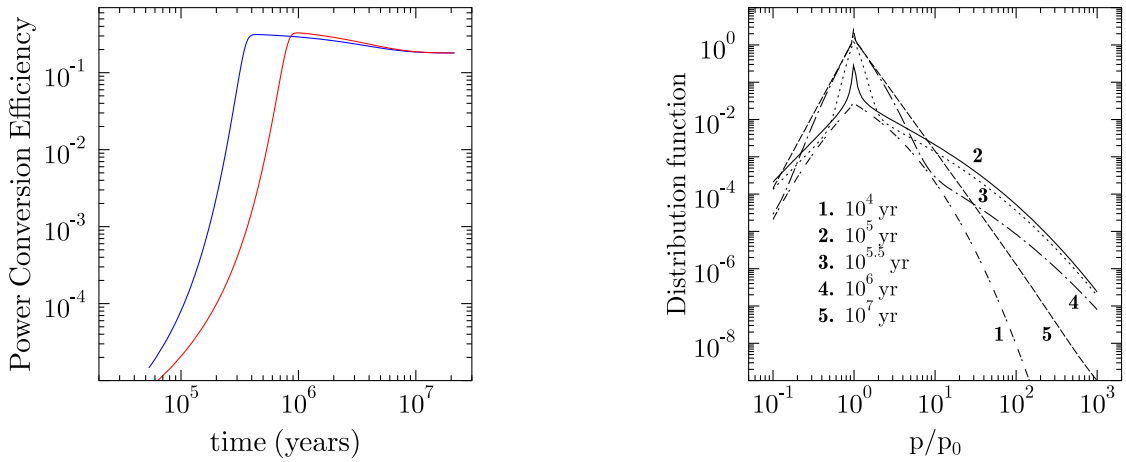

Figure 2: The evolution of nonthermal energetic particles in a superbubble, with the standard IMF. Monoenergetic injection was assumed with the injection energies 10 keV. The temporal evolution of the power conversion efficiency for two different IMF models (see Bykov 2001 for details) is presented in the left panel, while the particle distribution function is in the right panel.

the large-scale turbulence energy to energetic particles on ~ 0.1 Myr time scale. They also showed soft-hard-soft evolution of the particle spectra in 10 Myrs. The particle spectra are power-laws of indices between 1 and 3 with the time asymptotic power-law energy spectral index below 3 (see Fig.2). The superbubbles should be very plausible sites of cosmic ray particle acceleration (e.g. Bykov 2001, Parizot et al. 2004). Thermal and non-thermal X-ray emission observed recently with *Chandra* in the 30 Dor superbubble by Bamba et al. (2004) revealed the presence of some particle acceleration processes there. Magnetic fields in the extended superbubbles are the governing parameters to determine the maximal energies of the accelerated particles. There are different possible processes of magnetic field generation in a highly turbulent compressible medium in a superbubble environment. We shall discuss here a possible new mechanism of magnetic field generation associated with the particle acceleration process.

2.1 Magnetic fields in superbubbles

Supernova shocks in OB associations are sweeping out the matter destroying the honeycomb-like structure created by stellar winds. The matter inside the superbubble at that stage is very intermittent with patchy H_α emission structure indicating the presence of partially-ionized matter. It is known that incomplete ionization would result in ion-neutral damping of MHD waves and limit the maximal energies of accelerated particles. The effect has an important implication for nonthermal emission of supernova remnants interacting with clouds (Bykov et al. 2000). However, apart from the wave damping the presence of a neutral component is long-known to change the relation between local electromagnetic fields and the thermal plasma current — the generalized Ohm's law. The Ohm's law can be changed drastically even by a

relatively small amount of neutral atoms provided the plasma is highly magnetized. The effect of MHD fluctuation growth due to CR current in the upstream of MHD shock propagating along magnetic field in a partially ionized plasma with some (small) mass fraction of neutrals F was studied by Bykov & Toptygin (2005). Their analysis is valid for fluctuations of wavelength λ above the ion-neutral collision length and provides the magnetic fluctuation growth in the wavenumber ($k = 2\pi/\lambda$) range below the cosmic ray precursor length. The magnetic fluctuation growth in a collisionless shock may convert some fraction of the supersonic flow into magnetic fields of a parsec scale.

The ion-neutral collision length in the pre-shock gas can be estimated as $\lambda_{\rm in} \lesssim 2 \times 10^{16} \cdot (F \cdot n_{-2})^{-1}$ cm (for $T \leq 10^5$K). The fluctuation growth rate Γ depends on the fraction of energetic particles N_0/n_i. The value can be expressed through the ratio η of the CR energy density to the kinetic energy density in the upstream flow. For relatively strong shocks $N_0/n_i \approx \eta/2 \cdot (1-F) \cdot (u_{\rm sh}/c)^2/\ln\gamma_m$. The magnetic field growth rate can be presented as

$$\frac{\Gamma}{ku} \approx 10^2 \times \eta \cdot \frac{F \cdot (1-F) \cdot u_8^2 \cdot B_{-6}}{n_{-2} \cdot \ln\gamma_m \cdot T_4^{0.4}} \, , \qquad (3)$$

where u_8 is the shock velocity measured in 1,000 km s^{-1}, and number density n_{-2} in 10^{-2} cm^{-3}. In case of a moderate efficiency of ion acceleration with $\eta \sim 0.1$ and extended energy spectrum of accelerated ions with $\ln(\gamma_m) \sim 10$, the condition in the shock upstream $F \cdot (1-F) \cdot u_8^2 \cdot B_{-6} \cdot n_{-2}^{-1} \gtrsim 1$ must be satisfied for the fluctuations to grow.

The maximal upstream field amplitude calculation requires non-linear analysis of the instability. We can estimate the amplitude on the energetic ground as $B_m \sim (0.5 \cdot \eta \cdot n \; m_p \; u_8^2)^{1/2}$ providing $B_m \gtrsim$ 10 μG. The upstream field will be further compressed by the shock providing a few times higher downstream field, depending on the shock geometry. The resulting magnetic fields of $B \gtrsim 30\mu$G would allow cosmic ray acceleration up to the "ankle" energy region.

Acknowledgements

I would like to acknowledge my collaborators for fruitful cooperation. Support from the meeting organizers is gratefully acknowledged. The work was partially supported by RBRF grants 03-02-17433 and 04-02-16595.

References

Bamba A., Ueno M., Nakajima H., Koyama K., 2004, ApJ, 602, 257
Bykov A.M., 2001, Space Science Reviews, 99, 317
Bykov A.M., Chevalier R.A., Ellison D.C., Uvarov Yu.A., 2000, ApJ, 538, 203
Bykov A.M., Krassilchtchikov A.M., Uvarov Yu.A., et al., 2004, A&A, 427, L31
Bykov A.M., Toptygin I.N., 2005, Astron. Lett., 31, 748
Dougherty S.M., Williams P.M., 2000, MNRAS, 319, 1005
Eichler D., Usov V., 1993, ApJ, 402, 271
Mavromatakis F., 2003, A&A, 408, 237
Parizot E., Marcowith A., van der Swaluw E., et al., 2004, A&A, 424, 747
Rauw G., in *Cosmic Gamma-Ray Sources*, Eds. K. Cheng, G. Romero, p.105, Kluwer, 2004
Velázques P., Koenigsberger G., Raga A.C., 2003, ApJ, 584, 284

X-raying the super star clusters in the Galactic center

L. M. Oskinova

Astrophysik, Universität Potsdam, Germany

Abstract: The Galactic center harbors some of the most massive star clusters known in the Galaxy: the Arches and the Quintuplet. Based on the Chandra observations of these clusters (PI: Wang) which recently became public, I discuss the X-ray emission from the massive stars in these clusters. Confirming the general trend for Wolf-Rayet (WR) stars being X-ray dim, none of them is detected in the Quintuplet cluster. The most massive star known in the Galaxy, the Pistol star, is also not detected, invoking questions regarding the proposed binary nature of this object. X-ray emission in the Arches cluster is dominated by three stellar point sources. All three sources as well as the cluster's diffuse radiation show strong emission at 6.4–6.7 keV, indicating the presence of fluorescenting cool material. The Arches point sources may be identified as colliding wind binaries, albeit other possibilities cannot be ruled out.

The X-ray emission from young stellar clusters, such as the Arches and the Quintuplet, is tightly coupled with the massive stars evolution. When a massive star evolves from O type to WN type, and finally to WC type, it keeps its bolometric luminosity nearly constant while its X-ray luminosity is likely to decline (Oskinova 2005). This trend is confirmed by the study of WR stars in the Galaxy and the LMC (Guerrero et al. in prep., also these proceedings). In the 1–3 Myr old Arches cluster (Figer et al. 2002, F02), the majority of massive stars are of O type. The most massive stars are the most X-ray luminous ones due to the $\log L_{\rm X} = \log L_{\rm bol} - 7$ correlation. The stellar wind input into the intracluster medium is expected to result in diffuse cluster wind emission. The level of cluster wind emission scales with stellar mass-loss rates and wind kinetic energy (Chevalier & Clegg 1985). Both quantities rise sharply when stars evolve to the WR phase, characterized by conspicuously powerful stellar winds. Therefore, in the 3–5 Myr old Quintuplet cluster (Figer et al. 1999, FMM99) where a significant fraction of massive stars has evolved to the WR stage the level of cluster wind emission is expected to rise. The same time the stellar X-ray emission becomes much less prominent with the most massive stars evolving fast to the WC stage and becoming X-ray dim.

The Arches and the Quintuplet were recently observed with Chandra in a nearly 100 ksec exposure. Figure 1 shows the ACIS-I image of the Arches cluster. Three bright prominent point sources (see Table 1) coincide with the stars F02-6 (A1S), F02-7 (A1N) and F02-9 (A2)

"Massive Stars and High Energy Emission in OB Associations"; Proc. JENAM 2005 *Distant Worlds*, Liège (Belgium), eds. Rauw et al., p. 99-102

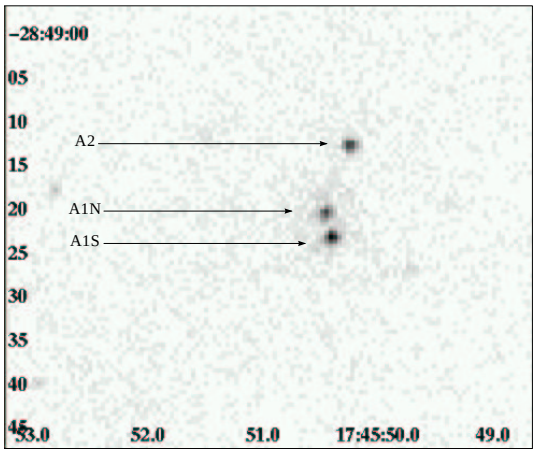

Figure 1: ACIS-I image of the Arches. The emission is dominated by three point sources, as indicated by arrows. Names of the sources are the same as in Law & Yusef-Zadeh (2004).

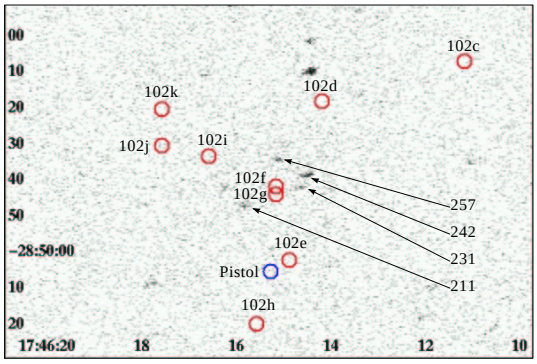

Figure 2: ACIS-I image of the Quintuplet. Positions of known WR stars (WR102c ... WR102k) and of the Pistol star are encircled. None of these is detected. Detected sources with known IR counterparts are indicated by arrows (object numbers are from FMM 99).

(numbers from Figer et al. 2002). F02-9 is an emission line star. The luminosities listed in the Table 1 are not corrected for absorption (the corrected L_X is ≈ 4 times higher). All three sources are suggested to be colliding wind binaries (Law & Yusef-Zadeh 2004). Their X-ray luminosity, however high, is not unique among Galactic binaries (e.g. HD 150136 has $L_X \approx 3 \times 10^{33}$ erg/s, Skinner et al. 2005). It is their X-ray spectra that are rather unusual (Figs. 3, 4).

Spectra of all three stars are remarkably similar in appearance, strongly resembling the spectrum of γ^2 Vel in the low state (Schild et al. 2004). The highly absorbed spectra of A1S, A1N and A2 can be fitted by a variety of models, all of them needing an additional component describing the dominant feature at 1.7-2.1 Å. The X-ray emitting plasma in stellar winds is conventionally modeled as a thermal collisional plasma. The spectra of the Arches stars can be fitted with temperatures above 2 keV and high absorption column densities (see Table 1). However, the flux predicted by such models at the iron K-shell line is a factor of 3 lower than the observed flux. The additional contribution can be attributed to the fluorescence of nearly neutral iron. The presence of the same $\lambda 1.7 - 2.1$Å emission feature in the spectra of the diffuse emission from the Arches supports this suggestion. However, the origin of cool fluorescenting material should be further explained. An exemplary fit with the *apec+gaussian* model to the spectrum of the emission line star A2 is shown in Fig. 4.

The Arches cluster contains hundreds of massive OB stars (F02), each of them expected to be an X-ray source. Yet only a handful of point sources is detected within the cluster radius. The scarcity of stellar X-ray sources in the Arches is naturally explained by the high interstellar absorption in the Galactic center. At the column density of $\sim 10^{23}$ cm^{-2} the photoelectric absorption attenuates photons up to energies of 2 keV. Only sources that are sufficiently luminous in the hard X-ray band (2.5 – 10 keV) can be observed.

X-ray temperatures of several keV are expected and have been observed in wide binary systems (e.g. WR140), where an *adiabatic* colliding wind shock is expected to occur. Antokhin et al. (2004) calculated X-ray spectra of *radiative* colliding winds shocks. They conclude that the presence of an "iron bump" at 6.7 keV can also be expected in relatively close binary systems (orbital period up to the order of 10 days).

However, by far not all binary stars show hard X-rays (harder than 2 keV). Many X-ray luminous spectroscopic binaries have X-ray temperatures not higher than the canonical 0.6 keV

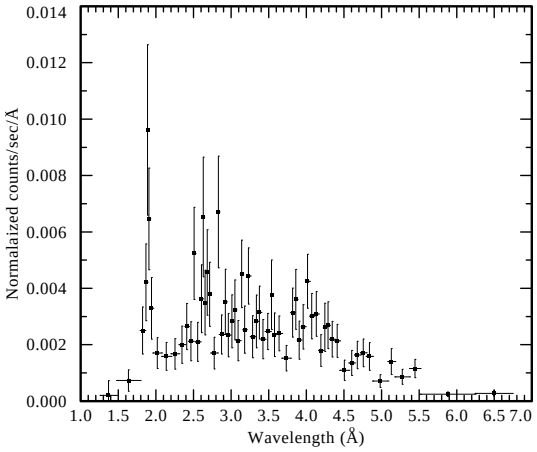

Figure 3: Observed background-subtracted spectrum of the brightest X-ray point source A1S (FMM 6) in the Arches cluster.

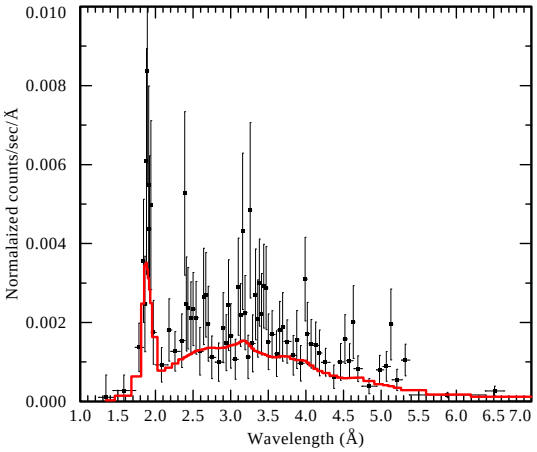

Figure 4: Observed background-subtracted spectrum of emission line star A2 (FMM 9). The solid line is a fitted thermal plasma model with $kT = 3.5 \pm 1.2$ keV with an additional gaussian component at 1.7-2.1Å.

Object	Count Rate [c/s]	$N_{\rm H}$ [cm^{-2}]	$L_{\rm X}$ [erg/s]
A1N	0.005	$\approx 7 \times 10^{22}$	6×10^{32}
A1S	0.009	$\approx 7 \times 10^{22}$	1×10^{33}
A2	0.006	$\approx 7 \times 10^{22}$	9×10^{32}

Table 1: X-ray emission from point sources in the Arches

predicted for single O stars from hydrodynamic models (Feldmeier et al. 1997). An interesting example of such a binary is HD 150136, one of the most X-ray luminous O stars (Skinner et al. 2005). The emission from this binary star is dominated by plasma with temperature $\approx$ 0.3 keV, with a small contribution of $\approx$ 1 keV plasma.

We employed the model used by Skinner et al. (2005) to fit the spectrum of HD 150136, but applied the interstellar absorption and distance appropriate for the Arches cluster. The flux of HD 150136 if it were located in the Arches would be at least thousand times smaller, and the system would remain undetected by this sensitive Chandra observation. The high interstellar absorption effectively selects sources with hard energy distribution. Soft sources, even intrinsically luminous, can not be seen in the Galactic center clusters.

A possible alternative to a colliding wind scenario to explain the hard X-rays from the Arches point sources is the generation of X-rays by magnetically confined wind flows, as observed in some young stars (e.g. θ^1 Ori C, Schulz et al. 2003). The hardness of the Arches sources spectra can be indicative for the presence of stellar or circumstellar magnetic fields. A study of the X-ray variability shall shed light on this proposition.

The Quintuplet cluster is 1–2 Myr older than the Arches, containing the largest conglomerate of WR stars known in the Galaxy (Figer et al. 1999). It is located in a similar environment and at approximately the same distance as the Arches (within 50 pc projected distance from the Galactic center). Its mass and stellar density are comparable with the Arches. Fig. 2 displays an ACIS-I image of the Quintuplet cluster.

There are a few luminous blue variable (LBV) candidates in the Quintuplet. LBVs are massive stars in a short phase of large, episodic mass loss. Famous is the Pistol star, which

is considered to be the most massive star known in the Galaxy. To reconcile its prodigious mass estimated as $\sim 150 - 250 M_\odot$ with the recently proposed upper mass cut-off at $150\,M_\odot$ it was suggested that the star is a binary. The Pistol star is not detected by the long Chandra exposure, implying an upper limit $\log L_{\rm X}/L_{\rm bol} < -8$. Thus there is no support for the binarity assumption from hard X-rays, which would be an indication of colliding stellar winds.

The scatter of X-ray luminosities among field WR stars is significantly larger than among O stars. The X-ray bright WR stars are rare and are binaries (sometimes suspected). Fig. 2 shows the position of known WR stars in the Quintuplet cluster. None of these stars is detected, putting an upper limit on their X-ray luminosity at 10^{32} erg/s. The fact that such a young and massive star cluster as the Quintuplet is barely visible on the X-ray sky tells that the X-ray luminosity of a massive star diminishes significantly when the star evolves.

Among a few weak point sources detected by Chandra, two (FMM 231 and FMM 211) are members of eponymous quintuplet of cocoon-like objects (Glass et al. 1999). The nature of these objects is under debate; their possible identification with dusty WC stars has been proposed. However, the X-ray emission from a single WC star is highly unusual and is not detected elsewhere.

To conclude: 1) the stellar X-ray sources in the Arches clusters may be attributed to colliding wind binaries; 2) the strong emission at 6.4–6.7 keV is observed in both stellar and diffuse emission sources in the Arches cluster. The level of this emission cannot be reproduced by thermal plasma models. The strong 6.4–6.7 keV emission may indicate the presence of cool fluorescenting material in the cluster; 3) the non-detection of X-rays from the Pistol star constrains the hypothesis about its binary nature; 4) none of the WR stars known in the Quintuplet cluster is detected in X-rays, confirming the general trend of WR stars being X-ray dim.

Acknowledgments

This research was supported by DFG grant FE 573/3-P.

References

Antokhin I.I., Owocki S.P., Brown J.C., ApJ, 2004, 611, 434
Chevalier R.A., Clegg A., 1985, Nature, 317, 44
Feldmeier A., Puls J., Pauldrach A.W.A., 1997, A&A, 322, 878
Figer D.F., McLean I.S., Morris M., 1999, ApJ, 514, 202 (FMM99)
Figer D.F., et al., 2002, ApJ, 581, 258 (F02)
Glass I.S., et al., 1999, MNRAS, 304, L10
Law C., Yusef-Zadeh F., 2004, ApJ, 611, 858
Oskinova L.M., 2005, MNRAS, 361, 679
Schild H., et al., 2004, A&A, 422, 177
Schulz N.S., et al., 2003, ApJ, 595, 365
Skinner S.L., et al., 2005, MNRAS, 361, 191

XMM-Newton observations of the Cyg OB2 association*

Gregor Rauw†, Michaël De Becker and Natacha Linder

Institut d'Astrophysique, Université de Liège, Belgium

Abstract: We present the first results of an observing campaign of the Cyg OB2 association with the *XMM-Newton* observatory. The brightest OB-type stars exhibit rather hard spectra suggesting that at least part of their X-ray emission arises in a wind-wind interaction. The EPIC images reveal a large number of fainter X-ray sources most of which are probably low-mass pre-main sequence stars belonging to Cyg OB2.

1 Introduction

The Cyg OB2 association is one of the richest and most massive young open clusters known in our Galaxy. These properties make it an ideal target for observations over a broad range of wavelengths from the radio to the γ-ray domain. Optical studies (e.g. Massey & Thompson 1991) are hampered by the heavy and patchy absorption by dense molecular clouds. A far more complete census of the cluster population can be obtained in the near infrared: Knödlseder (2000) analysed 2MASS data of Cyg OB2 finding that the cluster probably harbours about 2600 ± 400 OB stars among which 120 ± 20 O-stars. He accordingly suggested that Cyg OB2 could be a young globular cluster. Four cluster members have been extensively studied in the radio domain. Three of them are non-thermal radio emitters (Cyg OB2 #5, #8a and #9, see e.g. Waldron et al. 1998 and references therein), whilst the fourth one (Cyg OB2 #12) could be one of the most luminous stars in our Galaxy. At the other end of the electromagnetic spectrum, the error box of the unidentified *EGRET* γ-ray source 3EG J2033+4118 overlaps to a large extent with the cluster (Romero et al. 1999, Rauw 2004). Finally, X-ray emission from Cyg OB2 was discovered serendipitously when *EINSTEIN* was pointed at Cyg X-3 (Harnden et al. 1979). This was actually the first report of X-ray emission from OB stars. Since then, Cyg OB2 has been observed by every major X-ray satellite.

Here, we present the very first results of an observing campaign with the EPIC instruments onboard *XMM-Newton*.

*Based on observations with *XMM-Newton*, an ESA Science Mission with instruments and contributions directly funded by ESA Member states and the USA (NASA).

†Research Associate FNRS (Belgium)

2 *XMM-Newton* observations of Cyg OB2

Four pointings centered on Cyg OB2 #8a and separated by 10 days each were obtained in October - November 2004. The raw data were processed with SAS version 6.0. After rejecting some bad time intervals affected by high background events (so-called soft-proton flares), the remaining total exposure time was 75 ksec. A few stray-light features (due to singly reflected photons) from Cyg X-3 are visible in the lower right corner of the images. However, they do not affect the most interesting part of the field of view. The SAS routines detected a total of 221 sources in the combined EPIC images (outside the region affected by the stray-light) with fluxes down to 2×10^{-14} erg cm^{-2} s^{-1}. The EPIC spectra of the brightest X-ray sources were analysed with the `xspec` software. The spectra and the light curve of Cyg OB2 #8a are discussed by De Becker & Rauw (these proceedings) and we will not repeat this analysis here.

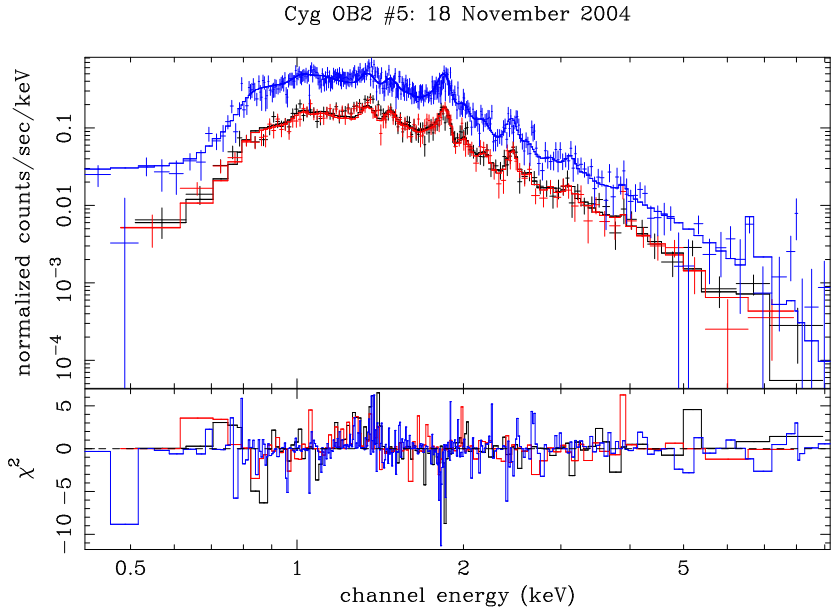

Figure 1: EPIC spectra of Cyg OB2 #5 as observed on 18 November 2004. The data were fitted with an absorbed two temperature optically-thin thermal plasma model (see text).

2.1 Cyg OB2 #5

Cyg OB2 #5 (= BD+40° 4220) is in fact a multiple system consisting (at least) of a short-period colliding wind binary (O6-7 Ia + Ofpe/WN9, Rauw et al. 1999) and a third visual component (most probably a B star, Contreras et al. 1997). The EPIC spectra of this source are well fitted with an absorbed two-temperature thermal plasma model (Fig. 1). In addition to the absorption by the neutral interstellar medium, we included a wind absorption model computed following the technique of Nazé et al. (2004). While the lower temperature of the fit ($kT_1 = 0.63 \pm 0.01$ keV) is quite typical of the intrinsic X-ray emission of early-type stars, the second component is much hotter ($kT_2 = 1.7 \pm 0.2$ keV) and arises most probably in a wind interaction zone. In fact, this multiple system most probably harbours several potential wind-wind collision regions. Unfortunately, the four observations of this system do not provide a good coverage of the 6.6 day orbital period of the close binary system, so that we presently cannot make any statement about the existence or absence of a phase-locked variability.

2.2 Cyg OB2 #9

This O5 If star is a variable non-thermal radio emitter (see also the contributions by Van Loo and by Blomme in these proceedings). Although the non-thermal emission is strongly believed to arise in a wind interaction zone, no spectroscopic evidence for binarity has been reported so far. As for Cyg OB2 #5 , the EPIC spectra are rather well fitted by an absorbed 2-T thermal plasma model (see Fig. 2). While the lower temperature ($kT_1 = 0.63 \pm 0.03$ keV) is again rather typical for O-type stars, the second temperature reaches $kT_2 = 2.4$ keV which corresponds by far to the hottest plasma in the O-type stars of Cyg OB2. This feature is quite consistent with a colliding wind scenario in a binary system where the winds reach their terminal velocities before they collide.

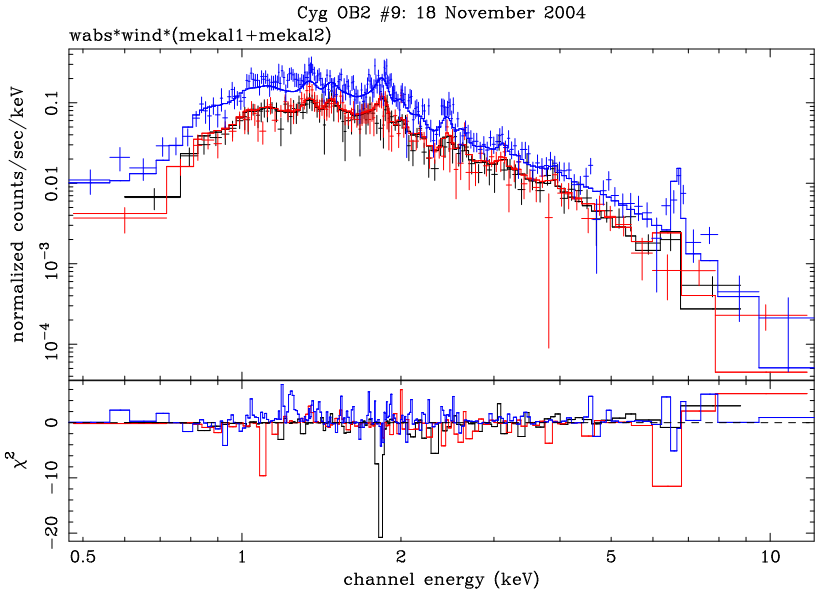

Figure 2: Same as Fig. 1 but for Cyg OB2 #9. Note the prominent Fe K line at 6.6 keV.

2.3 Cyg OB2 #12

The spectral type of this star is rather ill-defined and is probably variable. However, most investigations agree that Cyg OB2 #12 is an extremely luminous B supergiant that could be related to the LBV phenomenon. The EPIC spectra are well fitted with a thermal plasma model with $kT_1 = 0.73 \pm 0.16$ and $kT_2 = 1.8 \pm 0.4$ keV. The latter temperature is surprisingly high given the fact that the wind of the star is rather slow ($\sim 150\,\mathrm{km\,s^{-1}}$, Klochkova & Chentsov 2004). Kolchkova & Chentsov presented evidence for a line radial velocity gradient that they interpreted as an indication for infall of matter. However, even assuming head-on collisions of two flows, each at a velocity of $150\,\mathrm{km\,s^{-1}}$, the post-shock temperature would not be sufficient to account for the hard X-ray spectrum. Therefore, the most likely scenario seems again to be a colliding wind binary where the wind of the companion would have to be much faster.

2.4 Secondary sources

We have cross-correlated the positions of our 221 X-ray sources with the 2MASS point source catalogue. We found near-IR counterparts for 185 of them. Among these, there are 15 known

O-type stars. Beside these early-type objects, most X-ray sources have rather faint near-IR counterparts ($K > 11$). Their location in a $(J-K,\ K)$ colour-magnitude diagram (Fig. 3) suggests that they actually belong to Cyg OB2 and could be low-mass pre-main sequence stars. This latter interpretation is also supported by the flaring activity of some of these secondary sources. Evidence for an active star formation process in Cyg OB2 was already reported based on *IRAS* observations (e.g. Parthasarathy et al. 1992). The *XMM-Newton* results will help to shed more light on the star formation history of this extremely interesting cluster.

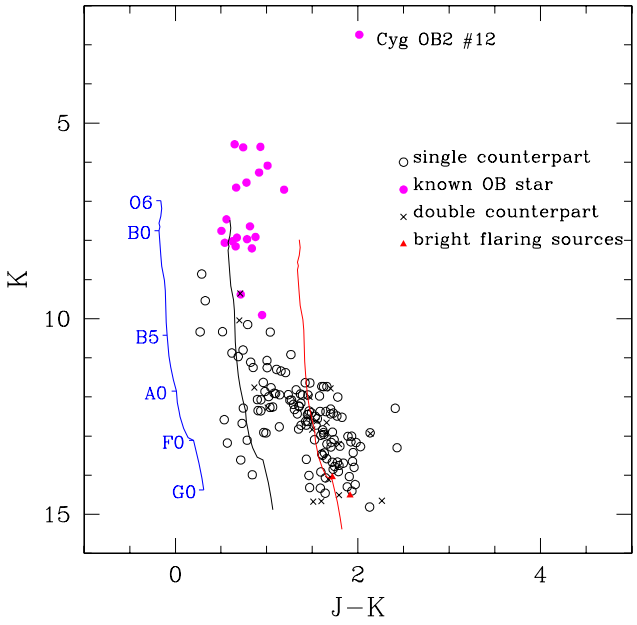

Figure 3: Near-IR colour-magnitude diagram of the 2MASS counterparts of the X-ray sources in Cyg OB2. The location of the main-sequence is shown for three different values of the reddening: from left to right, $A_V = 0$, 5 and 10 mag.

Acknowledgements

This research is supported in part by contract P5/36 IAP (Belspo) and through the XMM/INTEGRAL PRODEX contract.

References

Contreras M.E., Rodríguez L.F., Tapia M., et al., 1997, ApJ, 488, L153
Harnden F.R.Jr., Branduardi G., Elvis M., et al., 1979, ApJ, 234, L51
Knödlseder J., 2000, A&A, 360, 539
Kolchkova V.G., Chentsov E.L., 2004, Astronomy Reports, 48, 1005
Massey P., Thompson A.B., 1991, AJ, 101, 1408
Nazé Y., Rauw G., Vreux J.-M., De Becker M., 2004, A&A, 417, 667
Parthasarathy M., Jain S.K., Bhatt H.C., 1992, A&A, 266, 202
Rauw G., 2004, in *Cosmic Gamma-Ray Sources*, eds. K.S. Cheng & G. Romero, ASSL 304, 105
Rauw G., Vreux J.-M., Bohannan B., 1999, ApJ, 517, 416
Romero G.E., Benaglia P., Torres D.F., 1999, A&A, 348, 868
Waldron W.L., Corcoran M.F., Drake S.A., Smale, A.P., 1998, ApJS, 118, 217

The young open cluster NGC 6231: five years of investigations*

H. Sana†, G. Rauw‡ and E. Gosset‡

Institut d'Astrophysique et de Géophysique, Liège University, Belgium

Abstract: In this contribution, we present an overview of the main results obtained by the Liège multiwavelength (in the X-ray and optical domains) campaign on the young open cluster NGC 6231. We probe the distribution of the O star properties, and especially their binary nature. In this regard, we revise the O-type binary fraction and we briefly discuss the distribution of the binary parameters. We then present the latest developments of the canonical $L_{\rm X} - L_{\rm bol}$ relation. We discuss the causes of the observed deviations from this relation and of the X-ray variability among O-type stars. Probing the population of low mass pre-main sequence stars detected in the X-ray domain, we propose a scenario for the star formation history in NGC 6231.

1 Introduction

Located at about 1.6 kpc from the Earth, NGC 6231 hosts a rich early-type star population and has been chosen as the target of an extended multiwavelength campaign (in the optical and X-ray domains) by the Liège team. Since 1999, we have been acquiring high resolution spectra of most of the early-type stars of the cluster. The bulk of our data set was obtained with the ESO FEROS spectrograph. In 2001, the cluster was also the target of an X-ray monitoring campaign using the XMM-*Newton* observatory. Of a nominal duration of 180 ks, the campaign actually consisted of six separate pointings spread over a 5-day duration. This particular schedule aimed at the study of the variations of the X-ray flux of the early-type stars on different time-scales. More details about the Liège multiwavelength campaign can be found in Sana (2005).

2 Optical spectroscopy

Thanks to the high quality of our FEROS spectra, we have been able to provide an updated/new spectral classification for all the O-type stars in the XMM-*Newton* field of view (fov), and for 15 B-type stars. We derived SB2 orbital solutions for all 5 short period ($P < 6$ d) O-type

*Based on observations collected at the European Southern Observatory (La Silla, Chile) and with XMM-*Newton*, an ESA Science Mission with instruments and contributions directly funded by ESA Member States and the USA (NASA).

†FNRS Research Fellow ‡FNRS Research Associate

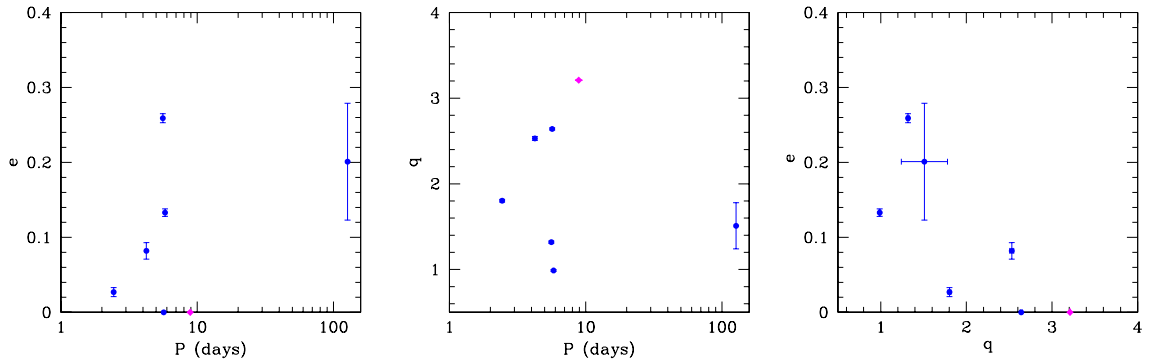

Figure 1: Distribution of various orbital and physical parameters (period, eccentricity, mass ratio) of the O-type binaries in NGC 6231. The diamond indicates the WR system HD 152270.

binaries (some of them for the first time). We also showed/confirmed that four other O-type objects were definitely longer period binaries ($P \sim$ a few months to a year) and we detected the signature of the secondary component for three of them. We are currently monitoring these objects to definitely upgrade their orbital solutions. Beside the 10 binaries (including the WR system WR 79), we also monitored the six remaining, presumably single, O-type stars of the cluster. We unveiled line profile variations (LPVs) for three of them, although these LPVs are probably not related to a binary nature. Accounting for the Wolf-Rayet system, we derive a binary fraction $f = 10/16 \sim 63\%$ for the O-type star population in NGC 6231. This is a somewhat lower value compared to the fraction $f \sim 79\%$ obtained by Garcìa & Mermilliod (2001, GM01 hereafter). This difference probably results from the lower quality of their spectra, as well as from their scarcer follow-up which did not allow them to distinguish RV-shifts most probably due to LPVs from those resulting from an orbital motion.

Fig. 1 presents the obtained distributions of the periods (P), eccentricities (e) and mass ratios (q). These are clearly different from those proposed by GM01. In particular, all the binaries have an eccentricity below 0.3 while GM01 obtained eccentricities ranging from 0.2 to 0.6. Reasons for this were already discussed in Sana et al. (2003) in the case of CPD $-41°7742$. The same discussion applies for the other systems as well. From Fig. 1, we note that the shortest period systems have a small eccentricity while the latter can be larger for longer periods. No obvious trend comes out of the period vs. mass-ratio diagram. It however indicates that the largest mass-ratio in our sample is about 3, which might reflect an observational bias. On the other hand, the eccentricity vs. mass-ratio diagram suggests the existence of an $e - q$ relation similar to the $P - e$ one. Systems with a higher mass-ratio indeed tend to display a smaller eccentricity. Accounting for the fact that all the points in the diagram come from binaries in the same cluster, thus with similar ages, this suggests that larger mass-ratio systems tend to circularize faster and, hence, that tidal dissipation is more efficient in such a configuration. Of course, there is so far only a limited sample of points in the diagram. We checked for SB2 O-type binaries in the 9th Spectroscopic Binary Catalogue and put them in the different diagrams. We observed the same trends for the first two plots of Fig. 1 while neither clear confirmation nor rejection of the existence of an $e - q$ relation could be established. It is possible that including objects from different ages actually hides an underlying relation. The next step in our analysis will be to check the quality of the different orbital solutions in the 9th Spectroscopic Binary Catalogue as well as to investigate the possible effect of the age on the obtained $e - q$ diagram.

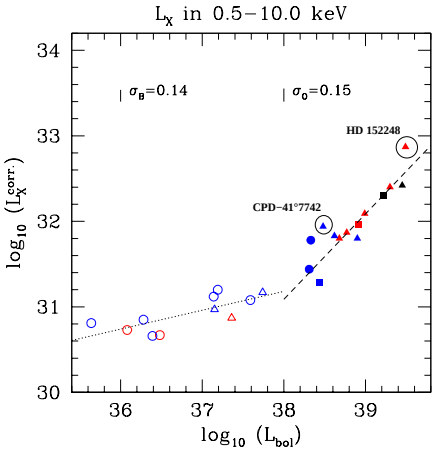

Figure 2: ISM-absorption corrected X-ray luminosities in the 0.5-10.0 keV band plotted vs. bolometric luminosities. Spectral type: O (filled symbols), B (open symbols). Luminosity class: supergiant (black), giant (red), main sequence (blue). Multiplicity: binary (triangles), single RV-variable star (squares), single constant-RV star (circles). Best-fit *canonical* relations for O (Eq. 1) and B (Eq. 2) stars are indicated by the dashed and the dotted lines respectively. $\sigma_{\rm O}$ and $\sigma_{\rm B}$ give respectively the related 1-σ deviation.

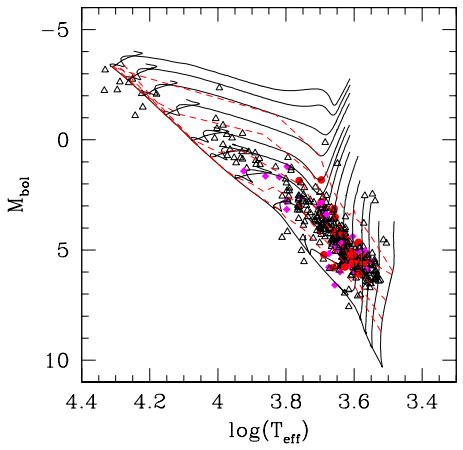

Figure 3: H-R diagram of the EPIC sources with optical counterparts in the Sung et al. (1998) catalogue. Evolutionary tracks from Siess et al. (2000) for masses of 0.2, 0.3, 0.4, 0.5, 0.7, 1.0, 1.5, 2.0, 2.5, 3.0, 4.0, 5.0, 6.0 and 7.0 $M_\odot$ are overplotted. Filled dots, filled diamonds and open triangles indicate respectively Hα emitting stars, Hα candidates and stars with no evidence for emission. The dashed lines correspond to isochrones for ages of 0.5, 1.5, 4.0, 10.0 and 20.0 Myr.

3 X-ray properties of the OB star population

All the O-type stars are detected as bright and relatively soft X-ray emitters while only about 20 % of the B-type stars can be associated with an X-ray source. Fig. 2 presents the obtained $L_{\rm X}$ vs. $L_{\rm bol}$ diagram, considering only the sources with good quality spectra (see details in Sana et al. 2006). Clearly, the O-type stars draw a linear relation in the $\log - \log$ plane. However, a couple of points display an enhanced extra X-ray emission compared to the expected linear relation. The two systems HD 152248 (Sana et al. 2004) and CPD $-41°7742$ (Sana et al. 2005a) are definitely colliding wind binaries for which we expect the wind interaction to produce a substantial amount of X-rays. Excluding those two points, a least-square fit yields:

$$\log L_{\rm X} - \log L_{\rm bol} = -6.912(\pm 0.153) \qquad (1)$$

This corresponds to a dispersion of the X-ray luminosity of about 40% around this new *canonical* relation. Within our sample, significant variability of the X-ray flux is solely observed for binaries, suggesting a wind interaction origin. This mechanism is also the only identified phenomenon that produces a significant deviation from the *canonical* relation.

Regarding the B-type stars, only about 20% of them could be associated with an X-ray source. They also seem to draw a line in the $\log - \log$ plane and a least-square fit yields:

$$\log L_{\rm X} = 0.22(\pm 0.06) \log L_{\rm bol} + 22.8(\pm 2.4) \qquad (2)$$

Note that we again observed a limited dispersion. However, the X-ray spectral properties are very similar to those of PMS stars and about one third of the sources displays flaring-like activity during the 180 ks of our campaign. It is therefore difficult to definitely decide whether the X-ray emission is associated to the B-type stars or if it is produced by PMS stars either located within a binary system or lying by chance along the same line of sight.

4 The optically faint X-ray sources

Beside the early-type stars, the combined EPIC image reveals several hundreds of sources (Sana et al. 2005b). Most of them are fainter but harder and are thought to be associated with PMS stars in the cluster. In total, about 80% of the detected X-ray sources could be associated with optical/IR counterparts, using different existing catalogues and, in particular, the UBV(RI)$_C$ H$_\alpha$ catalogue of Sung et al. (1998). For the latter objects, the location of the optically identified X-ray sources in the H-R diagram is presented in Fig. 3. Comparing with the PMS evolutionary tracks and isochrones from Siess et al. (2000), we get an idea of the masses and evolutionary ages of these objects. Most of them are low mass stars ($M < 2$ M$_\odot$) that started their formation about 2 to 5 Myr ago. However, the distribution of ages suggests that the star formation in NGC 6231 could have started at least 10 Myr ago at a relatively slow rate. This rate then slowly increased to culminate in a *starburst*-like event about 2 to 4 Myr ago, an epoch corresponding to the formation of the massive stars too.

5 Conclusions

We summarized the main achievements of the Liège multiwavelength campaign on the young open cluster NGC 6231. In the optical, our long-term monitoring of most of the early-type stars provides the best set of constraints obtained so far on their orbital and physical parameters. Clearly, it forms a firm basis for the X-ray analysis. On the other hand, the present XMM-*Newton* campaign is certainly one of the deepest X-ray observations of such a young cluster. It reveals a crowded fov, most sources being probably PMS stars, and provides insight into the cluster star formation history. Regarding the O stars, the limited dispersion observed around the *canonical* relation compared to the dispersion obtained by previous studies (e.g. Berghöfer et al. 1997) notably suggests that the *intrinsic* X-ray emission of single O-type star is rather stable, both in terms of brightness and variability. The present sample is however formed by a limited number of stars. The comparison of the present results with those derived in a homogeneous way from the studies of other young clusters will be of major interest.

Acknowledgements

The authors acknowledge support from the FNRS (Belgium), the PRODEX XMM and Integral Projects, as well as contracts P4/05 and P5/36 'Pôle d'Attraction Interuniversitaire' (Belgium).

References

Berghöfer T.W., Schmitt J.H.M.M., Danner R., Cassinelli J.P., 1997, A&A, 322, 167
Garcìa B., Mermilliod J.-C., 2001, A&A, 368, 122
Sana H., 2005, PhD thesis, Liège University, Belgium
Sana H., Hensberge H., Rauw G., Gosset E., 2003, A&A, 405, 1063
Sana H., Stevens I.R., Gosset E., Rauw G., Vreux J.-M., 2004, MNRAS, 350, 809
Sana H., Antokhina E., Royer P., et al., 2005a, A&A, 441, 213
Sana H., Gosset E., Rauw G., Sung H., Vreux J.-M., 2005b, A&A, in press
Sana H., Rauw G., Nazé Y., Gosset E., Vreux J.-M., 2006, MNRAS, submitted
Siess L., Dufour E., Forestini M., 2000, A&A, 358, 593
Sung H., Bessell M.S., Lee S.-W., 1998, AJ, 115, 734

A spectroscopic investigation of the young open cluster IC 1805*

Michaël De Becker† and Gregor Rauw‡

Institut d'Astrophysique et de Géophysique, Université de Liège, Belgium

Abstract: We present the main results of a spectroscopic campaign devoted to the O-type stars in the young open cluster IC 1805. This study aims at the investigation of the multiplicity and the line profile variability of its brightest massive members. We present new results concerning the line profile variability of He II λ 4686 and Hβ for HD 15570 and HD 15629. For these two stars, our radial velocity analysis does not reveal any variations compatible with a binary motion. We also significantly improve the orbital parameters of the long period binary HD 15558. For this latter system, we present for the first time evidence for the detection of the secondary, leading to spectral types of O5.5 and O7 respectively for the two components.

1 Introduction

IC 1805 contains 10 O-type stars, among which some of the most luminous and most massive early-type stars of the Galaxy. It is also supposed to harbour an unidentified EGRET gamma-ray source, whose relation to O-type stars is not excluded. Moreover, it contains the non-thermal radio emitter HD 15558, and constitutes therefore an interesting target for the investigation of the non-thermal emission from massive stars. This cluster was also proposed to be characterized by a very high binary fraction among its O-star members ($\sim 80\,\%$).

2 Data description

Spectra were obtained in the blue domain (4450 - 4900 Å) with the Aurélie spectrograph mounted on the T152 telescope at the Observatoire de Haute-Provence (OHP, France), for the 6 brightest O-stars of the cluster: HD 15558, HD 15570, HD 15629, BD+60° 497, BD+60° 501 and BD+60° 513 (see Rauw & De Becker 2004 for a study of the latter three targets). A more intense monitoring of HD 15558 was performed with the Elodie echelle spectrograph mounted on the T193 telescope at OHP. The aim of this study was to investigate the multiplicity of the O-stars of the cluster, along with their line profile variability and relate it to the various possible scenarios.

*Based on data collected at the Observatoire de Haute Provence (France)

†e-mail: debecker@astro.ulg.ac.be

‡Research Associate FNRS (Belgium)

3 Main results

In this section, we briefly describe the main results of our optical campaign devoted to the most massive members of IC 1805, namely HD 15558, HD 15570 and HD 15629. In Fig. 1, we present the blue spectrum obtained with the Aurélie spectrograph for the three stars.

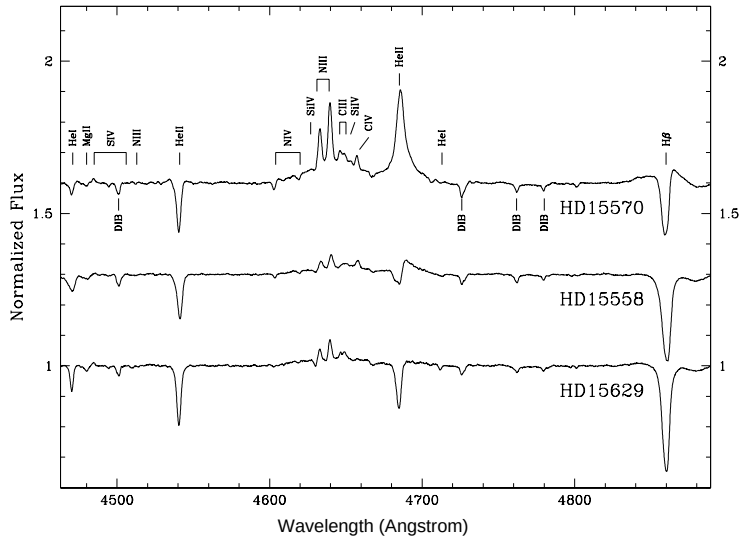

Figure 1: Optical spectra obtained in the blue domain for the three brightest O-stars of IC 1805. HD 15570: the main feature is the strong He II λ 4686 emission, along with the strong N III $\lambda\lambda$ 4639-4641 lines. Hβ is in P-Cygni. HD 15558: the emission lines are weaker, and He II λ 4686 displays a P-Cygni profile. HD 15629: the spectrum is typical of a single O5 main sequence star.

3.1 HD 15570

Our investigation of the radial velocity of HD 15570 (O4If$^+$) did not reveal any significant variations attributable to binarity on time-scales of a few days, or from one year to the next. However, we observed a significant line profile variability of He II λ 4686 and Hβ (see Fig. 2), with a recurrence time-scale of about 6 days. The equivalent width of He II λ 4686 presents a somewhat marginal modulation probably with a time-scale of about 6 days, but we note that this time scale is not very well defined.

Two scenarios could be envisaged to explain these profile variations:

- The variations could possibly be attributed to rotational modulations, the time-scale of 6 days being the rotational period.

- Another possibility to be considered is a wind-wind interaction within a binary system seen under a low inclination, but if the rotational and orbital axes are parallel this would lead to an excessive V_{rot} ($V_{rot} \sin i = 130\,\mathrm{km\,s^{-1}}$). For this reason, the rotational modulation scenario is slightly preferred (for details, see De Becker et al. 2005).

3.2 HD 15629

For this O5V((f)) star, our investigation did not reveal any significant radial velocity variation attributable to a binary motion on time-scales of a few days, or from one year to the next. However, we detected a significant variability of the profile of the He II λ 4686 and Hβ lines with a time-scale of a few days. We note that this variability is clearly detected during one observing run (September 2002) whilst it is marginal in other data sets. This suggests possible transient variations that require further investigation with more data (see De Becker et al. 2005).

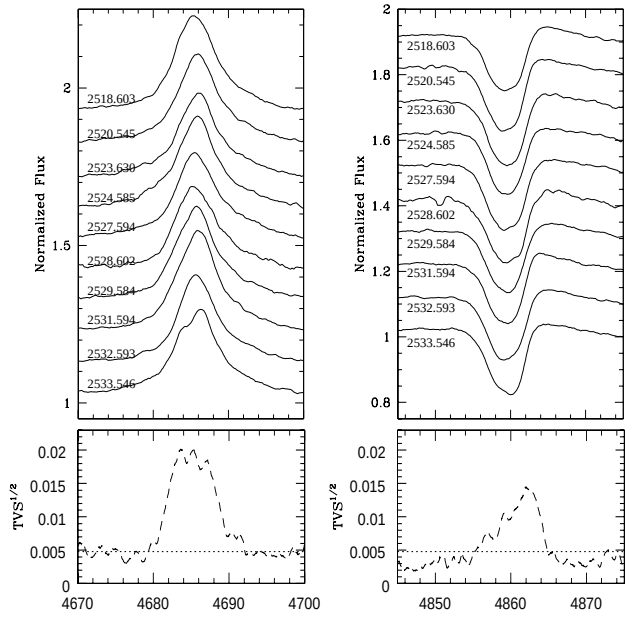

Figure 2: Line profile variability of He II λ 4686 (left) and Hβ (right) for HD 15570. The upper panels show the line profiles obtained with Aurélie in September 2002. The heliocentric Julian dates (- 2 450 000) are specified in each case. The profiles present correlated variations suggesting that more than one component contribute to the lines. In the lower panels, the Time Variance Spectra (TVS, see Fullerton et al. 1996) show variability levels well above the 90 % confidence threshold. For He II λ 4686, the variability is very high for the entire line. For Hβ, the variations are more significant in the emission part of the P-Cygni profile.

Table 1: Orbital parameters of HD 15558 determined from our times series obtained at OHP.

P	442 ± 12 d	K	40.9 ± 1.8 km s^{-1}
e	0.39 ± 0.03	ω	$116° \pm 6°$
T_o	$2\,451\,795.400 \pm 6.556$	a sin i	350.0 ± 15.2 R$_\odot$
γ	-50.2 ± 1.1 km s^{-1}	f(m)	3.0 ± 0.4 M$_\odot$

3.3 HD 15558

On the basis of 70 radial velocity measurements on the He II λ 4542 and N III $\lambda\lambda$ 4634,4641 lines spread over about 1600 days, we obtained a new SB1 solution (see Table 1).

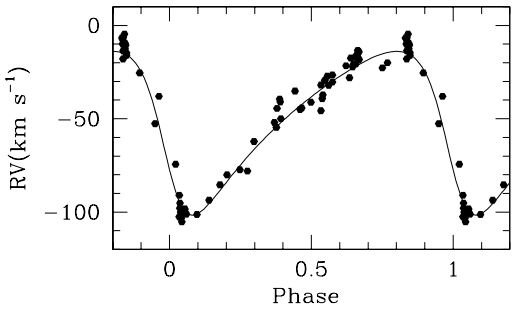

Figure 3: Radial velocity curve of HD 15558 for an SB1 orbital solution with a period of about 442 d. The data points are overplotted. Phase 0 corresponds to periastron.

As the profiles from the two stars are strongly blended at most of the phases, a disentangling method is needed to obtain an SB2 solution. However, we were able to separate to first order the profiles of the primary and of the secondary at phases close to the extrema of Fig. 3. Figure 4 presents the results obtained by fitting Gaussians to the profiles. From this approach, we determined the He I λ 4471/He II λ 4542 equivalent width ratio and hence the spectral types of the two stars, i.e. O5.5 and O7. A disentangling method is also needed to definitely determine the luminosity classes, but we tentatively propose they may be III and V respectively for the primary and the secondary. We note also that the He II λ 4686 P-Cygni profile of the primary

presents a significant variability on a time-scale of a few days, possibly attributable to rotational modulations (see De Becker & Rauw 2005).

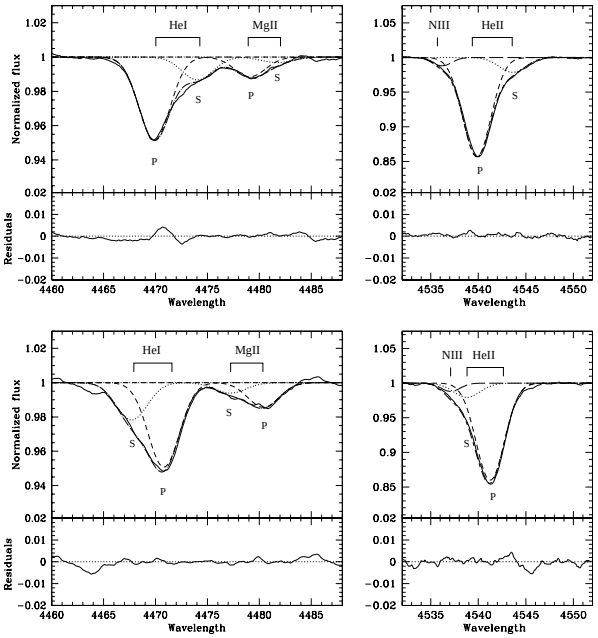

Figure 4: Simultaneous fit of Gaussians to the profiles of the He I λ 4471 , Mg II λ 4482 and He II λ 4542 lines of HD 15558. Upper part: phase $\sim$0.05. Lower part: phase $\sim$0.85. The P and S symbols stand respectively for the primary and secondary components of each line.

4 Summary and conclusions

Our radial velocity study did not reveal any significant variations for HD 15570 and HD 15629 on time scales of a few days or from one year to the next. This strongly supports the single star scenario for both stars. Both stars present significant profile variations of the He II λ 4686 and Hβ lines. For HD 15570, the recurrence time-scale is of about 6 d, and it might be attributed to rotational modulations. For HD 15629, the variability is mostly observed in only one data set, suggesting it might be transient. In the case of HD 15558, our intensive campaign led to the determination of a new orbital solution, based on a homogeneous set of spectral lines. For the first time, the companion is detected and we propose O5.5III and O7V spectral types respectively for the primary and the secondary.

Acknowledgements

This research was supported by FNRS for the rent of OHP telescopes, by contract PAI P5/36 (Belgian Federal Science Policy Office) and through the PRODEX XMM/INTEGRAL contracts.

References

De Becker M., Rauw G., 2005, in preparation
De Becker M., Rauw G., Eenens P., 2005, MNRAS, submitted
Rauw G., De Becker M., 2004, A&A, 421, 693
Fullerton A.W., Gies D.R., Bolton C.T., 1996, ApJS, 103, 475

A survey for gamma-ray emission from OB associations with *INTEGRAL*: some preliminary results

J.-C. Leyder [1,2] and G. Rauw [1*]

[1]Institut d'Astrophysique et de Géophysique, Université de Liège, Belgium

[2]INTEGRAL Science Data Center, Versoix, Switzerland

Abstract: Recent studies indicated that there might be a correlation between OB associations and unidentified gamma-ray sources from the 3EG catalogue. Moreover, when extrapolating the fluxes measured by EGRET at energies higher than 100 MeV with a power-law down to the energy range of ISGRI, the expected count rates should be large enough to be detected with *INTEGRAL*. As most of these OB associations are located within the Galactic plane, they are being observed by *INTEGRAL* as part of the Core Program (CP) during both the Galactic Plane Scans (GPS) and the Galactic Center Deep Exposure (GCDE). Combining public and CP data, we have performed a survey for gamma-ray emission from OB associations and the first results are presented in this paper.

1 OB Associations

OB associations are made up of a group of stars, specifically including O type stars, and eventually B type stars. As these stars are very massive, they exhibit features such as fast stellar winds :

$$v_\infty \simeq 2000 \text{ km s}^{-1},$$

and large mass loss rates :

$$\begin{aligned} \dot{M} &\simeq 10^{-5} M_\odot \text{yr}^{-1} \text{ (for O type stars)} \\ \dot{M} &\simeq 10^{-4} M_\odot \text{yr}^{-1} \text{ (for WR type stars).} \end{aligned}$$

The presence of massives stars also implies that they are rather young ($< 10^7$yr), and that these associations are found in star forming regions such as the spiral arms of the Galaxy. It should also be noted that the stars belonging to these associations are too far apart from each other to be bound by gravitation, as opposed to clusters.

OB associations are formed when an instability causes a cloud of interstellar matter to collapse, thus giving rise to a set of stars of all masses. When the most massive one reaches the end of its life and explodes as a supernova, it creates a shock front that will expand and cause the density in another region to increase.

O stars are detected in X-rays, and so are a fraction of B stars.

*Research Associate FNRS, Belgium

Figure 1: The Scorpius constellation, showing the Upper Scorpius OB association (Preibisch et al. 1998).

2 OB associations in γ-rays

Recent studies on the possible association of unidentified EGRET sources with different types of galactic objects indicated a significant correlation of sources from the 3 EG catalogue with OB associations (Romero, Benaglia & Torres 1999). Most of these OB associations, being usually located in the Galactic Plane, are observed during the *INTEGRAL* Core Programme. Deriving (accurate) positions and fluxes of these sources with the IBIS instrument onboard *INTEGRAL* might allow us to identify the counterparts of these sources. Furthermore, it might also help us determine whether the observed continuum emission is coming :

- from radio-quiet pulsars (as suggested by Romero et al. 1999);
- from shock fronts created by the interactions of the stellar winds of massive stars with the ambient ISM (Manchanda et al. 1996); or
- from hydrodynamic shocks in the winds :
  - of individual stars (Chen & White 1991); or
  - of massive colliding wind binary systems (Eichler & Usov 1993, Mücke & Pohl 2001, Benaglia et al. 2001).

The results of this study should help us to identify the so-far unknown counterparts of a large number of galactic γ-ray sources. For instance, in the third scenario hereabove, observations of non-thermal radiation at other energies (γ- and X-rays) should allow to constrain the properties of the relativistic electrons and hence provide an elegant means to measure the magnetic fields of early-type stars. Due to the spectral features of these stars, their magnetic fields cannot be measured by classical techniques (e.g. Zeeman splitting).

The sources listed by Romero et al. (1999) have photon indices near $\Gamma \sim 2$. Therefore, the number of photons at a given energy is $n(E) = \alpha \times E^{-\Gamma}$. According to Romero et al., the EGRET fluxes (> 100 MeV) are:
- 34×10^{-8} ph cm^{-2} s^{-1} for a typical WR counterpart,
- 47×10^{-8} ph cm^{-2} s^{-1} for a typical Of counterpart, and
- 45×10^{-8} ph cm^{-2} s^{-1} for a typical OB association counterpart.

For a power-law spectrum, the flux above 100 MeV is given by

$$\int_{100\,\mathrm{MeV}}^{\infty} n(E)\,dE = \alpha \int_{100\,\mathrm{MeV}}^{\infty} E^{-2}\,dE = \alpha/(10^5\,\mathrm{keV})$$

yielding
$\alpha_{\mathrm{WR}} = 34 \times 10^{-3}\,\mathrm{ph\,cm^{-2}\,s^{-1}\,keV}$,
$\alpha_{\mathrm{Of}} = 47 \times 10^{-3}\,\mathrm{ph\,cm^{-2}\,s^{-1}\,keV}$ and
$\alpha_{\mathrm{OB}} = 45 \times 10^{-3}\,\mathrm{ph\,cm^{-2}\,s^{-1}\,keV}$.
Extrapolating the power-law spectrum to the IBIS energy range (15 keV – 10 MeV), we find for a typical OB association a continuum flux of $45 \times 10^{-9}\,\mathrm{ph\,cm^{-2}\,s^{-1}\,keV^{-1}}$ @ 1 MeV.

3 Analysis with *INTEGRAL*

The preliminary results were first obtained with the Off-line Scientific Analysis (OSA) software, version 4.2. The analyses are being repeated with OSA 5.0 to take advantage of the better background reduction introduced with this new release.

The only instrument used up to now is ISGRI, a coded-mask imager offering a spatial resolution of $12'$ over an energy range from approximately 23 to 1000 keV (Lebrun et al. 2003).

4 Candidates and data

The data taken by *INTEGRAL* more than one year ago are now in the archive, which means that approximately one and a half year of data is available. Below is a table giving for each OB association (adapted from Humphreys 1978) in our sample the approximate time during which it was located in the fully coded field of view of the ISGRI instrument.

Region	Right Ascension [deg]	Declination [deg]	ISGRI time [ks]
Sgr OB1	272.0	-21.5	1091
Cyg OB3	301.2	35.8	2320
Cyg OB1	304.4	37.6	2470
Cyg OB8	303.2	41.0	1625
Cyg OB9	305.8	39.9	1861
Cyg OB2	308.1	41.3	2230
Cas OB5	359.1	61.6	2276
Cas OB6	40.8	61.4	39
Gem OB1	92.5	21.6	1241
Vel OB1	132.5	-45.0	1705
Car OB1	158.9	-59.1	1737
Coll 228	160.7	-60.0	1688
Car OB2	166.9	-59.8	1110
Ara OB1a	249.9	-46.8	1649
NGC 6204	251.6	-47.0	1601
Sco OB1	253.1	-42.2	1146

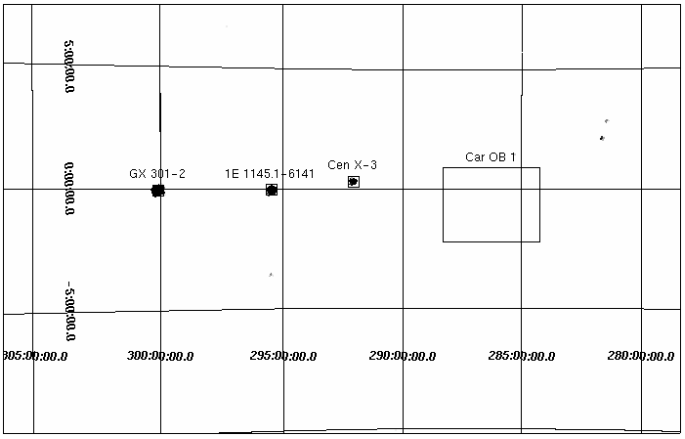

Figure 2: ISGRI significance map of the Car OB 1 region (20 – 40 keV), produced with OSA 5.0.

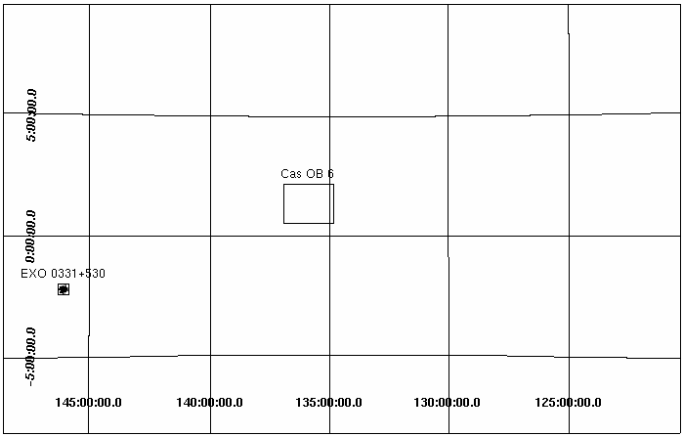

Figure 3: ISGRI significance map of the Cas OB 6 region (20 – 40 keV), produced with OSA 5.0.

5 Preliminary results

The first tests carried out using OSA 4.2 did not allow to detect any signal from the few OB associations that were studied. The improvements in OSA 5.0, especially in the background correction, might help change this situation.

References

Benaglia P., Romero G.E., Stevens I.R., et al., 2001, A&A, 366, 605
Chen W., White R.L., 1991, ApJ, 366, 512
Eichler D., Usov V., 1993, ApJ, 402, 271
Humphreys R., 1978, ApJS, 38, 309
Lebrun F., Leray J.P., Lavocat P., et al., 2003, A&A, 411, L141
Manchanda R.K., Polcaro V.F., Norci L., et al., 1996, A&A, 305, 457
Mücke A., Pohl M., 2001, in *Interacting Winds from Massive Stars*, eds. A.F.J. Moffat, N. St.-Louis, ASP Conf. Series, 260, 355
Preibisch Th., Guenther E., Zinnecker H., et al., 1998, A&A, 333, 619
Romero G.E., Benaglia P., Torres D.F., 1999, A&A, 348, 868